COMPARISON OF PHYTOPLANKTON BIOMASS AND COMMUNITY COMPOSITION IN THREE TEXAS ESTUARIES DIFFERING IN FRESHWATER INFLOW REGIME

A Thesis

by

TIFFANY LEE CHIN

BS, Dickinson College, 2016

Submitted in Partial Fulfillment of the Requirements for the Degree of

MASTER OF SCIENCE

in

MARINE BIOLOGY

Texas A&M University-Corpus Christi
Corpus Christi, Texas

August 2020

August 2020

COMPARISON OF PHYTOPLANKTON BIOMASS AND COMMUNITY COMPOSITION IN THREE TEXAS ESTUARIES DIFFERING IN FRESHWATER INFLOW REGIME

A Thesis

by

TIFFANY LEE CHIN

This thesis meets the standards for scope and quality of
Texas A&M University-Corpus Christi and is hereby approved.

Michael Wetz, PhD
Chair

Antonietta Quigg, PhD
Committee Member

Daniel Roelke, PhD
Committee Member

August 2020

ABSTRACT

Phytoplankton are at the base of the marine food web and are sensitive indicators of environmental change, such as changes to freshwater inflow in estuaries. Because freshwater inflows to Texas estuaries are projected to decrease in the coming decades as a result of increasing human freshwater demands and climate change, it is critical to understand ecosystem-level responses to freshwater inflow variability. This study examined phytoplankton community composition and biomass, along with relationships to environmental variables in three Texas estuaries with differing freshwater inflow regimes. The estuaries were San Antonio Bay (highest inflow levels), Nueces-Corpus Christi Bay (intermediate inflow levels), and Baffin Bay (lowest inflow levels). The goal was to understand the impacts of freshwater inflow variability and magnitude on phytoplankton dynamics. Baffin Bay had the highest phytoplankton biovolume, followed by NC and SA. Higher frequency and magnitude inflows in SA corresponded to overall lower biovolume and shifts of biovolume maxima downstream, while infrequent inflows in BB were followed by a sustained diatom bloom. Inflows to NC affected only the upper estuary, while the lower estuary appeared to be more influenced by ocean exchange. Large, faster-growing taxa, such as *Rhizosolenia*, were observed in greatest abundances in Baffin Bay, while slower-growing dinoflagellates dominated in NC and SA. Findings of lower biovolume and higher proportion of slow growing taxa in the high inflow estuary, SA, are contrary to our understanding based on the available literature and underscore the importance of understanding system-specific drivers for effective coastal management.

ACKNOWLEDGEMENTS

I would like to thank my advisor, Dr. Michael Wetz, for teaching and guiding me throughout this process. I am grateful as well to Dr. Antonietta Quigg and Dr. Daniel Roelke for serving on my committee and for their thoughtful feedback on my work. I thank the following entities for funding and support of this project: Harte Research Institute for Gulf of Mexico Studies, Texas Water Development Board, Texas A&M University-Corpus Christi Division of Research and Innovation and College of Science and Engineering.

I could not have completed this work without the invaluable assistance of my lab members and field crew - Natasha Breaux, Emily Cira, Ken Hayes, Josh Martin, Elani Morgan, Elizabeth Obst, Sarah Tominack, and Lily Walker. I would also like to thank Madden Bremer for her assistance with spatial analyses and all things maps. Thank you to the fellow students who helped me develop ideas and work through problems and who provided moral support and solidarity - Sophia Hoffman, Kelsey Martin, Meghan Martinez, Jill Thompson-Grim, and Abby Williams.

Finally, I would like to thank my undergraduate advisor, Dr. Kristin Strock, for sparking my interest in aquatic ecology and encouraging me to pursue research projects and further education. Thank you to my previous supervisors - Dr. Leslie Matthews, Kellie Merrell, Dr. Ed Rutherford, and Steve Smith – for the growth and knowledge I gained while working with you, and of course my family and friends who have encouraged me from afar. I would not be here without their support.

TABLE OF CONTENTS

LIST OF FIGURES

FIGURES PAGE

LIST OF TABLES

TABLES PAGE

INTRODUCTION

Freshwater inflows influence estuarine ecosystems through physical and chemical processes. Freshwater inflows bring new nutrients and sediment loads to estuaries, affecting biogeochemical processes (Brock 2001; An and Gardner 2002; Gardner et al. 2006; Bruesewitz et al. 2013) and light availability in the water column (Underwood and Kromkamp 1999; Azevedo et al. 2014). Additionally, the magnitude of freshwater entering the estuary affects mixing, circulation patterns, and hydraulic flushing regimes (Longley 1994; Montagna et al. 2018).

Phytoplankton are sensitive indicators of environmental change, making them an ideal organism to study for system-specific effects of freshwater inflow variability. While riverine nutrient loading may stimulate phytoplankton growth (Mallin et al. 1993), high magnitude inflows may also limit or reduce biomass accumulation if flushing times approach or exceed phytoplankton growth rates (Roelke et al. 2013; Azevedo et al. 2014). Under drought conditions, conflicting impacts on phytoplankton growth have been observed. For example, some studies have shown that estuarine phytoplankton can become nutrient limited (e.g., Wetz et al. 2011), while other studies have shown that phytoplankton growth can continue by utilizing regenerated nutrients (Longley 1994; Glibert et al. 2010). Aside from impacts on phytoplankton growth, freshwater inflow variability can favor different functional groups depending on the magnitude of inflow. For example, under high inflow regimes, large fast-growing taxa such as diatoms or motile chlorophytes are often favored, as they can rapidly uptake (and even store) new nutrients (Kennish and Paerl 2010; Paerl et al. 2014; Carstensen et al. 2015; Cloern 2017). Under lower inflow regimes, nutrient regeneration can occur through both water column processes and sediment interface interactions (Glibert et al. 2010), resulting in higher proportions of

ammonium and organic N in the water column than in river dominated systems (Burkholder et al. 2006; Glibert et al. 2007). These nitrogen forms are advantageous for small picocyanobacteria due to high surface area to volume ratios and also to mixotrophic dinoflagellates (Glibert et al. 2010, Ni Longphuirt et al. 2019), which are also advantaged by longer residence times due to their slower growth rates (Paerl and Justić 2013).

The effects of inflow also affect salinity regimes, which can affect phytoplankton community composition under extreme circumstances because of a lack of tolerance to high salinities by many, but not all taxa (Buskey et al. 1997; Hall et al. 2013). Phytoplankton taxa vary in their quality as a food source for higher organisms, making community composition important for water quality, food web dynamics, and whole ecosystem health (Cloern and Dufford 2005; Dorado et al. 2015). Diatoms are generally considered a superior food source (Paerl and Justić 2013), although there are exceptions. Grazing on diatoms can be inhibited by their morphology, making them unavailable as a food source (Koski et al. 2008), and diet studies of zooplankton have shown that a mono-specific diatom diet is inferior to a mixed diet of diatoms and cyanobacteria (Schmidt and Jónasdóttir 1997). Cyanobacteria and HAB-forming dinoflagellates species are considered poor food sources and can be toxic (Paerl 2006; Landsberg et al. 2009). Some cyanobacteria lack dietary lipids that make them less suitable diet items (Martin-Creuzberg and von Elert 2009), and toxic strains may cause zooplankton to stop feeding, as shown by Lampert (1987) to occur with *Microcystis*. However, there are also cyanobacteria species that are high quality food sources, such as *Phormidium* sp., which is used as a feedstock in aquaculture and performed better than other taxa in a nutritional experiment (Sivakumar et al. 2011).

Along the Texas Gulf Coast, there is a precipitation gradient from northeast to southwest (Montagna et al. 2011) that follows the shift from a humid, subtropical climate to an arid climate along the coast (Texas Water Development Board 2019). This gradient results in diminishing freshwater inflows along the coast, shifting from river-dominated estuaries on the north coast to low-inflow hypersaline systems on the south coast. Freshwater inflows are variable at the scale of individual bays and are dependent on both short-term weather patterns and long-term climatic variation. Under future climate change projections, droughts are expected to occur more frequently along the Texas Gulf Coast (IPCC 2014; Environmental Protection Agency 2016). Reduction of freshwater availability due to climate change, coupled with increasing freshwater demand from rising coastal populations and expanding urban centers (Montagna et al. 2002; Roelke et al. 2017; United States Census Bureau 2018), could result in a long-term decrease in freshwater inflow to Texas estuaries. This highlights the necessity of understanding how the ecology and health of Texas estuaries are affected by freshwater inflow variability.

In this study, we examined phytoplankton biomass and community composition in three Texas estuaries with different inflow regimes – San Antonio Bay, which is river-influenced, Nueces-Corpus Christi Bay, considered a neutral estuary, and Baffin Bay, which has no major river inflows and is frequently hypersaline. In literature pertaining to ecological impacts of freshwater inflow variability on estuaries, river-dominated estuaries tend to be over-represented compared to low inflow, lagoonal systems that are still numerically important (Largier 2010; Tweedley et al. 2019). The possibility of inflow declines in the future makes it critical to understand the functional differences in estuaries under different inflow regimes, particularly from a management standpoint. We aimed to evaluate three hypotheses: 1) nutrient concentrations and chlorophyll/phytoplankton biomass would be highest in the high inflow

estuary, San Antonio Bay, intermediate in Nueces-Corpus Christi Bay, and lowest in Baffin Bay as a result of decreasing inflow magnitude, 2) the phytoplankton community would be dominated by large and/or fast-growing in San Antonio Bay, with the fraction of small and/or slow-growing taxa increasing from Nueces-Corpus Christi Bay to Baffin Bay, and 3) phytoplankton biomass will peak at intermediate inflow magnitudes and biomass maxima will shift downstream during ephemeral inflow pulses.

METHODS

Site Descriptions

Three estuaries were chosen to represent the freshwater inflow gradient on the Texas Gulf Coast: San Antonio Bay, Nueces-Corpus Christi Bay, and Baffin Bay. San Antonio Bay (SA) is the northernmost of the three estuaries and is fed by the San Antonio and Guadalupe Rivers. It receives the highest rates of freshwater inflow of the three estuaries and has a positive inflow balance (Montagna et al. 2018). The average depth of SA is 2 m (USEPA 1999), and the average residence time is 38 days (Montagna et al. 2011). The SA watershed is dominated by agricultural lands and scrub (NOAA C-CAP). SA receives freshwater inflows from the Guadalupe and San Antonio rivers, and the watershed encompasses the city of San Antonio, which is rapidly expanding (US Census Bureau). The Nueces-Corpus Christi Bay system (NC) receives freshwater inflow from the Nueces River, as well as return flows from wastewater facilities. Salinity in NC is strongly influenced by exchange with coastal ocean water via a ship channel, and inflow balance is often neutral or slightly negative due to high evaporation rates and low inflow rates (Montagna et al. 2018). NC is shallow (3 m on average) (USEPA 1999), with average residence times of 356 days (Montagna et al. 2011). Land use in the watershed is

dominated by agriculture and developed areas (NOAA C-CAP). Baffin Bay (BB) is the southernmost of the three estuaries. It is a lagoonal estuary with an average negative inflow rate and frequent hypersalinity in the upper reaches of the bay (Wetz et al. 2017). Inflows in BB are from ephemeral streams, and the bay often experiences little to no inflows punctuated by periods of flooding during El Niño years. Land use coverage in the BB watershed is dominated by agriculture, scrub/shrub, and grassland (NOAA C-CAP).

Sampling

Monthly sampling was conducted in each bay from March 2018 to July 2019, with the exception of April 2019 when BB was not sampled due to inclement weather. Six sites in BB and four sites in each SA and NC (Fig. 1) were selected to capture the gradient from river influence to ocean exchange. At each site, surface water (0.1 m) was collected in brown HDPE bottles and stored on ice for nutrient, carbon, and chlorophyll *a* analysis. Additional water samples were collected in brown HDPE bottles and stored at ambient temperature for phytoplankton enumeration. Secchi depth as well as hydrographic depth profiles (every 0.5 m) of DO, pH, conductivity, salinity, and temperature were collected using a YSI multiparameter sonde.

Biogeochemical Analyses

Inorganic nutrient concentrations (nitrate + nitrite, nitrite, ammonium, orthophosphate, and silicate) were determined from the filtrate of water samples that were passed through 25 mm GF/F filters and stored frozen (-20 ºC) until analysis. After thawing to room temperature, samples were analyzed on a Seal QuAAtro autoanalyzer. Standard curves with five different concentrations were run daily at the beginning of each run. Fresh standards were made prior to

each run by diluting a primary standard with low nutrient surface seawater. Deionized water (DIW) was used as a blank, and DIW blanks were run at the beginning and end of each run, as well as after every 8-10 samples to correct for baseline shifts.

Total dissolved nitrogen (TDN) was determined using the filtrate of water samples that were passed through precombusted 25 mm GF/F filters and stored frozen (-20 ºC) until analysis. Samples were analyzed using the High Temperature Catalytic Oxidation method on a Shimadzu TOC-Vs analyzer with nitrogen module. Standard curves were run twice daily using a DIW blank and five concentrations of potassium nitrate. Three to five subsamples were taken from each standard and water sample and injected in sequence. Reagent grade glucosamine was used as a laboratory check standard and inserted throughout each run, as were Certified Reference Material Program (CRMP) deep-water standards of known TDN concentration. Dissolved organic nitrogen (DON) was determined by subtracting inorganic nitrogen (ammonium, nitrate + nitrite (N+N)) from TDN.

Phytoplankton Analyses

Chl *a* was obtained by filtering (<5 mm Hg) a known volume of water through Whatman 25 mm GF/F filters (pore size 0.7µm) that were then stored frozen (<-20 ºC) for future analysis. Whole water, <20 µm, and <3 µm size fractions were analyzed. <20 and <3 µm size fractions were pre-filtered with 20 µm mesh or Whatman GF/D filters (nominal pore size 2.7 µm, referred to here as 3 µm). Chl in the microplankton size range (>20 µm) was estimated by subtracting the <20 µm Chl from the whole water. Chl in the nanoplankton size range (3-20 µm) was estimated by subtracting the <3 µm Chl from the <20 µm Chl. Chl *a* was extracted from the GF/F filters by

soaking in 90% HPLC grade acetone for 16-24 hours. Fluorometric determination of chl *a* was performed with a Turner Trilogy fluorometer without acidification.

Samples for flow cytometric analysis were fixed with 80 µL glutaraldehyde to 4 mL sample water and stored at -20 ºC until analysis. Picoplankton and *Aureoumbra lagunensis* (brown tide) were enumerated on an Accuri C6 Plus flow cytometer. Samples were thawed in the dark at room temperature then filtered through 20 µm Nytex mesh. Samples for *A. lagunensis* enumeration then underwent a multistep polyclonal antibody staining process that is specific to *A. lagunensis*. Stained samples were analyzed on the flow cytometer along with unstained controls for *A. lagunensis* enumeration. Filtered unstained subsamples were used to enumerate picoplankton. The detection limit for *A. lagunensis* enumeration was 80,000 cells/mL (Cira and Wetz 2019), and values below detection limit were treated as zeros.

Nano- and microplankton were enumerated using the Utermohl method with samples that were preserved with 1 mL acid Lugol's solution to 60 mL sample water. 5 to 10 mL samples were settled for 24 hours and subsequently counted at 20x magnification using an Olympus 1X-71 inverted microscope. Transects of settled chambers were counted until a minimum of 100 cells of the most abundant genera were identified. Volume of sample settled and area of chamber counted were used to calculate number of cells per mL for each taxa present. Cell measurements were used to calculate biovolume using formulas determined by the geometric shape of cells, as described by Hillebrand et al. (1999) and Sun and Liu (2003). When there were conflicts between the formulas in these two sources, formulas from Sun and Liu (2003) were utilized (additional details in Appendix 1). Due to the difficulty of obtaining a third dimension for some taxa, missing cell dimensions were estimated based on relationships observed from cells for which all dimensions could be obtained. It is important to note that there are challenges inherent

to using biovolume calculations, including the aforementioned issue with estimates of dimensions, potential for human error in counting accuracy and the assumptions necessary to make these calculations (see Appendix 1).

Ancillary Environmental Data

Daily inflow data were obtained from USGS. Gauges from which data were obtained were: San Antonio River (#08188500) and Guadalupe River (#08176500) for SA, Nueces River (#08211000) for NC, and Los Olmos Creek (#08212400), San Fernando (#08211900), and Petronila Creek (#08212820) for BB. Seven-day averages of inflow prior to each sampling date were used to represent inflow conditions leading up to each sampling event. This seven-day timeframe was chosen based on best methods reported by Roelke et al. (2017).

Wind speed and precipitation data were obtained from NOAA's Tides and Currents database for SA or National Climate Data Center for NC and BB. Seadrift (station US1TXCLH015) was used to represent SA, Corpus Christi NAS (station USW00012926) was used to represent NC, and Kingsville NAS (station USW00012928) was used to represent BB.

Bay Volume-normalized Biomass Estimates

Estuary volumes were estimated using raster bathymetric data, downloaded from NOAA National Centers for Environmental Information using the Estuarine Bathymetric Digital Elevation Models for San Antonio Bay, Corpus Christi Bay, and Baffin Bay. Bathymetric data were imported into ArcPro (version 2.5), and segments were drawn in the state plane projection for Texas-South (NAD 1983 FIPS 4205). Each bay was divided into segments that corresponded to each sampling site (Fig. 2) by drawing polygons. Segments were then joined to raster

bathymetric data and volume estimated for each segment, followed by the estuary as a whole by adding each segment's volume. Bathymetric data were not available for Nueces Bay (encompassing NC1 and NC2), so volumes of the segments corresponding to NC1 and NC2 were estimated using the average depth of Nueces Bay published by USGS and the surface area of the corresponding segments.

Inflow normalized to bay volume for the 7-d period prior to each sampling were calculated by dividing the seven-day prior average inflow for each sampling date by the total volume of the bay. Volume adjusted chlorophyll and biovolume for each sampling date in each bay were calculated using methods detailed in Peierls et al. (2012). Values for each variable at each site were multiplied by the volume of the corresponding segment. These values were then summed and divided by the total estuary volume to provide volume-adjusted values for each sampling date in each bay.

Statistical Analyses

Kendall's tau correlations were used to determine relationships between phytoplankton functional groups or total biovolume and environmental factors. This non-parametric method was selected to handle non-normally distributed data with large outliers. Spatial differences in variables of interest within and between bays were analyzed using one-way ANOVA with appropriate post-hoc tests. Shaffer *p*-value adjustment was used for unbalanced data, and a Westfall *p*-value adjustment was used for balanced data. Environmental factors assessed include salinity, temperature, Secchi depth, ammonium, N+N, orthophosphate, silicate, DOC, DON, DIN:DIP, 7-day average discharge, wind speed, 7-day average wind speed, and 7-day total

rainfall. For all statistical analyses, functional groups that were absent at any date/site combination were treated as zero. All analyses were performed in R 3.6.2.

RESULTS

Environmental Conditions and Variability

All three bays experienced a shift from initially dry conditions to wet conditions, characterized by increased inflow and lower salinity. In SA and NC, this shift occurred in September 2018, while BB experienced increased inflow earlier, beginning in July 2018 (Fig. 3). Inflows into BB were episodic in nature and frequently at or near zero.

Early in the study when inflow was lower, all bays experienced relatively high salinities (Fig. 4). During this time, maximum salinity in SA was observed at SA2 (28.1 in June 2018), which is closest to ocean exchange. In contrast, maximum salinity in spring and summer 2018 in NC and BB occurred at upper estuary sites (37.6 in June 2018 at NC1 and 59.5 in June 2018 at BB5). Salinity at SA2 (closest to ocean exchange) was higher than all other sites in this system throughout the study period. Site BB6, which is closest to ocean exchange, had the lowest salinity of all BB sites when inflows were lowest (average salinity 47.0 ± 2.9 March-June 2018). Salinity minimums in all systems were concurrent with higher inflows and occurred at upper estuary sites. Secchi depth in SA was relatively shallow during the dry period (0.3 ± 0.1 m; March 2018-September 2018), but deeper and more variable throughout the rest of the study period (0.4 ± 0.3 m) (Fig. 5). There was also an increase in Secchi depth in NC following the increased inflows. Secchi depths were deepest at all sites in NC between January 2019 and March 2019, indicating a lagged response from the higher inflows that occurred between October 2018 and December 2018. Secchi depth in BB was deeper and more variable on average after

September 2018 (0.6 ± 0.3 m) than before (0.4 ± 0.1 m). Temperature was highest in July 2018 (SA: 30.3 ℃, NC: 29.8 ℃, BB: 30.5 ℃) and lowest in the winter (SA: 9.7 ℃ in January 2019, NC: 12.4 ℃ in December 2018, BB: 10.6 ℃ in March 2019) in all three systems (Fig. 6).

In SA, ammonium was highest in March 2018 (25.8 μM at site SA3) and then decreased to <15 μM throughout the rest of the study (Fig. 7). Ammonium in SA tended to be highest at intermediate salinities (Fig. 8). N+N was lowest in SA from June 2018-September 2018, then increased at all sites from October 2018-February 2019, with the maximum of 118.8 μM occurring at SA1 in January 2019 (Fig. 9). N+N tended to be highest at the freshwater endmember in SA (Fig. 10). DON declined slightly throughout the study, reaching a minimum of 8.7 μM at SA1 in June 2019 (Fig. 11). Variability in DON appeared to increase as salinity decreased, and DON decreased at salinity <5 (Fig. 12). In NC, ammonium and N+N were very low throughout the study (1.1 ± 1.5 μM, 0.6 ± 1.0 μM, respectively) (Figs. 7, 9). NC1, located in Nueces Bay and closest to the river mouth, experienced higher concentrations and greater variability in all nitrogen species than the other sites. However, the range of variability was still relatively small, from 0.1 to 11.2 μM for ammonium and 0.1 to 5.5 μM for N+N. Neither ammonium nor N+N displayed a clear pattern with salinity in NC (Figs. 8, 10). DON in NC was generally highest from May 2018 to October 2018, then decreased from November 2018 to February 2019, and finally increased thereafter (Fig. 11). In BB, ammonium concentrations were generally <1-2 μM, but episodic increases were observed (Fig. 7). For example, a brief increase was observed in June 2018 at all sites. An apparent prolonged increase began in February 2019 at most sites and concentrations remained elevated through summer 2019. Ephemeral increases were also observed at BB1 and BB6. Ammonium generally peaked at intermediate to high salinity levels (Fig. 8). N+N concentrations were consistently low among all sites from March

2018-November 2018 (Fig. 9). An ephemeral spike in N+N (18.1 μM) was observed at BB1 in December 2018. In May 2019, higher N+N concentrations were observed at all sites, but these were still <10 μM. There was no clear spatial pattern in DON in BB (Fig. 11). DON concentrations in BB were slightly lower from late 2018-early 2019 compared to other periods (Fig. 11). DON increased with decreasing salinities from March-September 2018 but appeared to decrease with decreasing salinities throughout the rest of the study period (Fig. 12).

Orthophosphate was highly variable across all sites in SA throughout the study, with the exception of a decline to near zero at all sites in Spring 2019 (Fig. 13). Phosphate was highest at low salinities and decreased as salinity increased (Fig. 14). Silicate concentrations varied considerably (from 26.6 to 301.3 μM), but followed consistent patterns across all sites, with concentrations rising to a maximum during fall 2018 (max: 301.1 μM at SA3) and falling to minimum (min: 26.6 μM at SA2) in spring 2019 (Fig. 15). Silicate concentrations increased towards the freshwater endmember (Fig. 16). In NC, orthophosphate and silicate increased from September-November 2018 concurrent with increased inflows (Figs. 13,15). Both analytes tended to increase towards the freshwater endmember (Figs. 14, 16). In BB, orthophosphate was ≤ 1 μM at all sites until June 2018, when concentrations increased at BB1 and remained elevated throughout the rest of the study (Fig. 13). Orthophosphate concentration at BB5 reached a baywide maximum of 8.2 μM in November 2018, but concentrations were < 1.5 μM for the rest of the study. In general, phosphate appeared to increase with decreasing salinities, especially at BB1 (Fig. 14). Silicate increased from March-October 2018, then declined sharply at all sites until reaching a minimum of 4.5 μM at BB3 in December 2018 (Fig. 15). Silicate increased again through February 2019, after which concentrations dropped and remained relatively low throughout the rest of the study. Silicate tended to increase with decreasing salinities (Fig. 16).

In SA, potential nutrient limitation was variable across sites and time (Fig. 17). P-limitation occurred at SA1 in winter 2018/2019 and spring 2019, and at SA3 in March 2018 and January 2019. A switch from N to P limitation at SA4 in September 2018 resulted from a decline in orthophosphate. NC was strongly N-limited throughout the study (Fig. 17). DIN:DIP was above the Redfield ratio of 16:1 at only two time points at site NC4 (April 2018 and February 2019). All other sites consistently had DIN:DIP ratios below 10:1. Most sites in BB were N-limited until May 2019 when all sites except BB1 became strongly P-limited (Fig. 17). This P-limitation regime persisted through July 2019. Neither SA nor NC experienced silicate limitation during this study (Fig. 18). DIN:silicate ratios in BB were generally low, indicating N limitation. An increase in DIN:silicate ratios was observed in all BB sites in December 2018, although only BB1 was >1, indicative of Si limitation.

System-specific Responses to Freshwater Inflow Variability

Volume-adjusted total biovolume and chlorophyll in SA did not exhibit clear patterns with normalized discharge, although peaks were noted at intermediate salinities (Figs. 19-20). Total biovolume was positively correlated with salinity and negatively correlated with 7-day average discharge (Table 1). Total biovolume was also positively correlated with temperature and wind speed, and negatively correlated with ammonium, N+N, and orthophosphate (Table 1). Volume-adjusted diatom biovolume in SA reach a peak at intermediate inflows (around $2x10^{-7}$) and then declined thereafter (Fig. 21). Volume-adjusted dinoflagellate biovolume increased with increasing normalized discharge until discharge exceeded $2x10^{-7}$, at which point biovolume dropped and remained lower until finally increasing again when discharge exceeded $6x10^{-7}$ (Fig. 22). However, no correlations were found between 7-day lag discharge and any of the functional

groups evaluated (diatoms, dinoflagellates, *Synechoccocus*, and *Mesodinium*) (Table 1). Diatom and dinoflagellate biovolume were positively correlated with salinity (Table 1). Diatom biovolume was negatively correlated with orthophosphate and silicate. Dinoflagellate biovolume was negatively correlated with ammonium, N+N, and orthophosphate and positively correlated with temperature and Secchi depth. *Synechococcus* biovolume was negatively correlated with N+N and positively correlated with temperature and wind speed, and *Mesodinium* was positively correlated with orthophosphate.

Volume-adjusted total biovolume in NC increased with increasing normalized discharge (Fig. 23). Total biovolume was positively correlated with salinity and DON (Table 2). Volume-adjusted total chlorophyll initially increased with increasing normalized discharge then plateaued as normalized discharge approached $5x10^{-9}$ before declining at the highest discharge value (Fig. 24). Volume-adjusted diatom biovolume in NC rapidly increased until normalized discharge approached $5x10^{-9}$, at which point diatom biovolume steadily declined (Fig. 25). Contrary to the trends observed in diatom biovolume, volume-adjusted dinoflagellate biovolume in NC increased as normalized discharge increases, although the rate of increase slowed once normalized discharge exceeded $5x10^{-9}$ (Fig. 26). Diatom biovolume was positively correlated with salinity and 7-day total rainfall and negatively correlated with orthophosphate, DOC, and 7-day lag discharge (Table 2). Dinoflagellate biovolume was positively correlated with DON, DOC, temperature, and wind speed. *Synechococcus* biovolume was positively correlated with ammonium, orthophosphate, silicate, DON, DOC, temperature, and wind speed. *Mesodinium* biovolume was positively correlated with orthophosphate. N+N and 7-day average wind speed, and Secchi depth did not correlate with any of the functional groups examined or total biovolume in NC.

Volume-adjusted total biovolume in BB rapidly increased with increasing normalized discharge and then declined, approaching initial values, once normalized discharge values exceeded $1x10^{-9}$ (Fig. 27). The same trends were observed between volume-adjusted total chlorophyll and normalized discharge (Fig. 28). Total biovolume was positively correlated with 7-day average discharge and negatively correlated with ammonium, silicate, DON, temperature and wind speed (Table 3). Volume-adjusted diatom biovolume rapidly increased with increasing normalized discharge until discharge approached $1x10^{-9}$, at which point diatom biovolume decreased (Fig. 29). Volume-adjusted dinoflagellate biovolume also increased rapidly with increasing normalized discharge until discharge approached $1x10^{-9}$ (Fig. 30). However, dinoflagellate biovolume reached a maximum when normalized discharge was around $2x10^{-9}$ and declined moderately thereafter. Diatom biovolume was negatively correlated with salinity, orthophosphate, silicate, and temperature (Table 3). Dinoflagellate biovolume was positively correlated with N+N, temperature, and wind speed and negatively correlated with 7-day average wind speed. *Synechococcus* biovolume was positively correlated with salinity, silicate, temperature, and wind speed and negatively correlated with ammonium, 7-day lag discharge, and 7-day average wind speed. *Mesodinium* was positively correlated with 7-day lag discharge and negatively correlated with salinity, silicate, temperature, and wind speed.

Interbay Differences in Nutrient Concentrations and Chlorophyll/Phytoplankton Biomass

Ammonium concentrations were significantly higher in SA (4.3 ± 4.9 μM) and BB (3.9 ± 3.8 μM) than NC (1.1 ± 1.5 μM) (Table 4). N+N concentrations were significantly higher in SA (22.2 ± 27.5 μM) than NC (0.6 ± 1.0 μM) or BB (1.5 ± 2.3 μM), and significantly higher in BB than NC (Table 4). DON concentrations in BB (65.7 ± 9.8 μM) were significantly higher than SA

(34.4 ± 9.6 µM) or NC (34.3 ± 8.9 µM). Phosphate concentrations were significantly higher in SA (3.2 ± 2.4 µM) than NC (1.5 ± 2.0 µM) or BB (0.8 ± 1.1 µM), and significantly higher in NC than BB. Silicate concentrations were significantly higher in SA (149.5 ± 60.5 µM) than NC (101.6 ± 95.5 µM) or BB (99.4 ± 55.6 µM), but there was no significant difference between NC or BB. DIN:DIP was significantly higher in BB (40.8 ± 119.2) than NC (2.6 ± 4.3) or SA (12.1 ± 19.5), and significantly higher in SA than NC. DIN:Si was significantly higher in SA (0.19 ± 0.22) than in BB (0.11 ± 0.22), which was significantly higher than NC (0.02 ± 0.02) (Table 4).

Chlorophyll *a* concentrations were significantly higher in SA (16.9 ± 11.7 µg/L) and BB (18.5 ± 3.4 µg/L) than in NC (9.5 ± 3.5 µg/L) (Figs. 31-33, Table 4), but not significantly different between SA and BB. Total phytoplankton biovolume in NC and SA were similar, while total biovolume in BB was significantly higher than both by over one order of magnitude (Table 4).

Interbay Differences in Phytoplankton Community Composition

In SA, total chlorophyll *a* concentration was dominated by nanoplankton (3-20 µm) (73.1 ± 16.3%) (Fig. 31). Picoplankton (<3 µm size class) were not a major contributor to total chlorophyll *a* concentrations at any site in SA throughout the study (9.8 ± 6.5%) (Fig. 31). All sites in NC were dominated by nanoplankton for most of the study (67.8 ± 18.5%), with a higher contribution of microplankton (>20 µm) to total chlorophyll during winter 2018/2019 in all sites (Fig. 32). Contributions of picoplankton to total chlorophyll *a* were greatest at NC1 (12.7 ± 8.2%), which is located in Nueces Bay and closest to the river mouth. Picoplankton were present at lower levels at the other three sites, with the exception of April 2018 at NC1 and NC2, when picoplankton constituted 28% and 54%, respectively, of total chlorophyll. Seasonality in

chlorophyll *a* size fractions was apparent in BB (Fig. 33). Spring and summer were characterized by dominance of nanoplankton (74.2 ± 12.9%), while the contribution of microplankton to total chlorophyll increased in fall and winter (46.5 ± 27.3%) over spring and summer (14.9 ± 11.2%). Picoplankton concentrations were highest in March and April 2018 at BB1 and BB2 (max 10.6 µg/L), which corresponded to the presence of brown tide.

Overall, the percentage of chlorophyll in the microplankton fraction was significantly lower in SA (17.4 ± 16.9%) than NC (23.9 ± 18.3%) and BB (29.2 ± 23.2%), but no significant difference was found between NC and BB (Table 4). The percentage of chlorophyll in the nanoplankton size class was significantly lower in BB (62.3 ± 21.1%) than in SA (73.1 ± 16.3%) and NC (67.8 ± 18.5%), but no significant difference was found between SA and NC (Table 4). The percentage of chlorophyll in the picoplankton was not significantly different between bays (Table 4).

Dinoflagellates often represented a major component of phytoplankton community composition in SA (Fig. 34). This was most pronounced in summer and fall 2018. High diatom biovolume was observed in March 2019, and picocyanobacteria increased at all sites from May 2019-July 2019. Phytoplankton community composition at SA3 did not follow the same trends as the other three sites. At this site, dinoflagellates were minor components of phytoplankton biovolume (11.2 ± 13.2%), and winter months were characterized by dominance of *Mesodinium rubra* (max 94.0% in January 2019). Community composition in NC was dominated by diatoms from March 2018-August 2018 (Fig. 35). A shift from diatom or mixed communities to dinoflagellate-dominated communities began in August 2018. The highest dinoflagellate biovolume in NC1 was observed in September 2018 (1.2×10^6 μm^3/mL), with *Gyrodinium sp.* as the dominant taxa in dinoflagellate community composition. The highest dinoflagellate

biovolume at NC3 ($4.4x10^6$ μm^3/mL) and NC4 ($1.1x10^6$ μm^3/mL) occurred a few months later in November 2018. Dinoflagellate community composition at these sites were also dominated by *Gyrodinium sp.* when biovolume was highest. In December 2018, NC2, NC3, and NC4 shifted from dinoflagellate-dominated to diatom-dominated. This shift occurred later in NC1, in January and February 2019. Summer 2019 (May-July 2019) was characterized by low total biovolume and higher biovolume of picocyanobacteria relative to previous months. In BB, the lowest biovolume occurred at all sites during summer months and early fall (May 2018-October 2018 and May 2019-July 2019), when community composition consisted of brown tide, picocyanobacteria, and relatively low biovolume of diatoms (Fig. 36). High diatom biovolume characterized the phytoplankton community at all sites during December 2018 and at all sites except BB2 during November 2018. Diatom blooms reach a maximum biovolume of $7.8 x10^8$ μm^3/mL at BB4 in December 2018. In January 2019, diatom biovolume decreased at all sites and total biovolume decreased at all sites except BB5 where a *Euglena* bloom occurred. *Euglena* biovolume was $3.4 x10^7$ μm^3/mL, which was 99.9% of total biovolume at this site. Diatom abundance increased at all sites in March 2019 but decreased again by May 2019. Picocyanobacteria displayed relatively low biovolume at all sites in summer-fall 2018 and summer 2019, and they were not an important contributor to total biovolume during the winter months.

Overall, diatoms constituted a significantly lower percentage of biovolume in SA (25.1 ± 29.8%) than in NC (40.3 ± 33.7%) (Table 4). Percentage of biovolume as diatoms in BB (38.3 ± 40.5%) was not significantly different from the other two bays. Dinoflagellates were a significantly smaller percentage of total phytoplankton biovolume in BB (12.4 ± 16.7%) than in SA (22.4 ± 25.2%) and NC (19.7 ± 21.5%). There were no site-specific differences in total

biovolume or diatom or dinoflagellate contribution to biovolume within any of the bays (Tables 5-7).

DISCUSSION

Phytoplankton are sensitive indicators of environmental change because of their ability to rapidly respond to changes in nutrient regimes, light, turbulence, and other environmental factors (Paerl et al. 2007; Lemley et al. 2016). This, as well as their position at the base of the estuarine food web, highlights the importance of understanding phytoplankton responses to large-scale environmental drivers such as freshwater inflow variability. Freshwater inflow influences nutrient regimes and flushing times in estuaries, with higher inflows generally equating to higher external nutrient loads and shorter flushing times. These two factors exert opposing controls on the growth of phytoplankton communities. Higher nutrient inputs stimulate phytoplankton growth, while increased flushing can limit biomass accumulation through displacement (Peierls et al. 2012; Azevedo et al. 2014). Higher inflows may also increase sediment loading, which could result in decreased light availability in the water column, introducing the potential for light limited growth as well (Lancelot and Muylaert 2011). Projected climatic changes on the Texas Gulf Coast indicate drier conditions over the next century, which will lead to reduced freshwater inflows to Texas estuaries (Montagna et al. 2002; Environmental Protection Agency 2016). Increasing freshwater demands from population growth in coastal areas are likely to exacerbate the effects of this freshwater inflow reduction (Montagna et al. 2013). These changes could impose stress on estuarine ecosystems by starving estuarine primary producers of limiting nutrients, and thereby negatively affecting food available to higher trophic levels (e.g., Nixon

2003). This oligotrophication has also been shown to cause a shift in phytoplankton community composition to favoring HAB species in other estuaries (Collos et al. 2009).

Over the course of the study, base inflow rates were highest in SA, followed by NC and BB. There were at least seven inflow events to SA where river discharge exceeded 100 m^3s^{-1}, compared to two in NC and one in BB. These observations are consistent with historical inflow conditions that exist because of a gradient of decreasing precipitation from the northern estuary (SA) to the southern estuary (BB) (Longley 1994; Montagna et al. 2018). As a result of this inflow gradient as well as high evaporation rates to the south, salinities were lowest on average in SA, intermediate in NC, and highest in BB.

Consistently higher concentrations of N+N, orthophosphate, and silicate were found in SA and likely resulted from the greater contribution of riverine nutrient inputs into this system. Higher inflow magnitude in SA throughout the study and higher concentrations of these nutrients at upper estuary sites in SA support this conclusion. Ammonium concentrations were approximately 4-fold higher in SA and BB than NC. Ammonium vs. salinity plots for both SA and BB indicate that the ammonium is likely derived from internal regeneration at intermediate salinities, consistent with previous work in these systems demonstrating the importance of regenerated N (Longley 1994). In addition, previous work has shown that dissimilatory nitrate reduction to ammonium (DNRA) rates can be quite high under higher salinity conditions, such as those found in Baffin Bay at times (An and Gardner 2002; Gardner et al. 2006). This would aid in the retention and availability of ammonium. DON concentrations in BB were approximately 2-fold higher than in SA or NC, where they were roughly equivalent. Previous work has also demonstrated this phenomenon and attributed it to excessive nutrient loading in the watershed (Wetz et al. 2017; Montagna et al. 2018). DON vs. salinity plots for BB show increasing DON at

lower salinities for dates up to and including the first significant rainfall event in summer 2018 (March to September 2018), but show a decreasing DON trend at lower salinities using dates after October 2018. We attribute this to a classic "first flush" effect, where the initial rainfall washed in DON that had accumulated in the watershed, whereas the next significant rainfall led to a dilution effect. Similar to what occurred during the secondary high rainfall period in BB, DON appears to decrease at lower salinities in SA, suggesting that a fraction of the DON in the bay is internally produced and may be diluted at high flows/low salinities. In NC, DON increased briefly during the wet fall of 2018, but the DON rapidly decreased thereafter, likely due to remineralization.

Before discussing differences between estuaries in terms of phytoplankton indicators, it is important to note that chlorophyll and phytoplankton biovolume patterns were occasionally inconsistent with one another, both within and between estuaries. For example, chlorophyll was high and equivalent between SA and BB, and lower in NC on average. Yet despite the high chlorophyll in SA, biovolume was relatively low in SA, especially when compared to BB. Interestingly, although chlorophyll was nearly 2-fold higher in SA than NC, biovolume was nearly equivalent between the two systems. One possibility for the apparent equivalence in biovolume between NC and SA, but higher chlorophyll in SA, is that the taxonomic makeup of the phytoplankton community favored cells with higher chlorophyll content in SA. This would be consistent with previous work showing that chl:C or chl:cell differs between taxa (Lewitus et al. 2005; Yacobi and Zohary 2010; Álvarez et al. 2017). However, here we found no clear relationship between the dominant functional group and chlorophyll to biovolume patterns in SA (data not shown). Another possibility is that the underwater light environment led to the inconsistent patterns of chlorophyll and biovolume. It has long been known that the amount of

chlorophyll per cell increases under light-limited conditions (Lewitus et al. 2005; Reynolds 2006). The shallow Secchi depth in SA compared to the other estuaries offers support to the light-limitation hypothesis. In addition, the ratio of Chl:biovolume was highest in SA and lowest in BB, also supporting the notion that light limitation may have been more pronounced in SA. Finally, the relatively high prevalence of dinoflagellates in SA also supports this, as many dinoflagellate taxa employ mixotrophy that allows them to persist in low light conditions (Jones et al. 1995; Stoecker 1999). Studies in other systems with relatively high freshwater inflow have also shown occasional to persistent light limitation of phytoplankton growth due to inputs of light-absorbing allochthonous organic matter (Gameiro et al. 2011; Andersson et al. 2018). Additional work is clearly needed on the chlorophyll to biovolume disparity observed here, as it confounds our understanding of inflow-phytoplankton relationships, especially given the large differences in chlorophyll observed between these estuaries that were not reflected in biovolume measurements. These findings also indicate that chlorophyll, which is perhaps the most widely used indicator of nutrient and algal biomass enrichment in coastal monitoring programs, should not be relied on as direct evidence of algal biomass per se.

Despite the noted inconsistencies between chlorophyll and biovolume, some key patterns were observed. Both chlorophyll and phytoplankton biovolume were lowest on average in NC, highest in BB, and inconsistent (high chlorophyll, lower biovolume) for SA. Aside from the role of light availability, consideration must be given to the availability of nitrogen (N) for these large-scale differences. N has been argued to be the main phytoplankton growth limiting nutrient in many Texas estuaries (Örnólfsdóttir et al. 2004; Wetz et al. 2017). As noted above, SA had relatively high inorganic N concentrations throughout the study due to consistently higher inflow levels as well as internal regeneration. Likewise, BB had relatively high DON concentrations,

some of which is accessible to mixotrophic phytoplankton (Wetz et al. 2017). New work has also indicated the potential for high rates of photoammonification in BB, which would further increase bioavailability of the DON (H. Abdulla, unpubl. data). In addition, previous work has shown that internal ammonium regeneration rates can be quite high in BB (Gardner et al. 2006), providing a continuous N source for blooms. In contrast, persistent N-limitation is likely in NC, as noted by the very low N:P ratio and the previously discussed low inorganic N levels, even during/after flood events.

Correlation analyses revealed short-term relationships (either at lags of 7 d or instantaneous) between phytoplankton biovolume and environmental factors. In terms of relationships with freshwater inflow, phytoplankton biovolume was negatively correlated with inflow in SA, showed no correlation in NC, and was positively correlated in BB. In SA, where inflows were consistently higher and the magnitude of episodic pulses was higher, biomass accumulation at upper estuary sites may have initially been limited by higher flushing rates. This finding is consistent with another study of SA that found the upper bay to be rapidly flushed with inflow pulses (Roelke et al. 2017). Additionally, previous research has shown that maximum biovolume accumulates further downstream in estuaries when inflows are high (Mallin et al. 1993; Roelke et al. 2017), which is consistent with the site-specific differences seen here (Fig.37). Highest biomass in SA occurred lower in the estuary at a lag from the decline at upper estuary sites, supporting the conclusion that increased flushing rates altered the spatial patterns of biomass accumulation.

In NC, rapid assimilation of freshwater-derived nutrients near the river mouth may explain the lack of correlation between total biovolume and inflows in the system as a whole. The low nutrient concentrations observed here are consistent with those reported in Turner et al.

(2015), who also demonstrated low inorganic N concentrations over the course of a year at several sites in Corpus Christi Bay. Even though the flood conditions that were observed during late 2018 caused a noticeable drop in salinities of NC, there was little to no discernible effect on inorganic N concentrations in either Nueces or Corpus Christi Bay. This suggests that external N loads to the system were quickly removed from the water column. There was a sharp increase in phytoplankton biomass at the upper Corpus Christi Bay site (NC3) in October to December 2018. However, we would have also expected higher phytoplankton biomass further upstream in Nueces Bay if phytoplankton uptake was a factor in the lack of apparent increase in inorganic N concentrations downstream. Instead, phytoplankton biomass decreased at the Nueces Bay sites during the wet/low salinity period, leaving us to speculate that any riverine inorganic N loads to NC are rapidly denitrified. Prior work by Gardner et al. (2006) showed that the relative importance of denitrification (an N removal pathway) compared to DNRA (an N retention pathway) increased at lower salinities in Texas estuaries. Likewise, Bruesewitz et al. (2013) showed that in nearby Copano Bay, denitrification rates increased following storm events and indicated that the estuary was a net sink for N during high inflow conditions.

The positive correlation between inflows and total biovolume in BB was a reflection of the rapid increases in total biovolume that were observed in response to inflow pulses. Interestingly, the volume-normalized discharge rates that stimulated phytoplankton biomass accumulation in BB were much lower than in SA. It is possible that a smaller freshwater inflow pulse may be required for an impact on phytoplankton growth in BB because its watershed streams are more eutrophic than those of the other estuaries (Wetz, unpubl. data from Texas Commission on Environmental Quality). Additionally, higher retention times in BB due to lack of ocean exchange may allow for both biomass accumulation and maintenance of the high

biomass due to internal nutrient cycling. Extended blooms lasting months to years are common in lagoonal estuaries where they are sustained by regenerated forms of nutrients (Glibert et al. 2010).

While the correlation analyses resolved instantaneous or short-term relationships between biovolume and environmental factors, plots of biovolume and inflow normalized to estuary volume offer a glimpse at the larger-scale impact of inflows. SA and BB experienced a biomass peak at intermediate inflows, while biovolume continuously increased with discharge in NC. In other estuaries, biovolume peaks have been observed at intermediate inflows for two apparent reasons. In many cases, riverine-derived nutrients are sufficient, but flushing is not so high as to prevent biomass accumulation at intermediate inflows (Peierls et al. 2012; Azevedo et al. 2014; Paerl et al. 2014). Others have shown that circulation patterns under moderate inflows balance opposing forces of tidal flux into the estuary and freshwater inflow out of the estuary, such that cells are retained in the estuary (Cloern et al. 1983). Minimal tidal ranges (<0.2m) on the Texas coast likely rule out the possibility of tidal forcing as a reason for this observation, and the highest flushing rates observed are still below typical phytoplankton growth rates (Örnólfsdóttir et al. 2004). In SA, light limitation under relatively high inflows may have been responsible for the decline in total biovolume at higher inflow rates. It is less likely that this was the driver of biovolume declines in BB, as Secchi depth generally deepened or was unchanged following ephemeral inflows. Another possible driver of declining biomass under higher inflows in BB is an increase in grazing pressure (Buskey et al. 1997), although this was not explored in this study.

In contrast, the volume-normalized comparison showed continuously increasing total biovolume versus inflows in NC. This relationship appears to be driven by dinoflagellate biovolume, which seemed to increase in a logarithmic manner with volume-normalized

discharge, not only in NC but also in the other two estuaries. The observed dinoflagellate trend is contrary to our general understanding of dinoflagellates as slow growers that would be disadvantaged by short residence times associated with high freshwater inflows (Hart et al. 2015). Previous studies of inflow effects on community composition have found dinoflagellates to be inversely related to inflows (Roelke et al. 2013) and to be favored when vertical mixing is limited (Dorado et al. 2015). Nonetheless, there are some studies that have shown dinoflagellate blooms associated with high inflows. This has been attributed to density-driven stratification that favors dinoflagellates (Cohen 1985; Garcon et al. 1986), resuspension of cysts from sediments (Cohen 1985), or advection of oceanic taxa into the estuary in bottom water flowing upstream (Cloern et al. 1983; Malone et al. 1988). Strong salinity stratification in NC occurred at upper estuary sites (NC1 and NC2) during periods of high inflows, but stratification did not extend to lower estuary sites (NC3 and NC4) where high dinoflagellate biovolume was observed. This suggests that either resuspension of cysts or advection into the estuary were more likely drivers of the dinoflagellate bloom observed in NC. Nutrient stimulation of dinoflagellate growth can also be ruled out given that most of the biomass accumulation occurred in the lower estuary, which did not directly receive riverine nutrient inputs and showed no obvious increase in nutrients with increasing flows.

The percentage of biovolume as diatoms was lowest in SA, which was not expected given the higher magnitude inflows and prevalence of inflow pulses in this system. Estuaries with shorter residence times, on the order of days to weeks, typically favor faster-growing taxa such as diatoms, while longer residence times, on the order of months to years, favor large slow-growing dinoflagellates (Hart et al. 2015). In addition, diatoms can take advantage of a short-term freshwater inflow/nutrient pulse events due to their high nutrient uptake rates (Paerl et al.

2014). Pulsed inflows, as opposed to continuous inflow, have been shown to increase the proportion of diatoms in phytoplankton community composition (Örnólfsdóttir et al. et al. 2004; Miller et al. 2008). With this in mind, we hypothesized that diatoms would be favored in SA, while slower growing taxa would be favored in NC or BB. However, dinoflagellates were more common in SA, and diatom blooms in SA were short-lived. Dinoflagellates are adapted to assimilate ammonium (Ni Longphuirt et al. 2019), and the higher ammonium concentrations in SA early in the time series may have favored these taxa over others. Diatoms, which preferentially utilize nitrate (Ni Longphuirt et al. 2019), dominated only when N+N concentrations were highest. Additionally, community composition in SA included some freshwater taxa, particularly in the fall and winter, that were not observed in the other systems and likely originated in the river. When inflows were highest, total biovolume at SA3, closest to river inflow, was low and community composition was dominated by *Mesodinium*. Winter community dominance by *Mesodinium* has been observed in other estuaries (Sanders 1995; Johnson et al. 2013). However, temperature alone must not have been the only contributing factor in *Mesodinium* abundance in SA, as high abundances of *Mesodinium* were not seen in the other two systems during cooler temperatures. Relatively high inorganic nitrogen concentrations (Sanders 1995) and temperatures around 15°C (Taylor et al. 1971) have both been shown to favor high abundances of *Mesodinium*. These conditions were observed in SA while *Mesodinium* dominated community composition, but they do not explain their outcompetition of diatoms since diatoms often proliferate when riverine nutrients are replete, particularly nitrate, and have wide ranges for optimal temperature (Carstensen et al. 2015). Cloern et al. (1994) found that *Mesodinium* and some dinoflagellates displayed nonseasonal growth patterns related to short-term weather conditions which included warm, sunny days and calm winds. It is possible that

similar drivers are responsible here, however finer resolution meteorological and phytoplankton data is needed to understand potential relationships between these factors. None of the functional groups in SA correlated with inflows despite a negative correlation with total biovolume, indicating that the inflow regime did not consistently favor one group over another.

The largest diatom blooms were observed in BB and consisted mainly of *Rhizosolenia* sp. These blooms occurred in the winter following ephemeral inflows when nutrient-enriched conditions promoted preferential growth of large, solitary diatom cells (Lancelot and Muylaert 2011; van de Poll et al. 2013; Carstensen et al. 2015). Concurrent with higher inflows into BB, silicate increased at all sites and began declining once the diatom bloom formed. It is possible that nutrient loadings from ephemeral inflows stimulated the diatom bloom, then once inflows ceased cells were not advected out of the estuary but continued to proliferate while nutrients were still plentiful due to internal recycling (Lancelot and Muylaert 2011). Additionally, the timing of the bloom in winter indicates that grazing pressures may have been lower, as zooplankton grazing is often differentially affected by lower temperatures compared to diatoms (Murrell et al. 2002; Rose and Caron 2007). The large cell size of *Rhizosolenia* sp. may also make it a poor prey item for the grazers that remained, allowing it to flourish when other species could not (Fahnenstiel et al. 1995; Strom et al. 2007). Large *Rhizosolenia* blooms have been observed before in BB. Buskey et al. (2001) observed a community succession pattern in BB that was characterized by a decline in brown tide (*A. lagunensis*) to low or background levels, a *Rhizosolenia* bloom, then dominance by *Synechococcus* after the *Rhizosolenia* bloom subsided. This succession pattern was observed here as well, at least in terms of organismal abundances. However, *Synechococcus* did not reach the high biomass levels of the *Rhizosolenia* bloom. Persistent brown tide blooms of *A. lagunensis* have proliferated in the past (Buskey et al. 2001;

Wetz et al. 2017), but *A. lagunensis* was observed here in only low biomass and only at upper estuary sites early in the study. The disappearance of brown tide from BB was likely due to a decline in salinity, which allowed other taxa to outcompete (Buskey et al. 1998). Overall, seasonality appears to be an important driver of phytoplankton community composition in BB, as temperature was a highly significant driver for all functional groups examined. The high summer temperatures in particular may favor cyanobacteria and/or dinoflagellates. Strong relationships between *Synechococcus* and temperature have been observed before, both in other ecosystems (Agawin et al. 1998; Phlips et al. 1999; Moisan et al. 2010) and in laboratory studies (Fu et al. 2007). The positive relationship with wind speed is confusing however, as it conflicts with other studies. For example, *Synechococcus* blooms in Florida Bay were associated with a change in wind direction, but not in wind magnitude (Phlips et al. 1999), and in ocean studies *Synechococcus* abundance declined following wind-driven surface mixing events (van den Engh et al. 2017). Dinoflagellate blooms have also been previously associated with higher temperatures (Cloern et al. 2005; Carstensen et al. 2015), although they tend to be associated with lower wind and water column stability as well (Cloern et al. 2005). In this instance, the positive relationship with wind speed may simply be an artifact of higher winds co-occurring with higher temps, as wind speed tends to be highest in summer in this region.

Results from this study have implications for understanding and projecting impacts of long-term reductions in freshwater inflow that have been observed on the central Texas coast. In the case of NC, long-term decreases in inflow have led to increases in salinity and a decrease in chlorophyll (Montagna and Palmer 2012; Kim et al. 2014; Palmer and Montagna 2015; Bugica et al. 2020). Also, relatively low phytoplankton biovolume and chlorophyll was observed here. The consequences are unclear, although studies in other systems have shown that this

oligotrophication can lead to reductions in upper trophic level production (Nixon et al. 2003). As observed in our study, it appears that riverine N inputs to NC are rapidly removed prior to having an impact on the bay itself. It is worth speculating on potential future impacts of lower inflows/higher salinities in NC. One possibility is the oligotrophication noted above. However, an alternate future is also possible. Specifically, previous work showing that the relative importance of denitrification to DNRA decreases with increasing salinity is relevant. This increasing importance of DNRA with increasing salinities would conceivably increase ammonium availability and N retention in the system. This then could lead one to speculate that NC may see less effective denitrification/more effective DNRA in the future under decreasing inflow scenarios, causing it to become more sensitive to external loads. This is important given the rapid urbanization and growing influence of stormwater and wastewater-derived nutrients in the system (Rebich et al. 2011). Further work is clearly needed, given that the negative effects of nutrient retention are already manifesting in the other low inflow estuary, BB. In BB, watershed nutrients brought in during episodic inflow events appear to cause rapid, lasting bloom development and changes in phytoplankton community composition. However, as noted by a long-term increase in chlorophyll and nutrients in the system (Wetz et al. 2017), the system appears to be ineffective at removing these nutrients over longer timescales. Furthermore, dense and/or prolonged blooms of *A. lagunensis* (brown tide) using organic and/or recycled nutrients during lower rainfall conditions cause harm to the ecosystem overall (see e.g., Wetz et al. 2017). Drier conditions in the future may lead to more estuaries experiencing similar conditions to BB, with periods of hypersalinity and extended blooms resulting from internal recycling of riverine nutrients received during episodic inflows. The differing responses of each of these ecosystems

to freshwater inflow highlight the importance of system-specific management plans and consistent monitoring programs in coastal estuaries.

REFERENCES

Agawin, N. S. R., C. M. Duarte, and S. Agustí. 1998. Growth and abundance of *Synechococcus* sp. in a Mediterranean Bay: seasonality and relationship with temperature. Mar. Ecol. Prog. Ser. 170: 45–53. doi:10.3354/meps170045

Álvarez, E., E. Nogueira, and Á. López-Urrutia. 2017. *In vivo* single-cell fluorescence and size scaling of phytoplankton chlorophyll content. Appl. Environ. Microbiol. 83:e03317-16. doi:10.1128/AEM.03317-16

An, S., and W. S. Gardner. 2002. Dissimilatory nitrate reduction to ammonium (DNRA) as a nitrogen link, versus denitrification as a sink in a shallow estuary (Laguna Madre/Baffin Bay, Texas). Mar. Ecol. Prog. Ser. 237: 41–50.

Andersson, A., S. Brugel, J. Paczkowska, O. F. Rowe, D. Figueroa, S. Kratzer, and C. Legrand. 2018. Influence of allochthonous dissolved organic matter on pelagic basal production in a northerly estuary. Estuarine, Coastal Shelf Sci. 204: 225–235. doi:10.1016/j.ecss.2018.02.032

Azevedo, I. C., A. A. Bordalo, and P. Duarte. 2014. Influence of freshwater inflow variability on the Douro estuary primary production: A modelling study. Ecol. Modell. 272: 1–15. doi:10.1016/j.ecolmodel.2013.09.010

Brock, D. A. 2001. Nitrogen budget for low and high freshwater inflows, Nueces Estuary, Texas. Estuaries 24: 509. doi:10.2307/1353253

Bruesewitz, D. A., W. S. Gardner, R. F. Mooney, L. Pollard, and E. J. Buskey. 2013. Estuarine ecosystem function response to flood and drought in a shallow, semiarid estuary: Nitrogen cycling and ecosystem metabolism. Limnol. Oceanogr. 58: 2293–2309. doi:10.4319/10.2013.58.6.2293

Bugica, K., B. Sterba-Boatwright, and M. S. Wetz. 2020. Water quality trends in Texas estuaries. Mar. Pollut. Bull. 152: 110903. doi:10.1016/j.marpolbul.2020.110903

Burkholder, J. M., D. A. Dickey, C. A. Kinder, and others. 2006. Comprehensive trend analysis of nutrients and related variables in a large eutrophic estuary: A decadal study of anthropogenic and climatic influences. Limnol. Oceanogr. 51: 463–487. doi:10.4319/lo.2006.51.1_part_2.0463

Buskey, E. J., P. A. Montagna, A. F. Amos, and T. E. Whitledge. 1997. Disruption of grazer populations as a contributing factor to the initiation of the Texas brown tide algal bloom. Limnol. Oceanogr. 42: 1215–1222. doi:10.4319/lo.1997.42.5_part_2.1215

Buskey, E. J., B. Wysor, and C. Hyatt. 1998. The role of hypersalinity in the persistence of the Texas “brown tide” in the Laguna Madre. J. Plankton Res. 20: 1553–1565. doi:10.1093/plankt/20.8.1553

Buskey, E. J., H. Liu, C. Collumb, and J. G. F. Bersano. 2001. The decline and recovery of a persistent Texas brown tide algal bloom in the Laguna Madre (Texas, USA). Estuaries 24: 337–346.

Carstensen, J., R. Klais, and Cloern, James E. 2015. Phytoplankton blooms in estuarine and coastal waters: Seasonal patterns and key species. Estuarine, Coastal Shelf Sci. 162: 98–109. doi: 10.1016/j.ecss.2015.05.005

Cira, E. K., and M. S. Wetz. 2019. Spatial-temporal distribution of *Aureoumbra lagunensis* ("brown tide") in Baffin Bay, Texas. Harmful Algae 89: 101669. doi:10..1016/j.hal.2019.101669

Cloern, J. E., A. E. Alpine, B. E. Cole, R. L. J. Wong, J. F. Arthur, and M. D. Ball. 1983. River discharge controls phytoplankton dynamics in the Northern San Francisco Bay Estuary. Estuarine, Coastal Shelf Sci. 16: 415–429.

Cloern, J. E., B. E. Cole, and S. W. Hager. 1994. Notes on a *Mesodinium rubrum* red tide in San Francisco Bay (California, USA). J. Plankton Res. 16: 1269–1276. doi:10.1093/plankt/16.9.1269

Cloern, J. E., and R. Dufford. 2005. Phytoplankton community ecology: Principles applied in San Francisco Bay. Mar. Ecol. Prog. Ser. 285: 11–25.

Cloern, J. E., T. S. Schraga, C. B. Lopez, N. Knowles, R. Grover Labiosa, and R. Dugdale. 2005. Climate anomalies generate an exceptional dinoflagellate bloom in San Francisco Bay. Geophys. Res. Lett. 32. doi:10.1029/2005GL023321

Cloern, J. E. 2017. Why large cells dominate estuarine phytoplankton. Limnol. Oceanogr. doi:10.1002/lno.10749

Cohen, R. R. H. 1985. Physical processes and the ecology of a winter dinoflagellate bloom of *Katodinium rotundatum*. Mar. Ecol. Prog. Ser. 26: 135–144.

Collos, Y., B. Bec, C. Jauzein, E. Abadie, T. Laugier, J. Lautier, A. Pastoureaud, P. Souchu, and A. Vaquer. 2009. Oligotrophication and emergence of picocyanobacteria and a toxic dinoflagellate in Thau lagoon, southern France. J. Sea Res. 61: 68–75. doi:10.1016/j.seares.2008.05.008

Dorado, S., T. Booe, J. Steichen, A. S. McInnes, R. Windham, A. Shepard, A. E. B. Lucchese, H. Preischel, J. L. Pinckney, and others. 2015. Towards an understanding of the interactions between freshwater inflows and phytoplankton communities in a subtropical estuary in the Gulf of Mexico. PLoS One 10: e0130931. doi:10/1372/journal.pone.0130931

van den Engh, G. J., J. K. Doggett, A. W. Thompson, M. A. Doblin, C. N. G. Gimpel, and D. M. Karl. 2017. Dynamics of *Prochlorococcus* and *Synechococcus* at Station ALOHA revealed through flow cytometry and high-resolution vertical sampling. Front. Mar. Sci. 4. doi:10.3389/fmars.2017.00359

Environmental Protection Agency. 2016. What climate change means for Texas.

Fahnenstiel, G. L., M. J. McCormick, G. A. Lang, D. G. Redalje, S. E. Lohrenz, M. Markowitz, B. Wagoner, and H. J. Carrick. 1995. Taxon-specific growth and loss rates for dominant phytoplankton populations from the northern Gulf of Mexico. Mar. Ecol. Prog. Ser. 117: 229–239.

Fu, F.-X., M. E. Warner, Y. Zhang, Y. Feng, and D. A. Hutchins. 2007. Effects of increased temperature and CO_2 on photosynthesis, growth, and elemental ratios in marine *Synechococcus* and *Prochlorococcus* (cyanobacteria). J. Phycol. 43: 485–496. doi:10.1111/j.1529-8817.2007.00355.x

Gameiro, C., J. Zwolinski, and V. Brotas. 2011. Light control on phytoplankton production in a shallow and turbid estuarine system. Hydrobiologia 669: 249. doi:10.1007/s10750-011-0695-3

Garcon, V. C., K. D. Stolzenbach, and D. M. Anderson. 1986. Tidal flushing of an estuarine embayment subject to recurrent dinoflagellate blooms. Estuaries 9: 179–187. doi:10.2307/1352129

Gardner, W. S., M. J. McCarthy, S. An, D. Sobolev, K. S. Sell, and D. Brock. 2006. Nitrogen fixation and dissimilatory nitrate reduction to ammonium (DNRA) support nitrogen dynamics in Texas estuaries. Limnol. Oceanogr. 51: 558–668.

Glibert, P. M., C. E. Wazniak, M. R. Hall, and B. Sturgis. 2007. Seasonal and interannual trends in nitrogen and brown tide in Maryland's coastal bays. Ecological Applications 17: S79–S87. doi:10.1890/05-1614.1

Glibert, P. M., J. N. Boyer, C. A. Heil, C. J. Madden, B. Sturgis, and C. S. Wazniak. 2010. Blooms in lagoons: Different from those of river-dominated estuaries, In M.J. Kennish and H.W. Paerl [eds.], Coastal lagoons: Critical habitats of environmental change. CRC Press.

Hall, N. S., H. W. Paerl, B. L. Peierls, A. C. Whipple, and K. L. Rossignol. 2013. Effects of climatic variability on phytoplankton community structure and bloom development in the eutrophic, microtidal, New River Estuary, North Carolina, USA. Estuarine, Coastal Shelf Sci. 117: 70–82. doi:10.1016/j.eccs.2012.10.004

Hart, J. A., E. J. Phlips, S. Badylak, N. Dix, K. Petrinec, A. L. Mathews, W. Green, and A. Srifa. 2015. Phytoplankton biomass and composition in a well-flushed sub-tropical estuary: The contrasting effects of hydrology, nutrient loads and allochthonous influences. Mar. Environ. Res. 112: 9–20. doi:10.1016/j.marenres.2015.08.010

Hillebrand, H., C.-D. Durselen, D. Kirschtel, U. Pollingher, and T. Zohary. 1999. Biovolume calculation for pelagic and benthic macroalgae. J. Phycol. 35: 403–424.

IPCC. 2014. Climate Change 2014: Synthesis Report. Contribution of Working Groups I, II, and III to the Fifth Assessment Report of the Intergovernmental Panel on Climate Change. IPCC.

Johnson, M. D., D. K. Stoecker, and H. D. Marshall. 2013. Seasonal dynamics of *Mesodinium rubrum* in Chesapeake Bay. J. Plankton Res. 35: 877–893.

Jones, H. L. J., P. Durjun, B. S. C. Leadbeater, and J. C. Green. 1995. The relationship between photoacclimation and phagotrophy with respect to chlorophyll *a*, carbon and nitrogen content, and cell size of *Chrysochromulina brevifilum* (Prymnesiophyceae). Phycologia 34: 128–134. doi:10.2216/i0031-8884-34-2-128.1

Kennish, M. J., and H. W. Paerl, eds. 2010. Coastal lagoons: Critical habitats of environmental change, CRC Press.

Kim, H.-C., S. Son, P. Montagna, B. Spiering, and J. Nam. 2014. Linkage between freshwater inflow and primary productivity in Texas estuaries: Downscaling effects of climate variability. J. Coastal Res. SI: 65–73.

Koski, M., T. Wichard, and S. H. Jónasdóttir. 2008. “Good” and “bad” diatoms: development, growth and juvenile mortality of the copepod *Temora longicornis* on diatom diets. Mar. Biol. 154: 719–734. doi:10.1007/s00227-008-0965-4

Lampert, W. 1987. Laboratory studies on zooplankton-cyanobacteria interactions. N. Z. J. Mar. Freshwater Res. 21: 483–490. doi:10.1080/00288330.1987.9516244

Lancelot, C., and K. Muylaert. 2011. Trends in estuarine phytoplankton ecology. *In* E. Wolanski and D. McLusky [eds.], Treatise on Estuarine and Coastal Science. Elsevier. doi: 10.1016/B978-0-12-374711-2.00703-8

Landsberg, J. H., L. J. Flewelling, and J. Naar. 2009. *Karenia brevis* red tides, brevetoxins in the food web, and impacts on natural resources: Decadal advancements. Harmful Algae 8: 598–607. doi:10.1016/j.hal.2008.11.010

Largier, J. L. 2010. Low-inflow estuaries: hypersaline, inverse and thermal scenarios. In: Contemporary Issues in Estuarine Physics, A. Valle-Levinson (editor), Cambridge University Press, Cambridge.

Lemley, D. A., J. B. Adams, and G. C. Bate. 2016. A review of microalgae as indicators in South African estuaries. S. Afr. J. Bot. 107: 12–20. doi:10.1016/j.sajb.2016.04.008

Lewitus, A. J., D. L. White, R. G. Tymowski, M. E. Geesey, S. N. Hymel, and P. A. Noble. 2005. Adapting the CHEMTAX method for assessing phytoplankton taxonomic composition in Southeastern U.S. estuaries. Estuaries 28: 160–172. doi:10.1007/BF02732761

Longley, W. L. 1994. Freshwater Inflows to Texas Bays and Estuaries: Ecological Relationships and Methods for Determination of Needs. Texas Water Development Board and Texas Parks and Wildlife Department.

Mallin, M. A., H. W. Paerl, J. Rudek, and P. W. Bates. 1993. Regulation of estuarine primary production by watershed rainfall and river flow. Mar. Ecol. Prog. Ser. 93: 199–203.

Malone, T., L. Crocker, S. Pike, and B. Wendler. 1988. Influences of river flow on the dynamics of phytoplankton production in a partially stratified estuary. Mar. Ecol. Prog. Ser. 48: 235–249. doi:10.3354/meps048235

Martin-Creuzburg, D., and E. von Elert. 2009. Good food versus bad food: the role of sterols and polyunsaturated fatty acids in determining growth and reproduction of *Daphnia magna*. Aquat. Ecol. 43: 943–950. doi:10.1007/s10452-009-9239-6

Miller, C. J., D. L. Roelke, S. E. Davis, H.-P. Li, and G. Gable. 2008. The role of inflow magnitude and frequency on plankton communities from the Guadalupe Estuary, Texas,

USA: Findings from microcosm experiments. Estuarine, Coastal Shelf Sci. 80: 67–73. doi:10.1016/j.eccs.2008.07.006

Moisan, T. A., K. L. Blattner, and C. P. Makinen. 2010. Influences of temperature and nutrients on *Synechococcus* abundance and biomass in the southern Mid-Atlantic Bight. Cont. Shelf Res. 30: 1275–1282. doi:10.1016/j.csr.2010.04.005

Montagna, P. A., M. Alber, P. Doering, and M. S. Connor. 2002. Freshwater inflow: Science, policy, management. Estuaries 25: 1243–1245.

Montagna, P., B. Vaughan, and G. Ward. 2011. The Importance of Freshwater Inflows to Texas Estuaries, p. 107–127. *In* R.C. Griffin [ed.], Water Policy in Texas: Responding to the Rise of Scarcity. The RFF Press.

Montagna, P. A., and T. A. Palmer. 2012. Water and sediment quality status and trends in the Coastal Bend - phase 2: Data analysis. Coastal Bend Bays & Estuaries Program for project 1206 78. 78 Harte Research Institute for Gulf of Mexico Studies, Texas A&M University - Corpus Christi.

Montagna, P. A., T. A. Palmer, and J. Beseres Pollack. 2013. Hydrological changes and estuarine dynamics, Springer New York.

Montagna, P. A., X. Hu, T. A. Palmer, and M. Wetz. 2018. Effect of hydrological variability on the biogeochemistry of estuaries across a regional climatic gradient. Limnol. Oceanogr. 63: 2465–2478. doi:10.1002/lno.10953

Murrell, M. C., R. S. Stanley, E. M. Lores, G. T. DiDonato, and D. A. Flemer. 2002. Linkage between microzooplankton grazing and phytoplankton growth in a Gulf of Mexico estuary. Estuaries 25: 19–29. doi:10.1007/BF02696046

Ni Longphuirt, S., G. McDermott, S. O'Boyle, R. Wilkes, and D. B. Stengel. 2019. Decoupling abundance and biomass of phytoplankton communities under different environmental controls: A new multi-metric index. Front. Mar. Sci. 6:312. doi:10.3389/fmars.2019.00312

Nixon, S. W. 2003. Replacing the Nile: Are anthropogenic nutrients providing the fertility once brought to the Mediterranean by a Great River? Ambio 32: 30–39.

Örnólfsdóttir, E., S. E. Lumsden, and J. Pinckney. 2004. Nutrient pulsing as a regulator of phytoplankton abundance and community composition in Galveston Bay, Texas. J. Exp. Mar. Biol. Ecol. 303: 197–220. doi:10.1016/j.jembe.2003.11.016

Paerl, H. W. 2006. Assessing and managing nutrient-enhanced eutrophication in estuarine and coastal waters: Interactive effects of human and climatic perturbations. Ecological Engineering 26: 40–54. doi:10.1016/j.ecoleng.2005.09.006

Paerl, H. W., L. M. Valdes-Weaver, A. R. Joyner, and V. Winkelmann. 2007. Phytoplankton indicators of ecological change in the eutrophying Pamlico Sound System, North Carolina. Ecological Applications 17: S88–S101. doi:10.1890/05-0840.1

Paerl, H. W., and D. Justić. 2013. Estuarine Phytoplankton, p. 85–110. *In* J.W. Day Jr., B.C. Crump, W.M. Kemp, and A. Yáñez-Arancibia [eds.], Estuarine Ecology. John Wiley & Sons, Inc.

Paerl, H. W., N. S. Hall, B. L. Peierls, K. L. Rossignol, and A. R. Joyner. 2014. Hydrologic variability and its control of phytoplankton community structure and function in two shallow, coastal, lagoonal ecosystems: the Neuse and New River Estuaries, North Carolina, USA. Estuaries Coasts 37: S31–S45. doi:10.1007/s12237-013-9686-0

Palmer, T. A., and P. A. Montagna. 2015. Impacts of droughts and low flows on estuarine water quality and benthic fauna. Hydrobiologia 753: 111–129. doi:10.1007/s10750-015-2200-x

Peierls, B. L., N. S. Hall, and H. W. Paerl. 2012. Non-monotonic responses of phytoplankton biomass accumulation to hydrologic variability: A comparison of two coastal plain North Carolina estuaries. Estuaries Coasts 35: 1376–1392. doi:10.1007/s12237-012-9547-2

Phlips, E. J., S. Badylak, and T. C. Lynch. 1999. Blooms of the picoplanktonic cyanobacterium *Synechococcus* in Florida Bay, a subtropical inner-shelf lagoon. Limnol. Oceanogr. 44: 1166–1175. doi:10.4319/lo.1999.44.4.1166

van de Poll, W. H., G. Kulk, K. R. Timmermans, and others. 2013. Phytoplankton chlorophyll *a* biomass, composition, and productivity along a temperature and stratification gradient in the northeast Atlantic Ocean. Biogeosciences 10: 4227–4240. doi:10.5194/bg-10-4227-2013

Rebich, R. A., N. A. Houston, S. V. Mize, D. K. Pearson, P. B. Ging, and C. E. Hornig. 2011. Sources and delivery of nutrients to the Northwestern Gulf of Mexico from streams in the South-Central United States. J. Am. Water Resour. Assoc. 47: 1061–1086. doi:10.1111/j.1752-1688.2011.00583.x

Reynolds, C. S. 2006. The ecology of phytoplankton, Cambridge University Press.

Roelke, D. L., H.-P. Li, N. J. Hayden, C. J. Miller, S. E. Davis, A. Quigg, and Y. Buyukates. 2013. Co-occuring and opposing freshwater inflow effects on phytoplankton biomass, productivity and community composition of Galveston Bay, USA. Mar. Ecol. Prog. Ser. 477: 61–76. doi:10.3354/meps10182

Roelke, D. L., H.-P. Li, C. J. Miller-DeBoer, G. M. Gable, and S. E. Davis. 2017. Regional shifts in phytoplankton succession and primary productivity in the San Antonio Bay System

(USA) in response to diminished freshwater inflows. Mar. Freshwater Res. 68: 131–145. doi:10.1071/MF15223

Rose, J. M., and D. A. Caron. 2007. Does low temperature constrain the growth rates of heterotrophic protists? Evidence and implications for algal blooms in cold waters. Limnol. Oceanogr. 52: 886–895.

Sanders, R. W. 1995. Seasonal distributions of the photosynthesizing ciliates *Laboea strobila* and *Myrionecta rubra* (= *Mesodinium rubrum*) in an estuary of the Gulf of Maine. Aquat. Microb. Ecol. 9: 237–242. doi:10.3354/ame009237

Schmidt, K., and S. Jónasdóttir. 1997. Nutritional quality of two cyanobacteria: How rich is "poor" food? Mar. Ecol. Prog. Ser. 151: 1–10. doi:10.3354/meps151001

Sivakumar, N., M. Sundararaman, and G. Selvakumar. 2011. Efficacy of micro algae and cyanobacteria as a live feed for juveniles of shrimp *Penaeus monodon*. Afr. J. Biotechnol. 10: 11594–11599. doi:10.5897/AJB11.710

Stoecker, D. K. 1999. Mixotrophy among dinoflagellates. J. Eukaryotic Microbiol. 46: 397–401. doi:10.1111/j.1550-7408.1999.tb04619.x

Strom, S. L., E. L. Macri, and M. B. Olson. 2007. Microzooplankton grazing in the coastal Gulf of Alaska: Variations in top-down control of phytoplankton. Limnol. Oceanogr. 52: 1480–1494. doi:10.4319/lo.2007.52.4.1480

Sun, J., and D. Liu. 2003. Geometric models for calculating cell biovolume and surface area for phytoplankton. J. Plankton Res. 25: 1331–1346. doi:10.1093/plankt/fbg096

Taylor, F. J. R., D. J. Blackbourn, and J. Blackbourn. 1971. Red-water ciliate *Mesodinium rubrum* and its "incomplete symbionts": A review influencing new ultrastructural observations. J. Fish. Res. Board Can. 28: 391–407. doi:10.1139/f71-052

Texas Water Development Board. 2019. Bays & Estuaries.

Turner, E. L., B. Paudel, and P. A. Montagna. 2015. Baseline nutrient dynamics in shallow well mixed coastal lagoon with seasonal harmful algal blooms and hypoxia formation. Mar. Pollut. Bull. 96: 456–462. doi:10.1016/j.marpolbul.2015.05.005

Tweedley, J. R., S. R. Dittmann, A. K. Whitfield, K. Withers, S. D. Hoeksema, and I. C. Potter. 2019. Hypersalinity: Global distribution, causes, and present and future effects on the biota of estuaries and lagoons, *In* E. Wolanski, J.W. Day, M. Elliott, and R. Ramachandran [eds.], Coasts and estuaries. Elsevier.

Underwood, G., and J. Kromkamp. 1999. Primary production by phytoplankton and microphytobenthos in estuaries. Adv. Ecol. Res. 29: 93–153. doi:10.1016/S0065-2504(08)60192-0

United States Census Bureau. 2018. Coastline County Population Continues to Grow. The United States Census Bureau.

USEPA. 1999. Ecological condition of estuaries in the Gulf of Mexico. EPA 620-R-98-004. EPA 620-R-98-004 U.S. Environmental Protection Agency, Office of Research and Development, National Health and Environmental Effects Research Laboratory.

Wetz, M. S., E. A. Hutchinson, R. S. Lunetta, H. W. Paerl, and J. C. Taylor. 2011. Severe droughts reduce estuarine primary productivity with cascading effects on higher trophic levels. Limnology and Oceanography 56: 627–638. doi:10.4319/lo.2011.56.2.0627

Wetz, M. S., E. K. Cira, B. Sterba-Boatwright, P. A. Montagna, T. A. Palmer, and K. C. Hayes. 2017. Exceptionally high organic nitrogen concentrations in a semi-arid South Texas estuary susceptible to brown tide blooms. Estuarine, Coastal Shelf Sci. 188: 27–37. doi: 10.1016/j.ecss.2017.02.001

Yacobi, Y. Z., and T. Zohary. 2010. Carbon:chlorophyll *a* ratio, assimilation numbers and turnover times of Lake Kinneret phytoplankton. Hydrobiologia 639: 185–196. doi:10.1007/s10750-009-0023-3

FIGURES

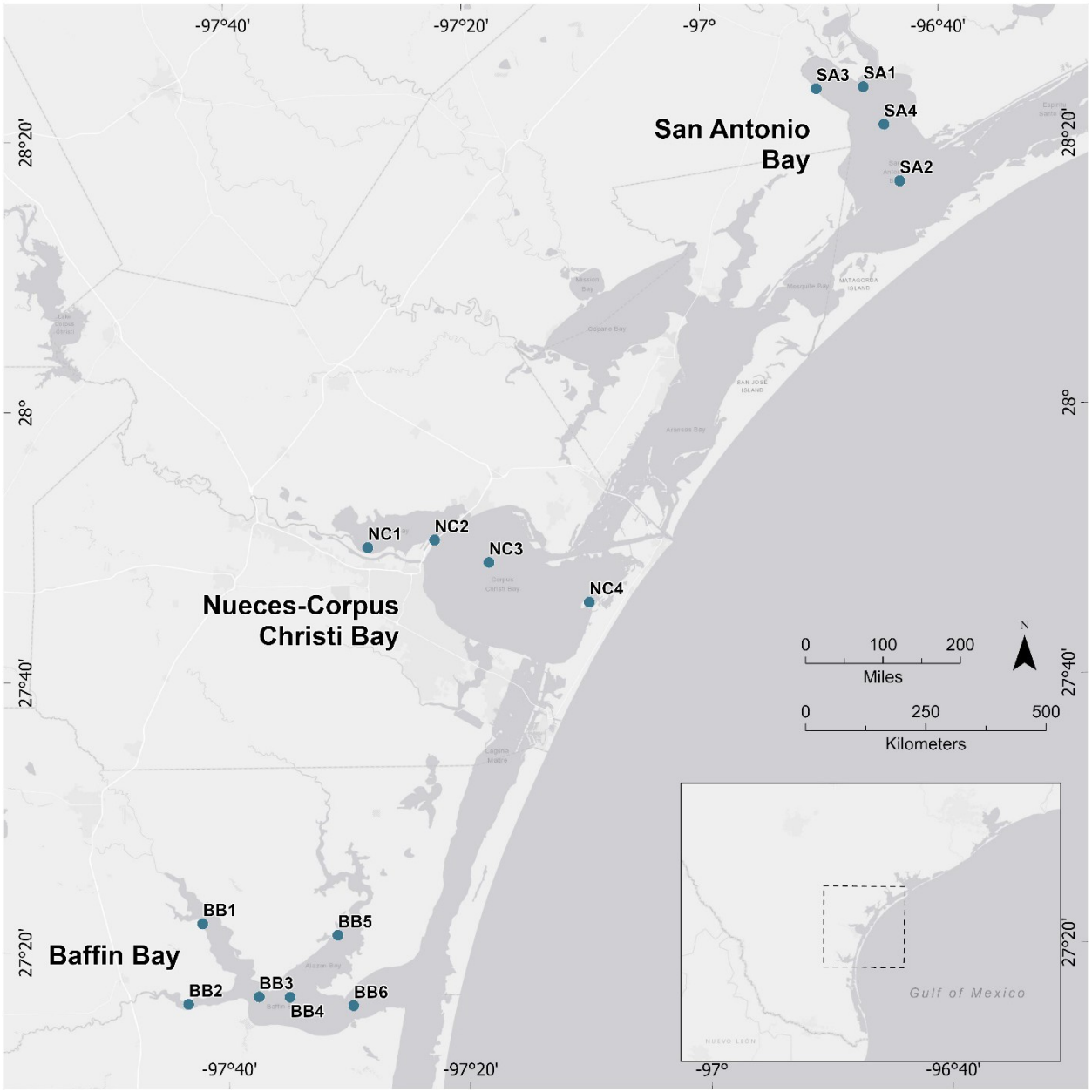

Figure 1. Map of sample sites in each estuary.

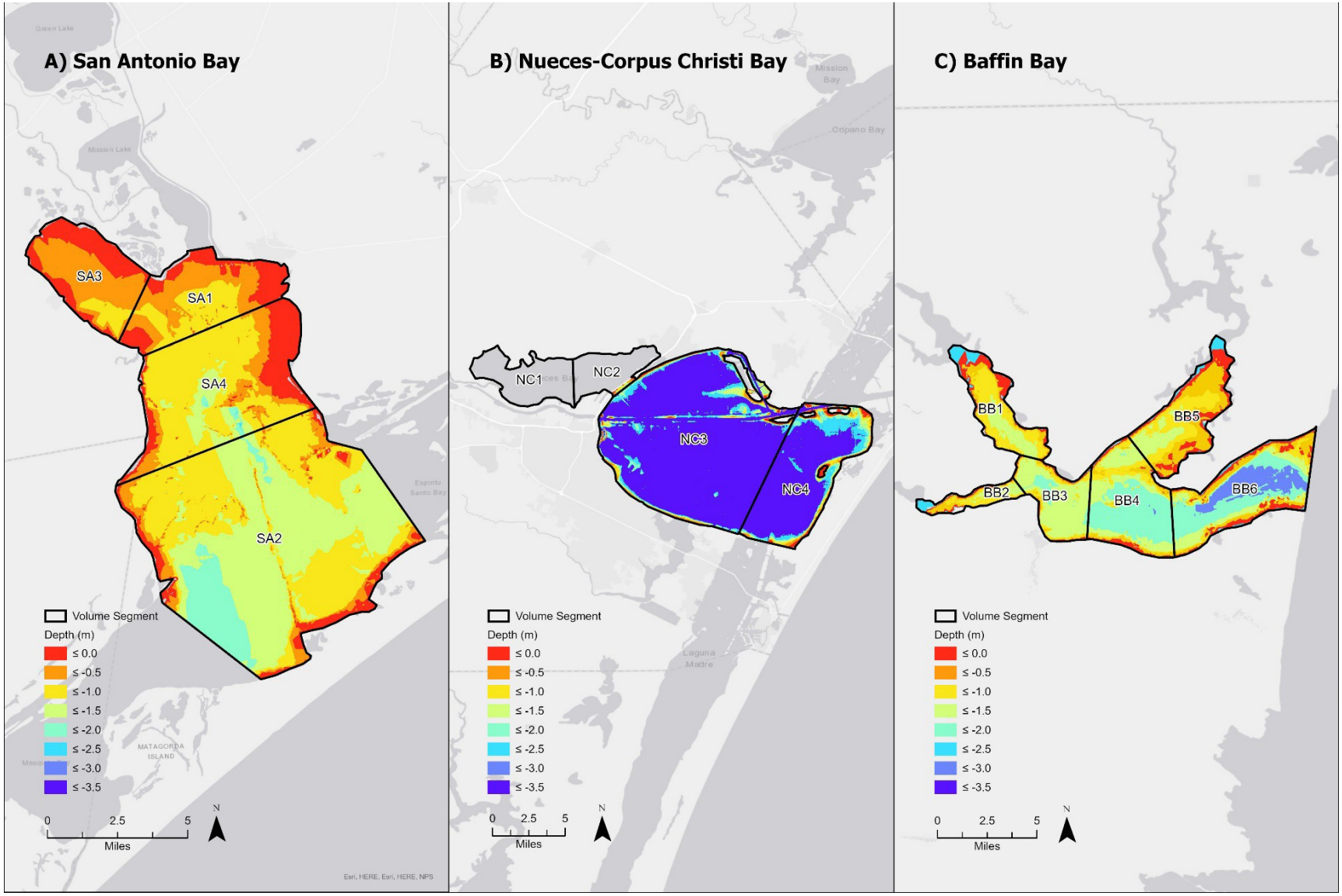

Figure 2. Maps of bathymetry and segments used to calculate volume and normalized variables. Bathymetric data were not available for Nueces Bay (NC1 and NC2), so published average depth was used for to calculate volume for those segments.

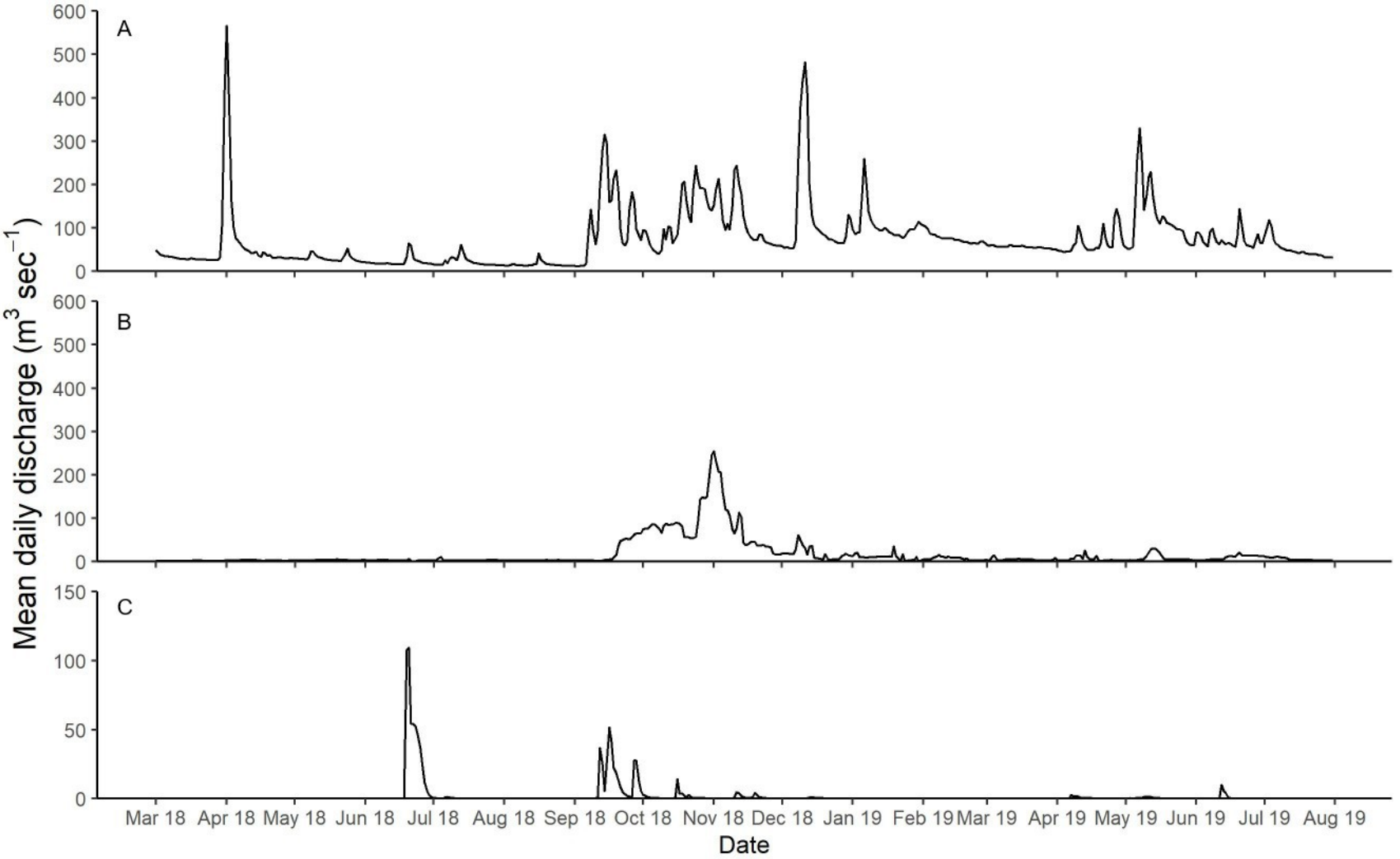

Figure 3. Mean daily river discharge for A) Guadalupe and San Antonio Rivers into San Antonio Bay, B) Nueces River into Nueces-Corpus Christi Bay, and C) Petronila, Los Olmos, and San Fernando Creeks into Baffin Bay.

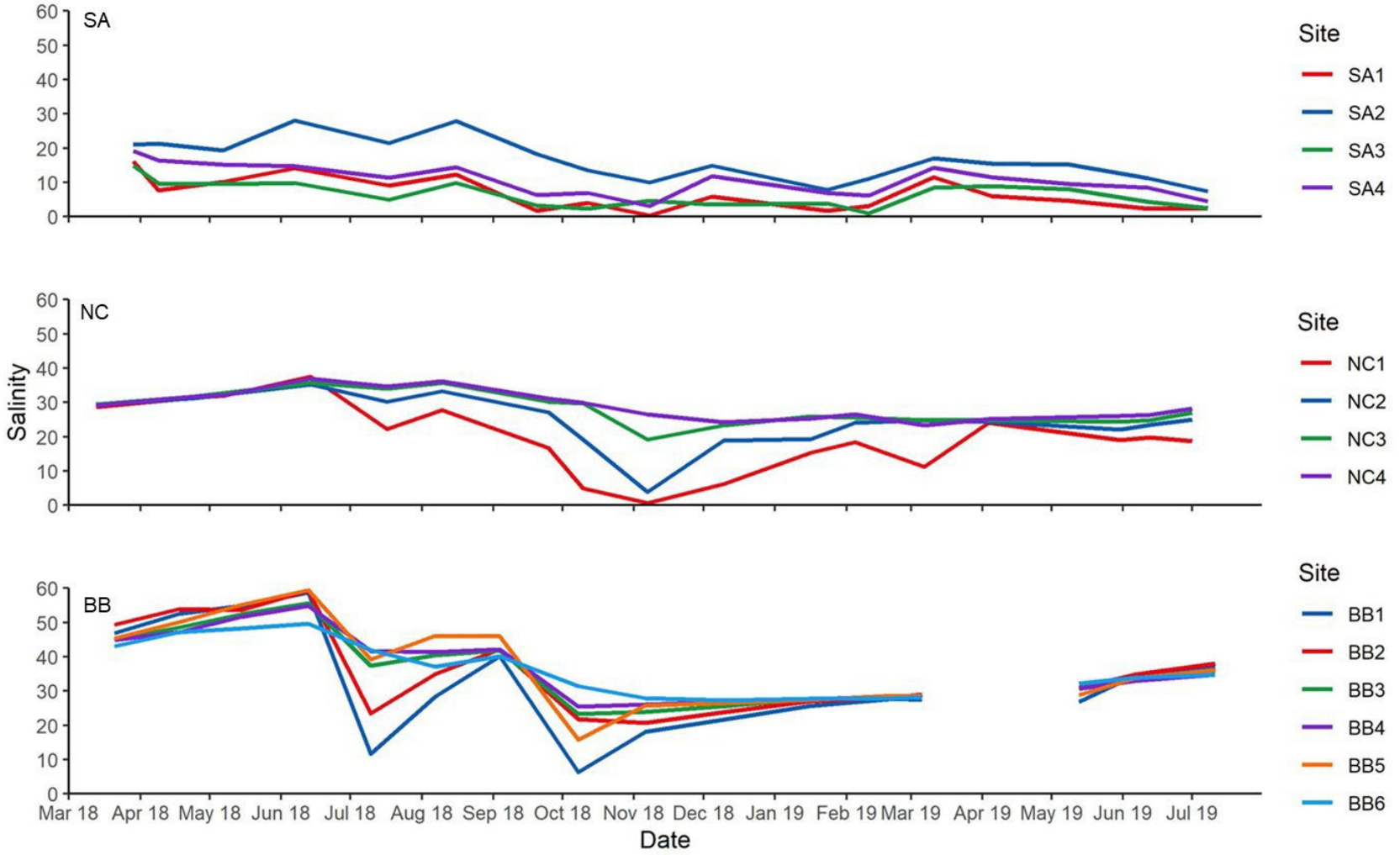

Figure 4. Salinity at each site from March 2018-July 2019.

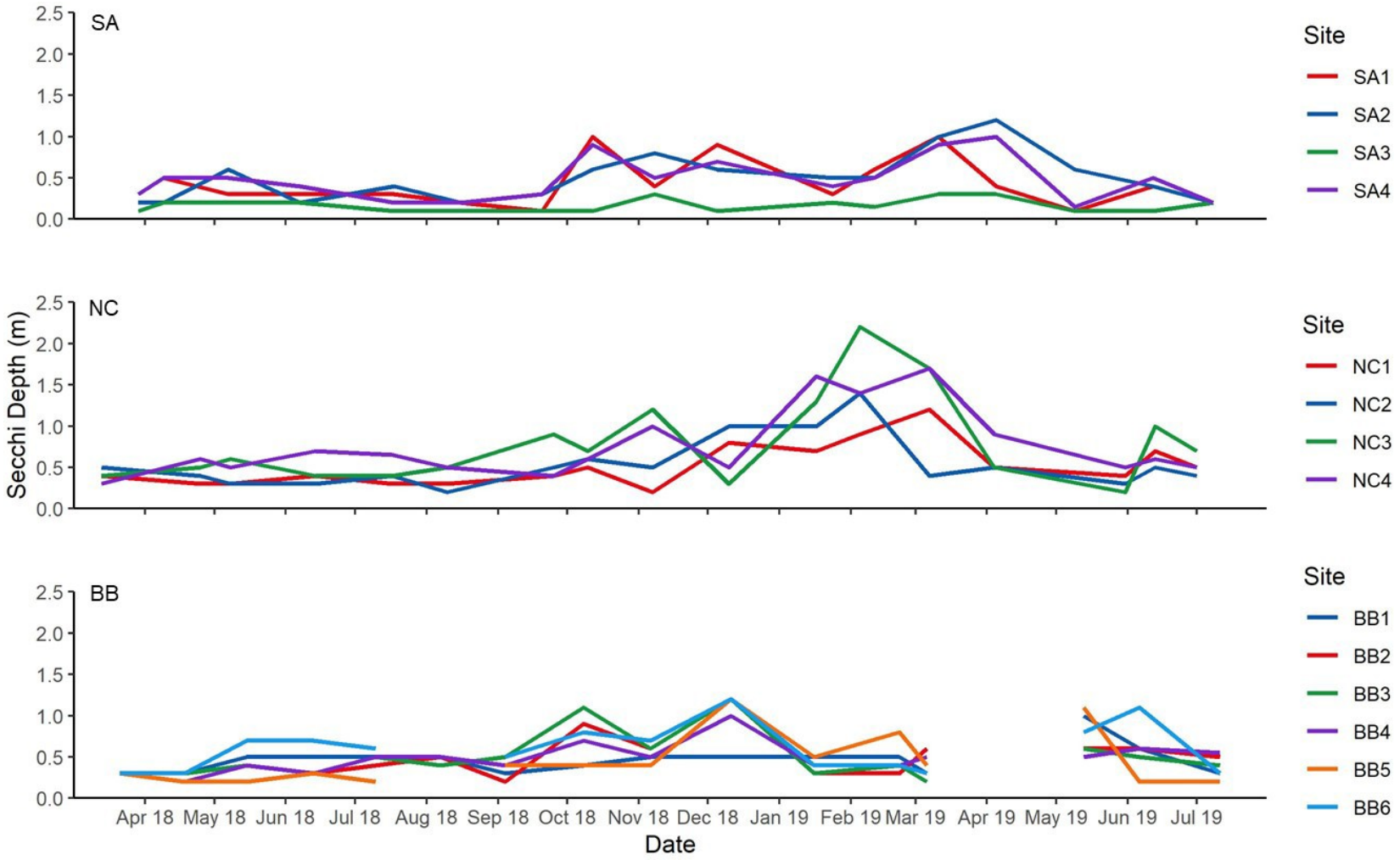

Figure 5. Secchi depth at each site from March 2018-July 2019.

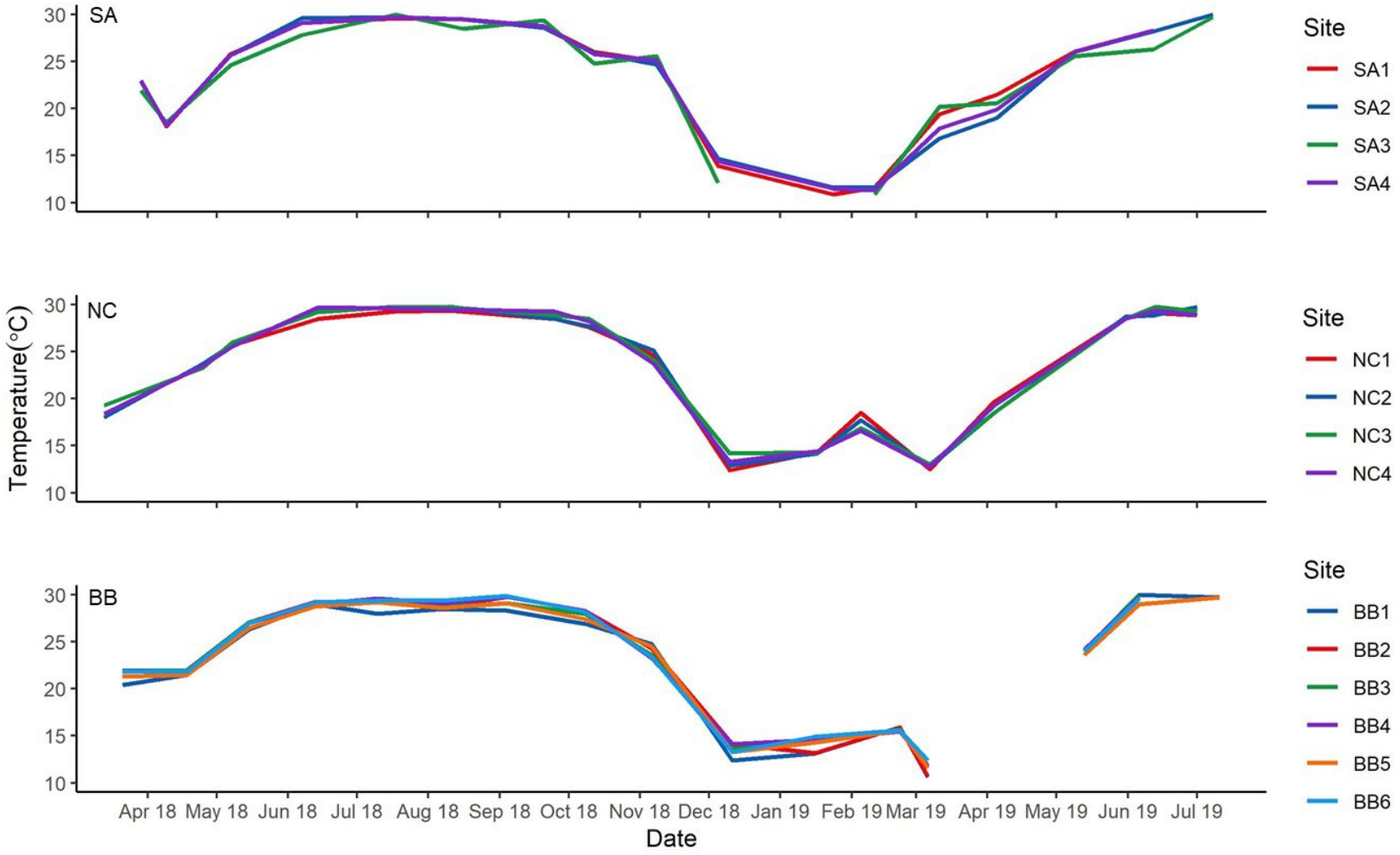

Figure 6. Temperature at each site from March 2018-July 2019.

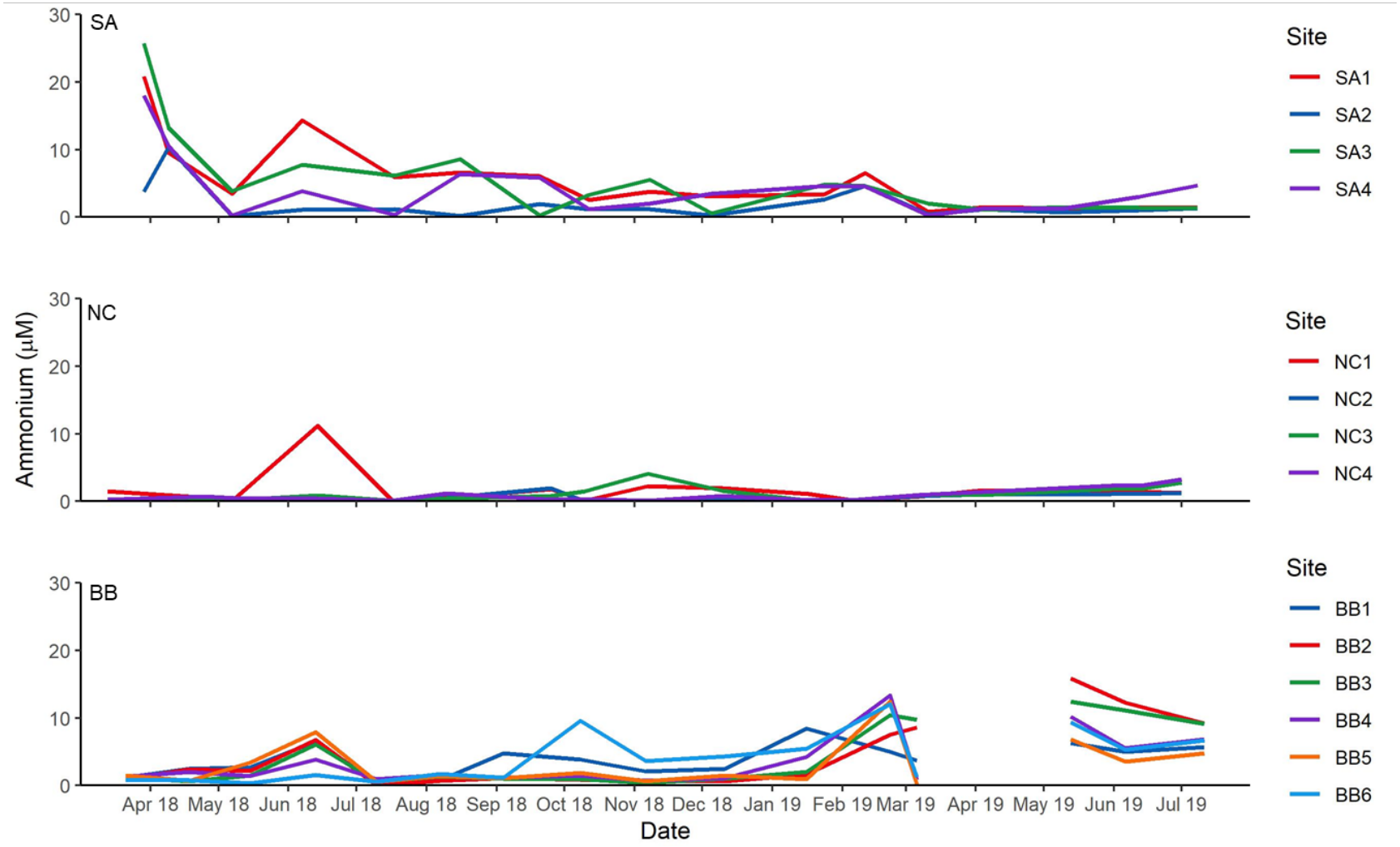

Figure 7. Ammonium concentrations at each site from March 2018-July 2019.

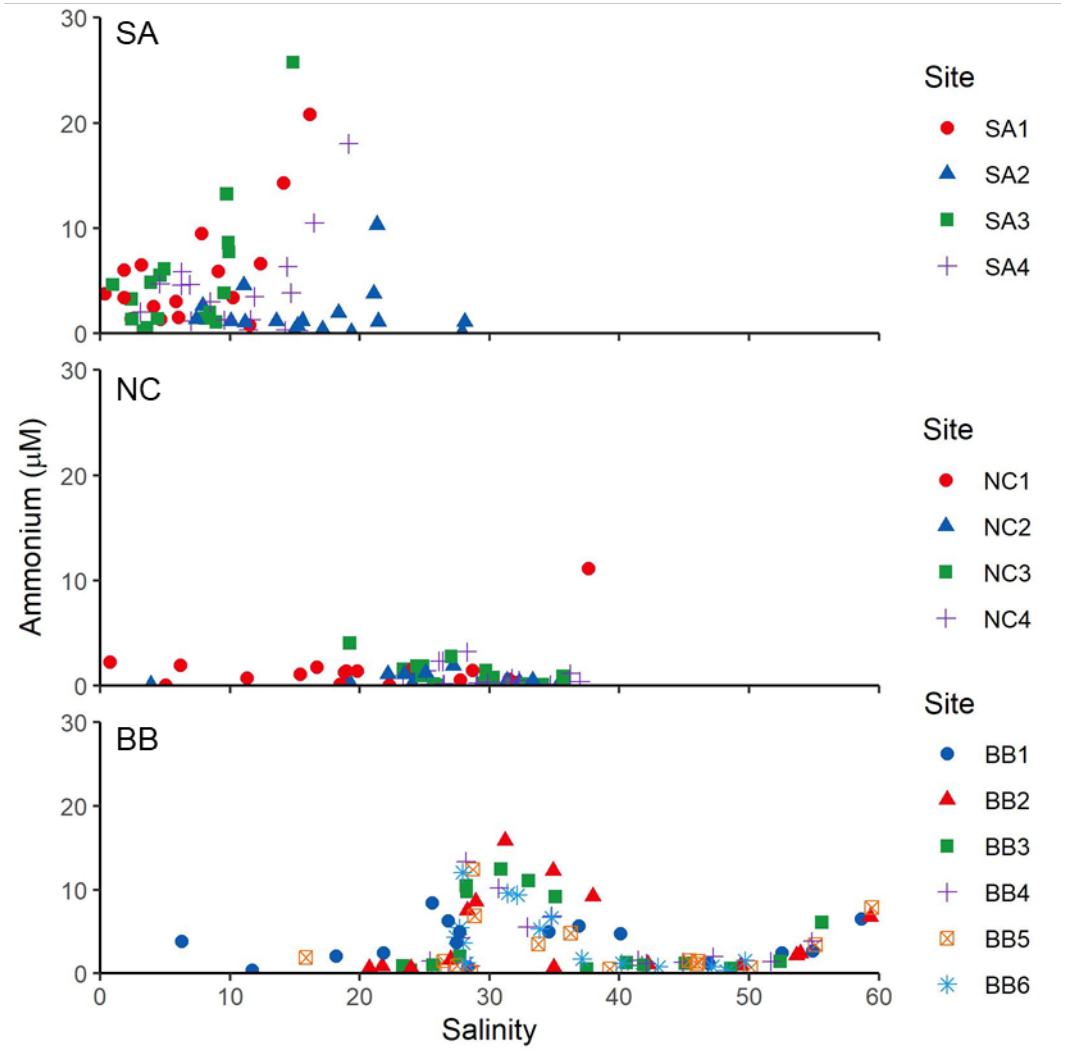

Figure 8. Ammonium concentrations over salinity for each site and sample date.

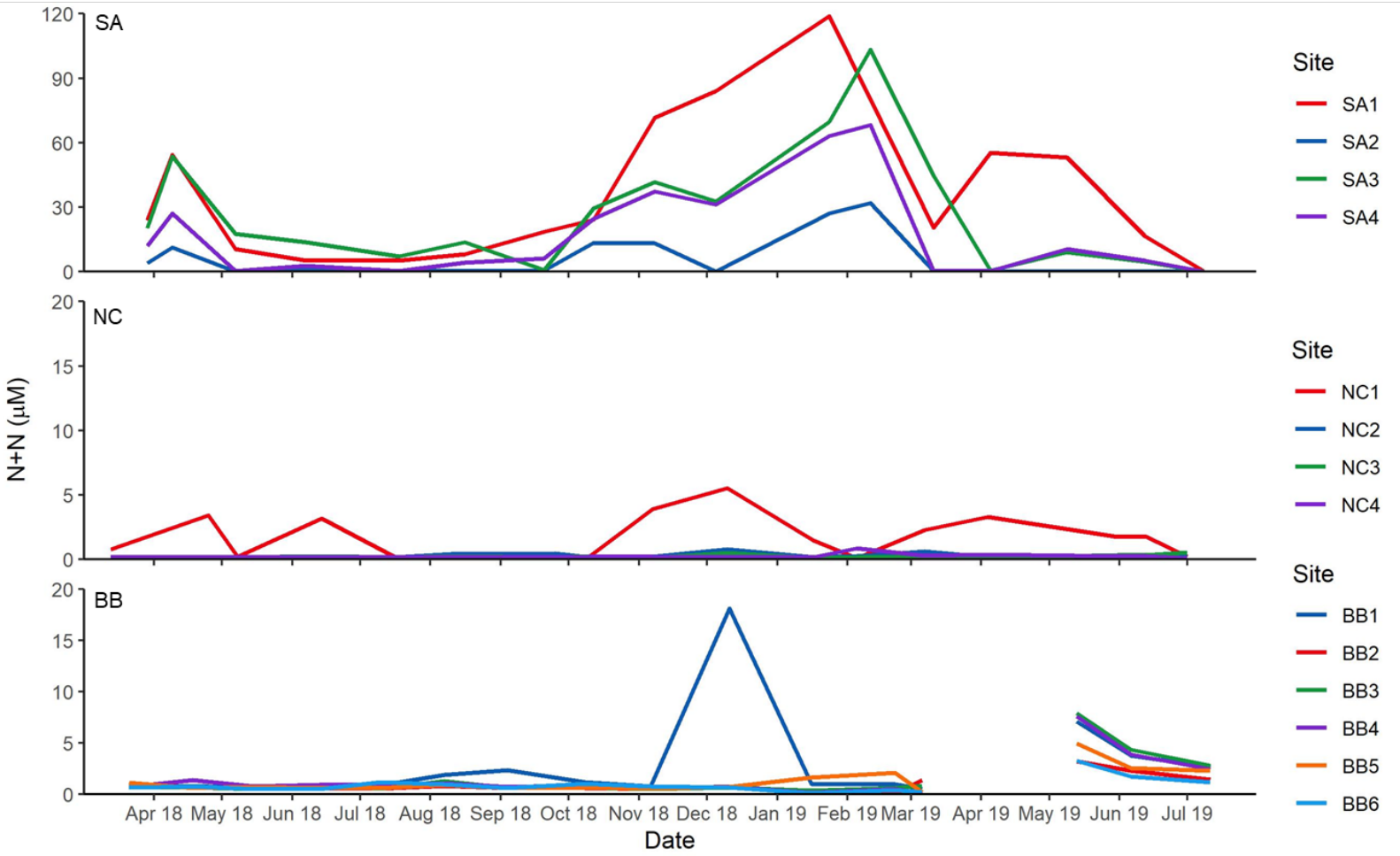

Figure 9. N+N concentrations for each site from March 2018-July 2019.

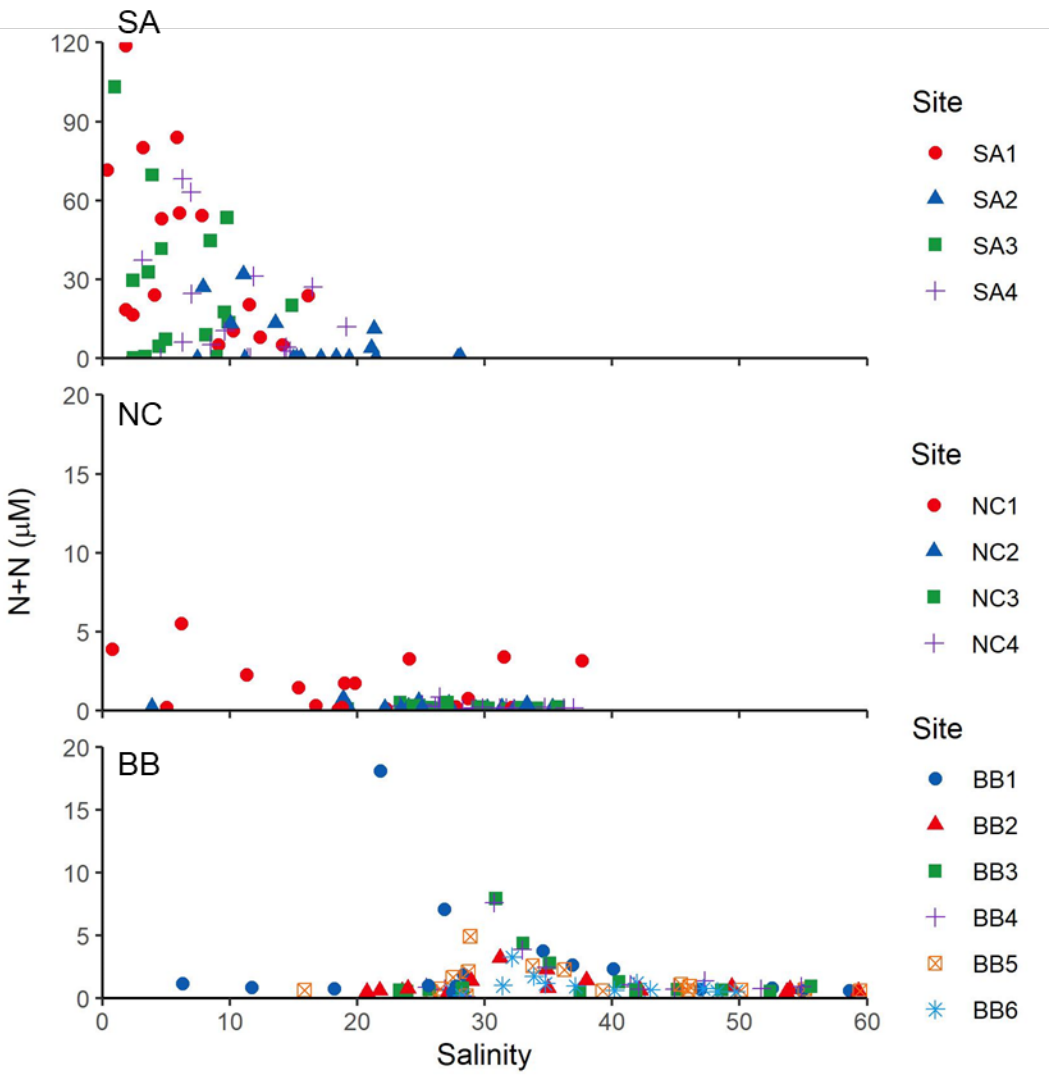

Figure 10. N+N concentrations over salinity for each site and sample date.

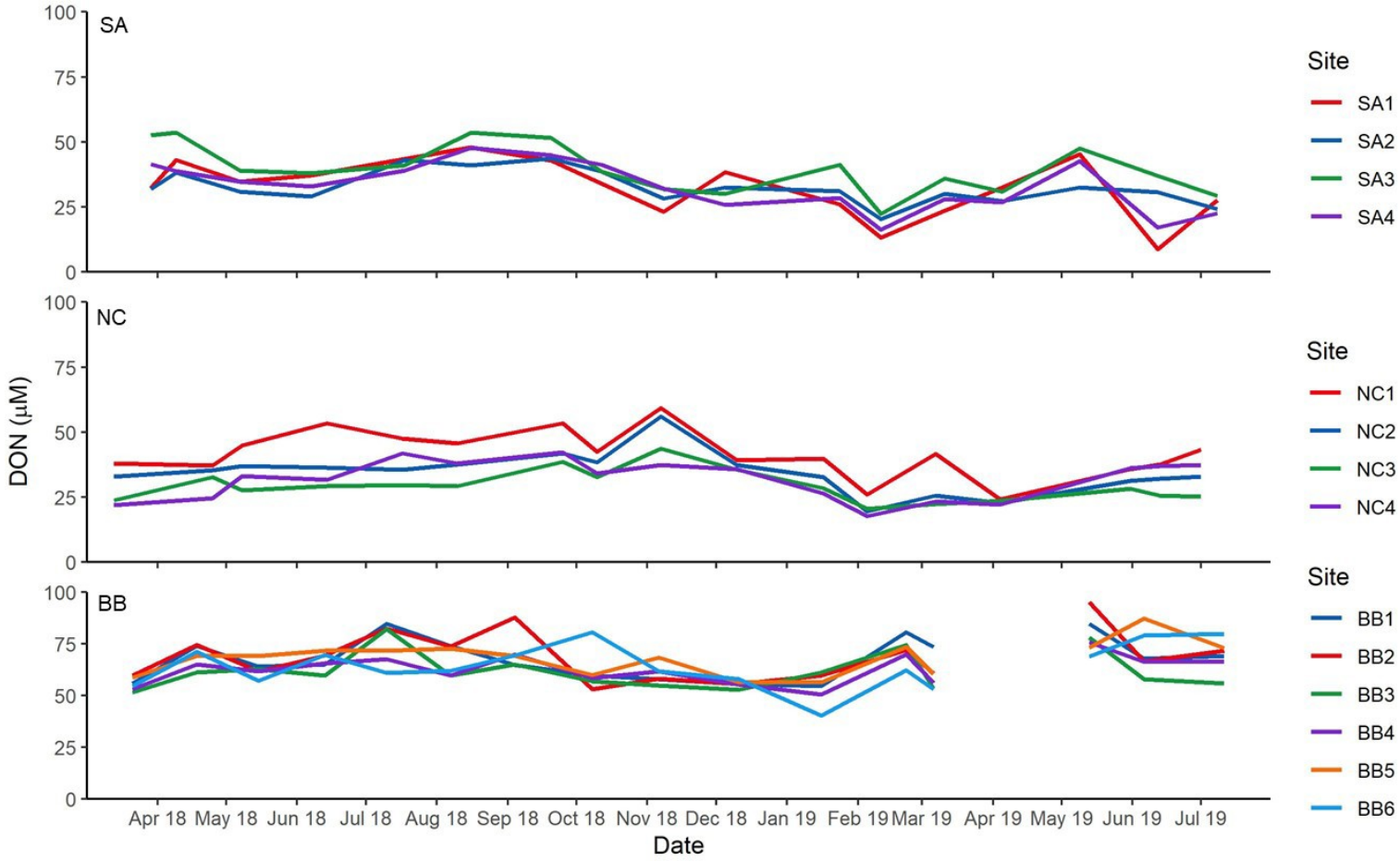

Figure 11. DON concentrations for each site from March 2018-July 2019.

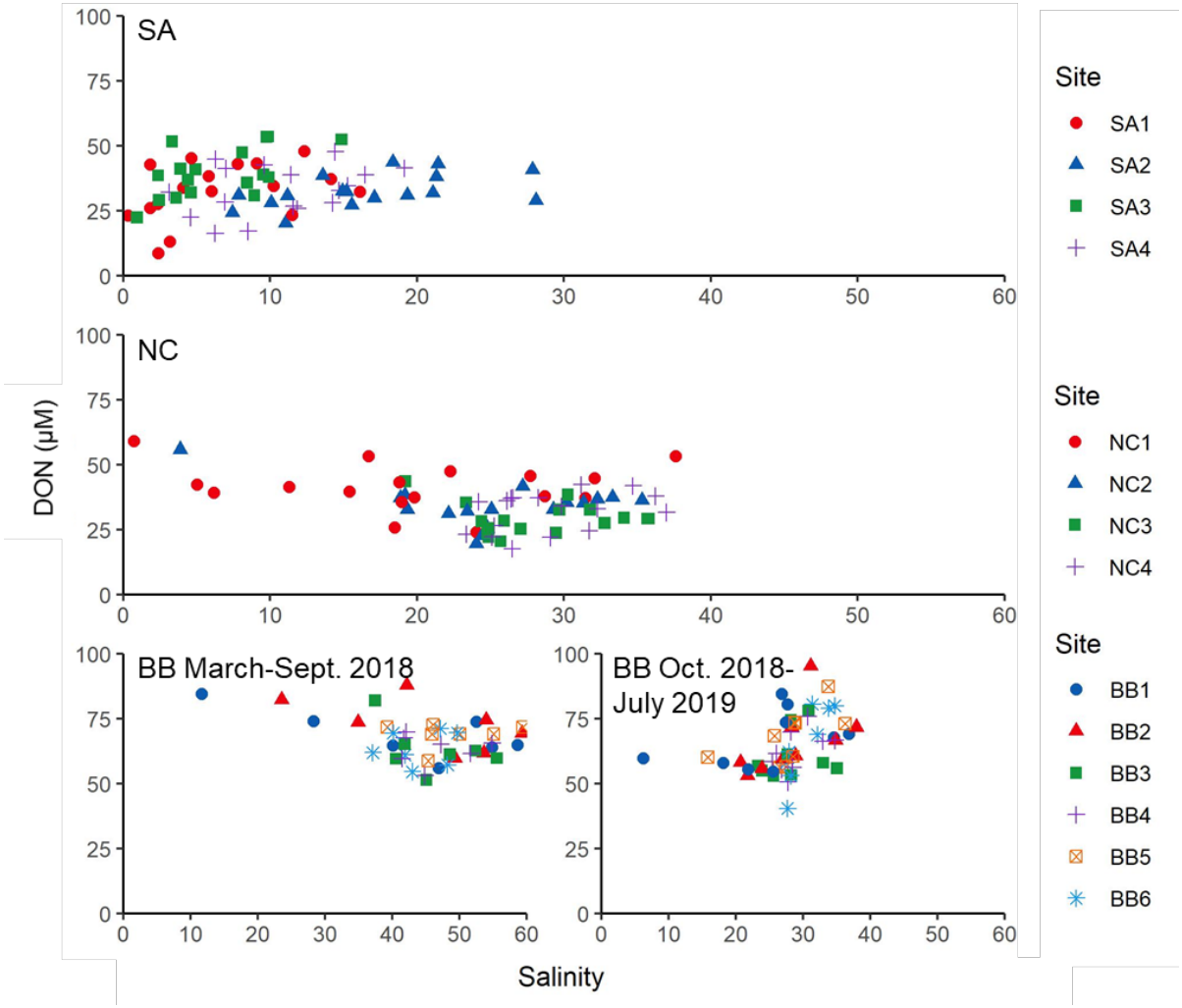

Figure 12. DON concentrations over salinity for each site and sample date. BB concentrations are split across two plots to show different behaviors in the first half of the study (March-September 2018) and in the second half of the study (October 2018-July 2019).

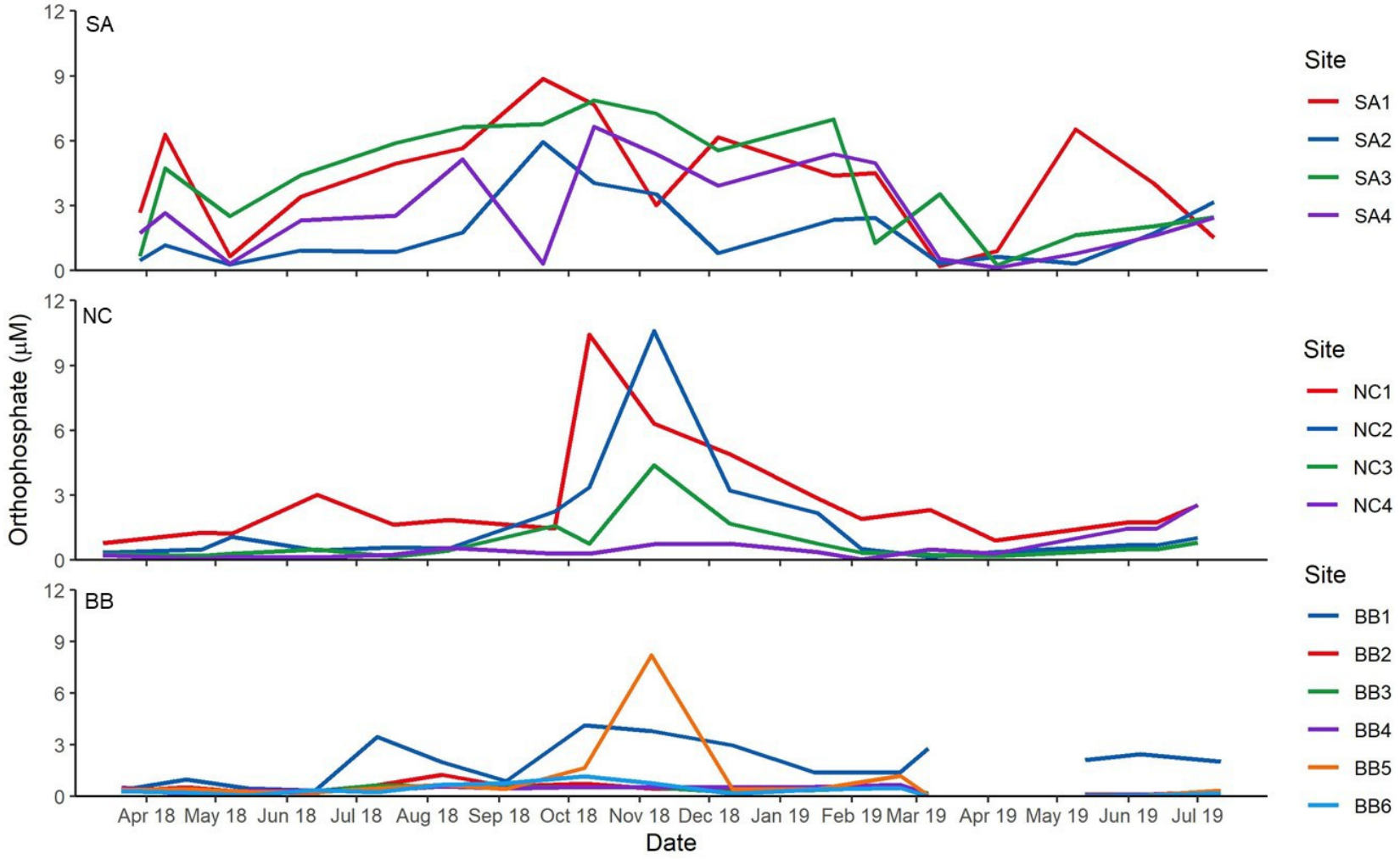

Figure 13. Orthophosphate concentrations for each site from March 2018-July 2019.

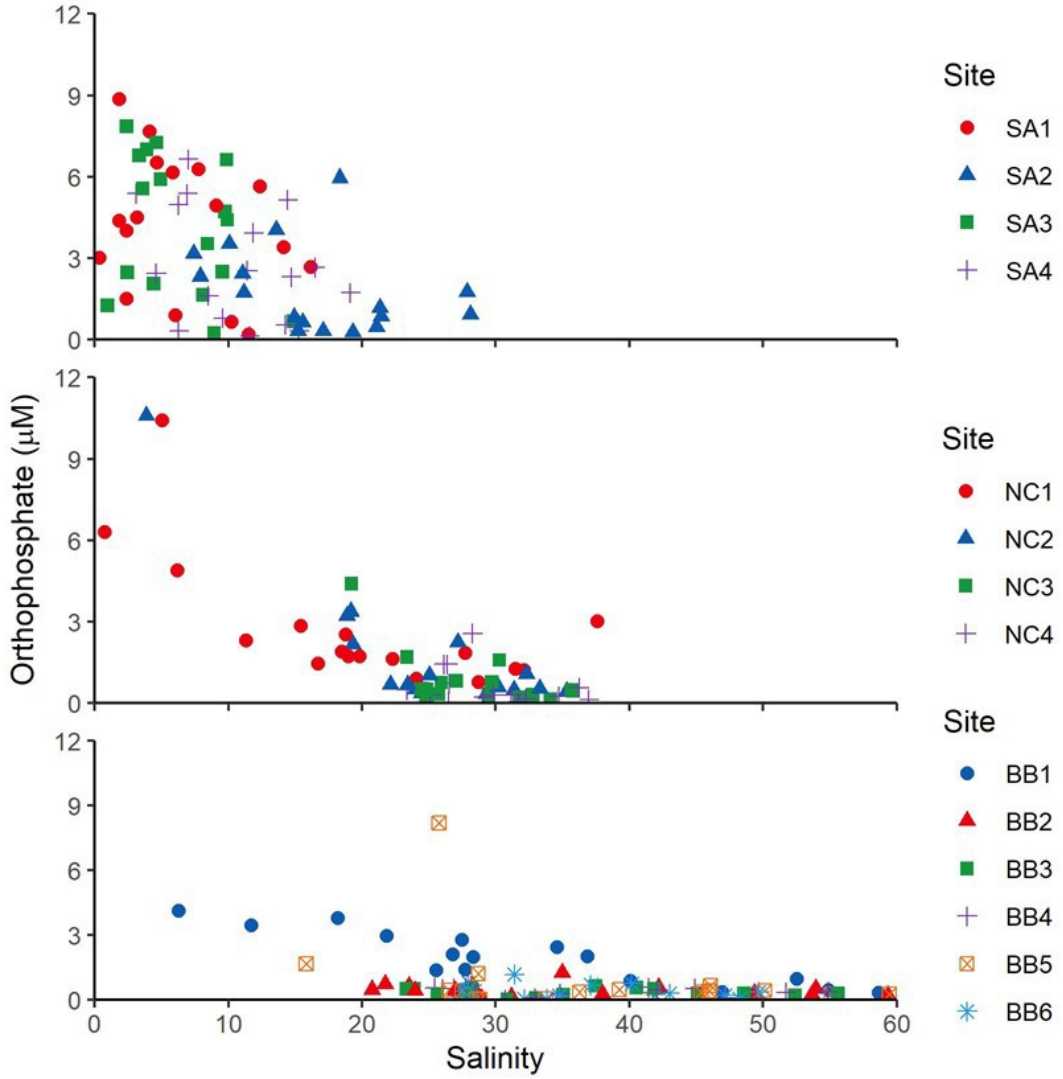

Figure 14. Orthophosphate concentrations over salinity for each site and sample date.

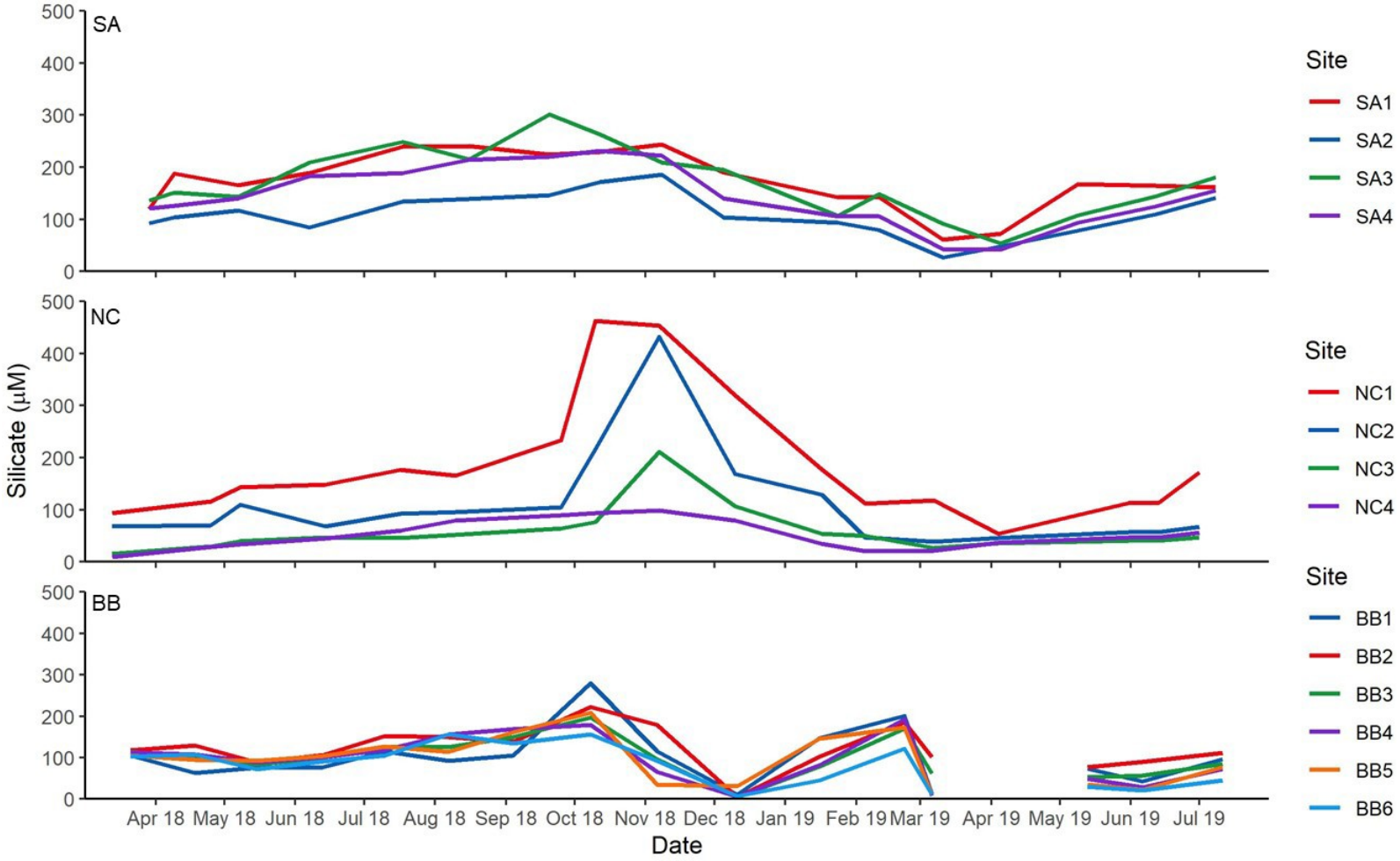

Figure 15. Silicate concentrations for each site from March 2018-July 2019.

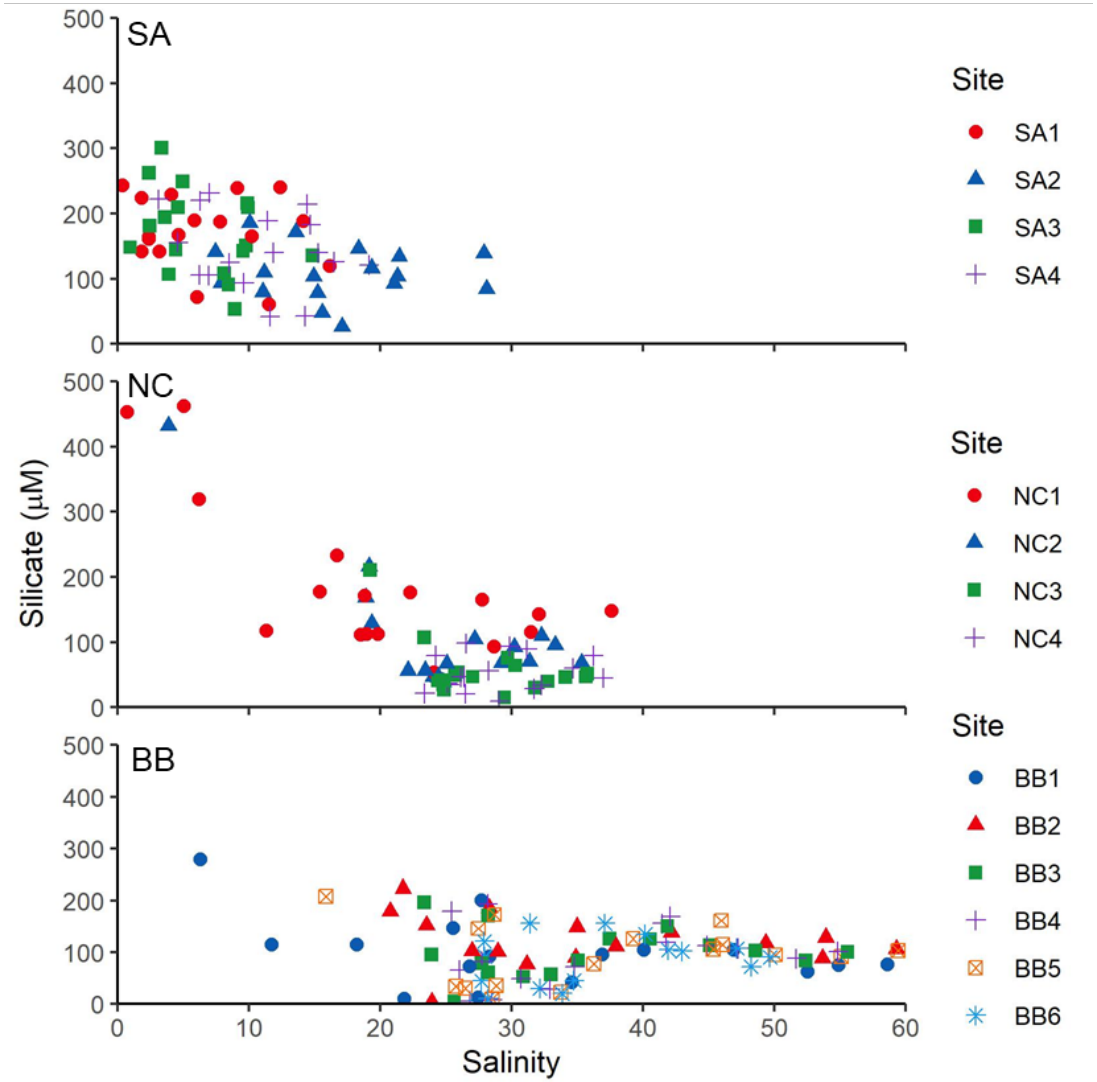

Figure 16. Silicate concentrations over salinity for each site and sample date.

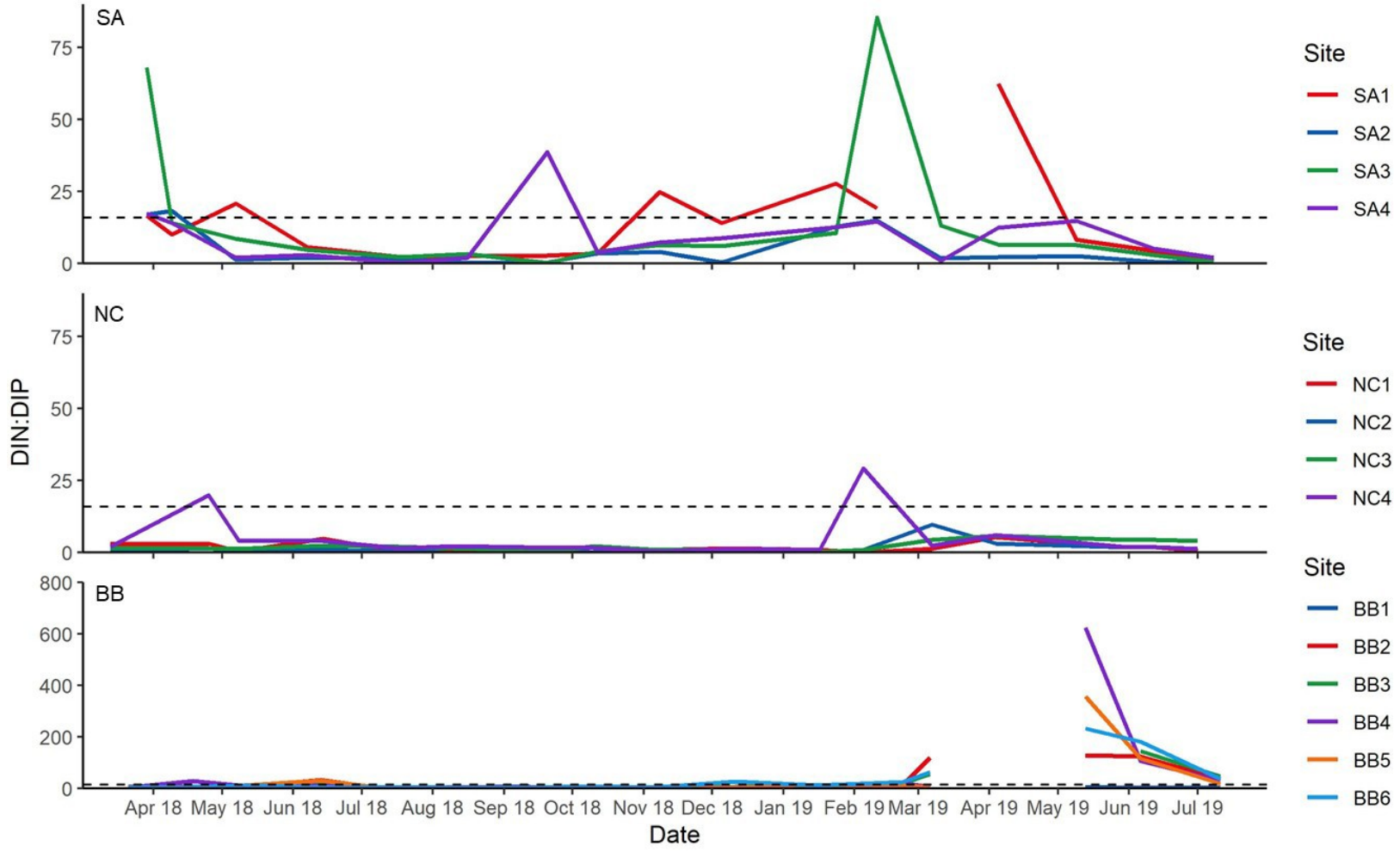

Figure 17. DIN:DIP ratio for each site from March 2018-July 2019. Dotted line represents the Redfield ratio of 16:1.

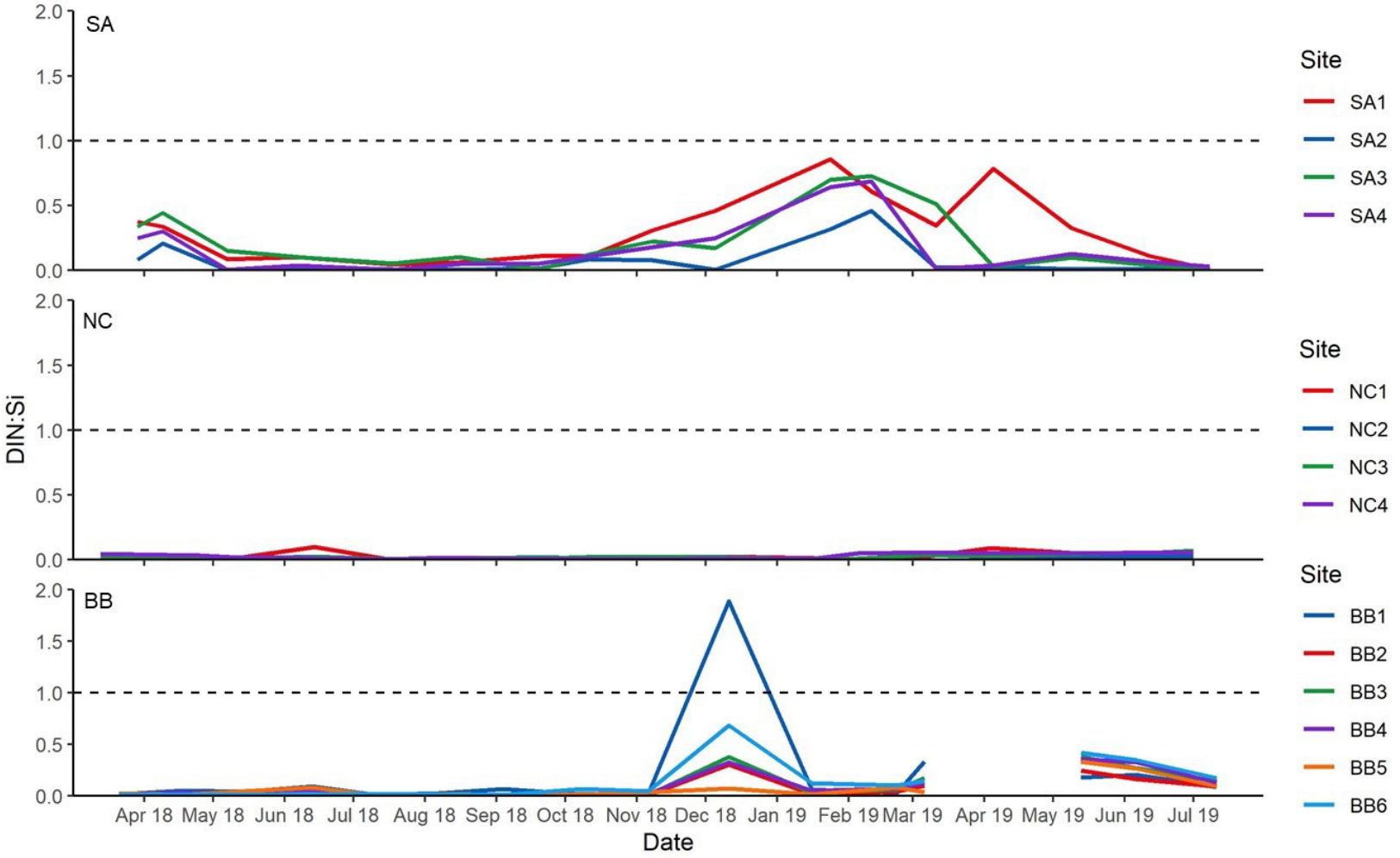

Figure 18. DIN:Si ratio for each site from March 2018-July 2019. Dotted line represents 1:1 ratio.

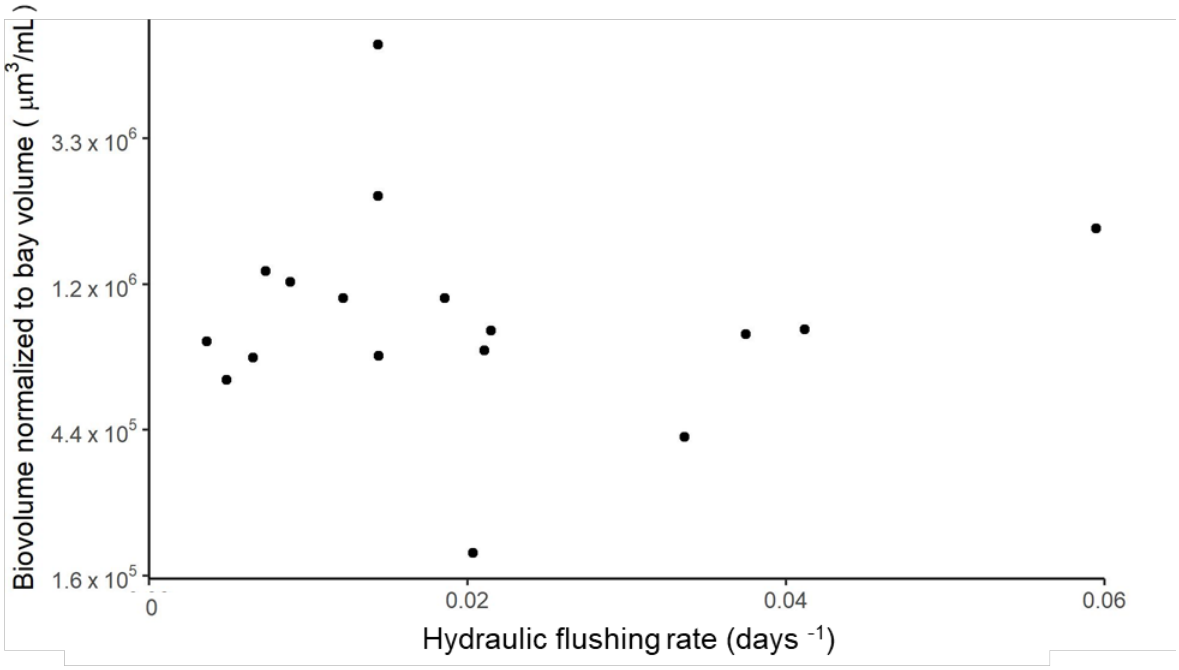

Figure 19. San Antonio Bay volume-adjusted total phytoplankton biovolume, plotted on a natural log scale, over hydraulic flushing rate.

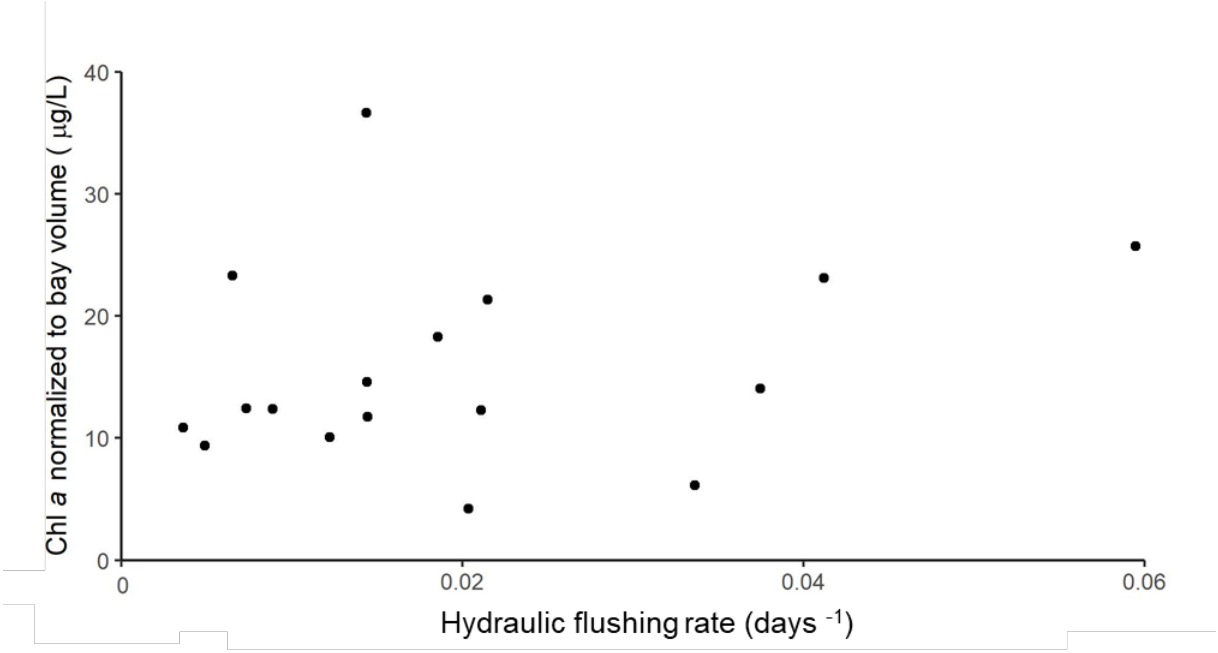

Figure 20. San Antonio Bay volume-adjusted total chlorophyll *a* over hydraulic flushing rate.

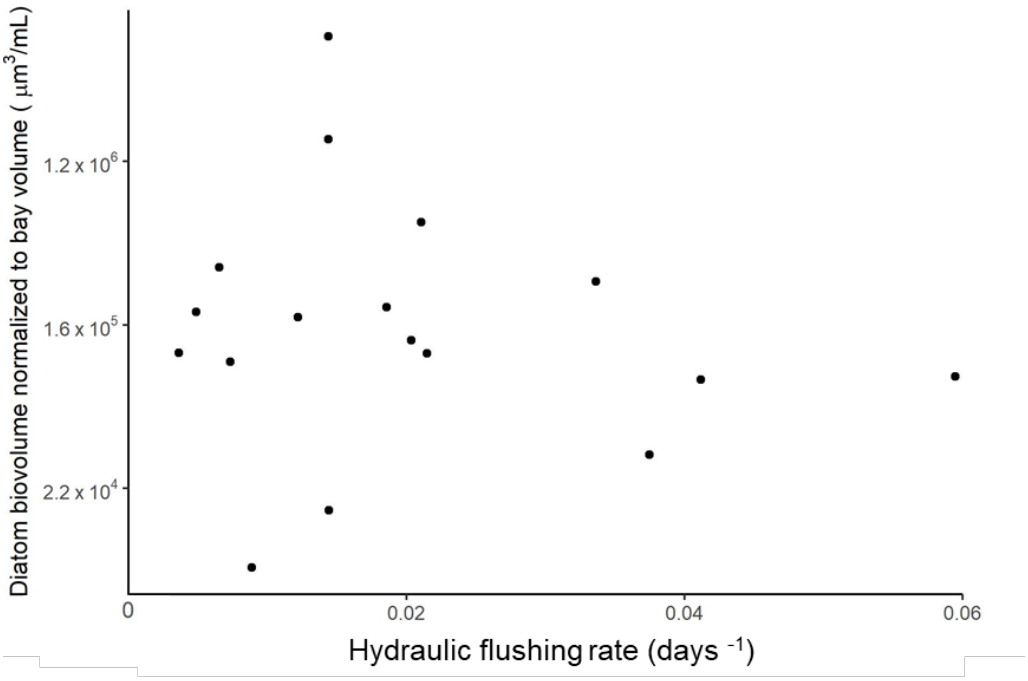

Figure 21. San Antonio Bay volume-adjusted diatom biovolume, plotted on a natural log scale, over hydraulic flushing rate.

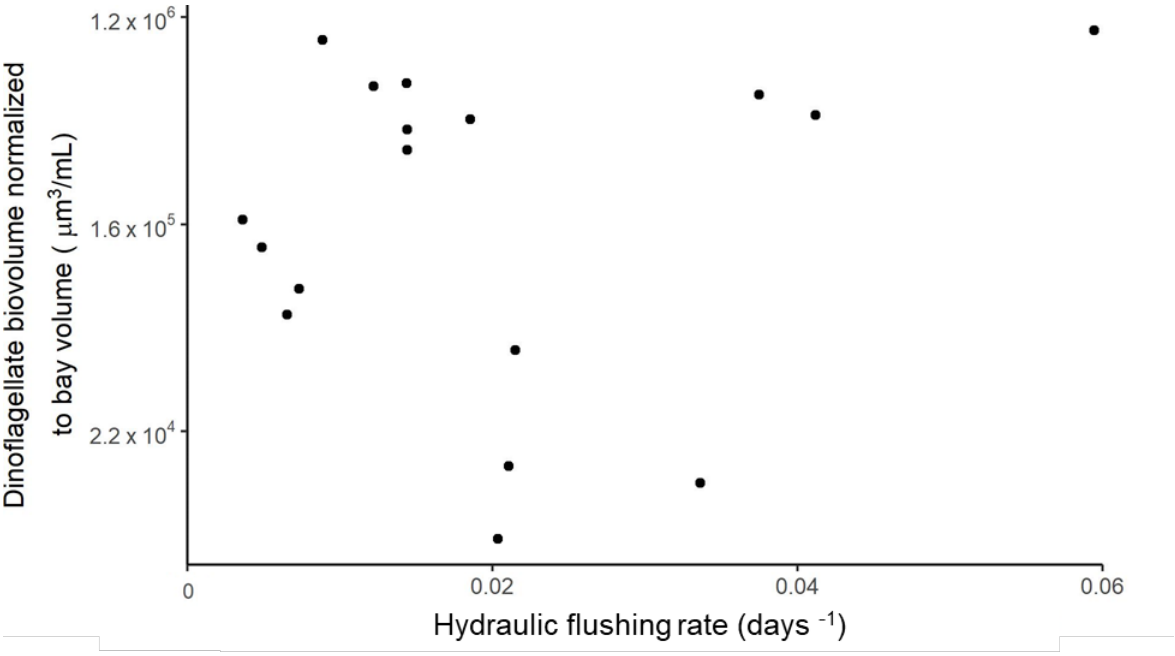

Figure 22. San Antonio Bay volume-adjusted dinoflagellate biovolume, plotted on a natural log scale, over hydraulic flushing rate.

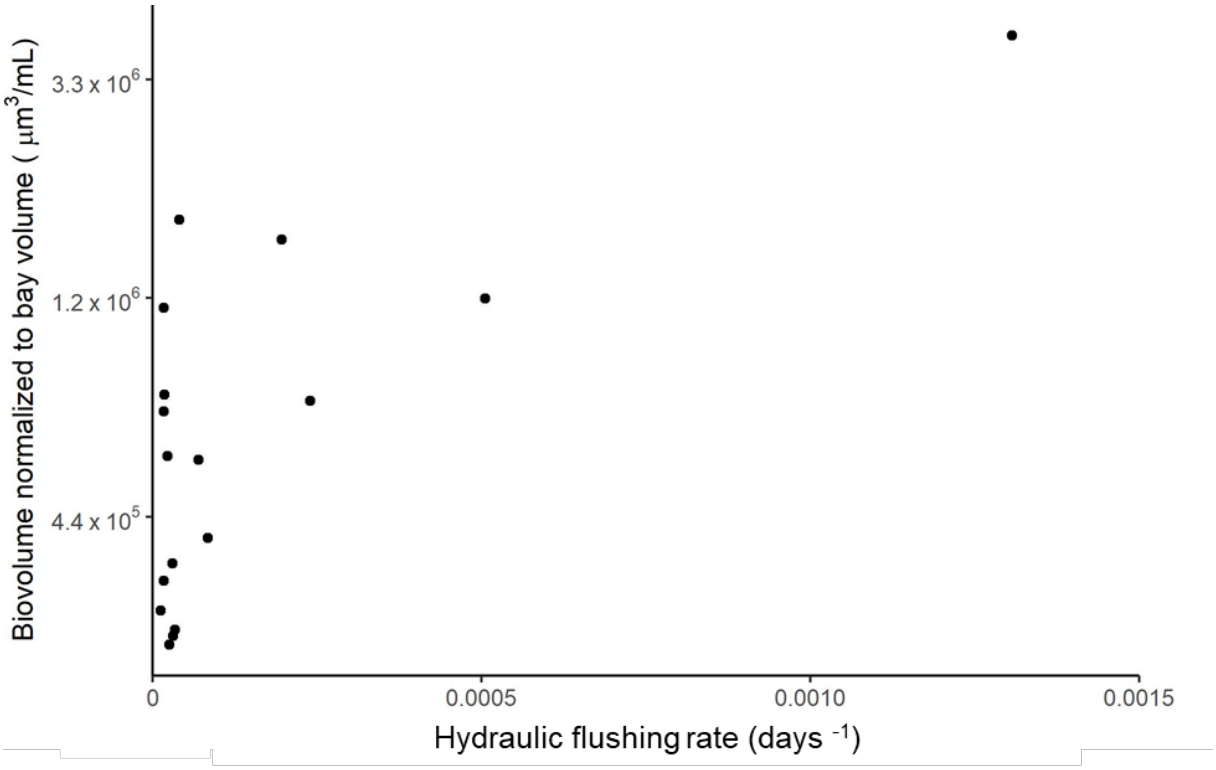

Figure 23. Nueces-Corpus Christi Bay volume-adjusted total phytoplankton biovolume, plotted on a natural log scale, over hydraulic flushing rate.

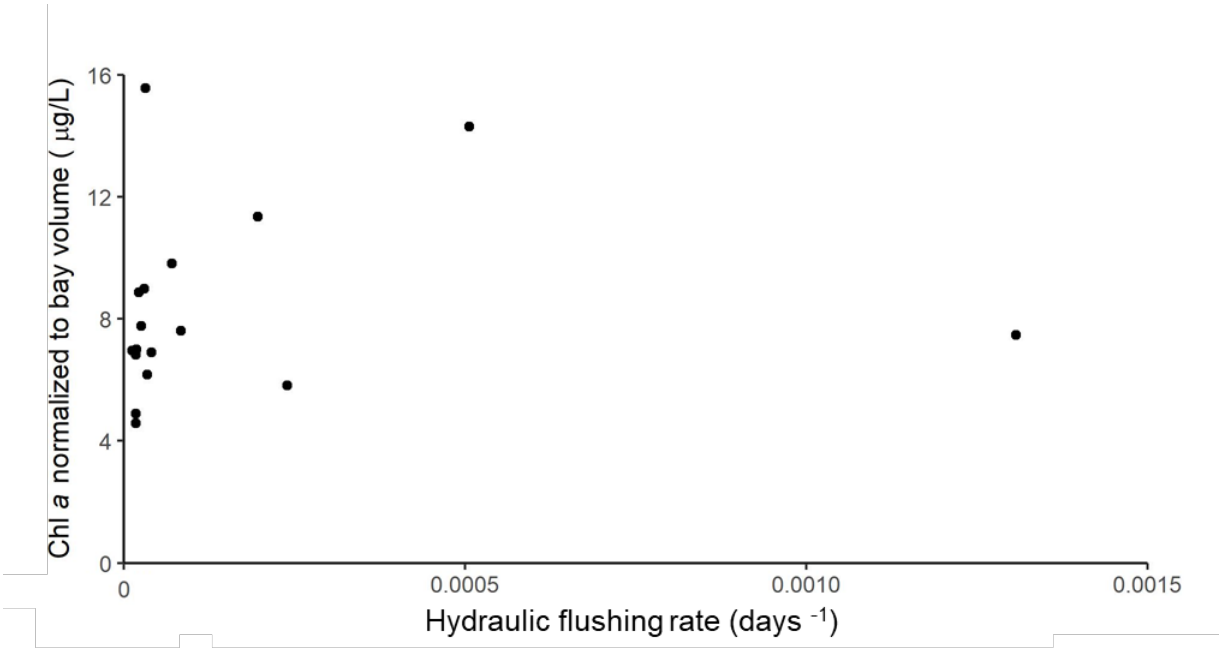

Figure 24. Nueces-Corpus Christi Bay volume-adjusted total chlorophyll *a* over hydraulic flushing rate.

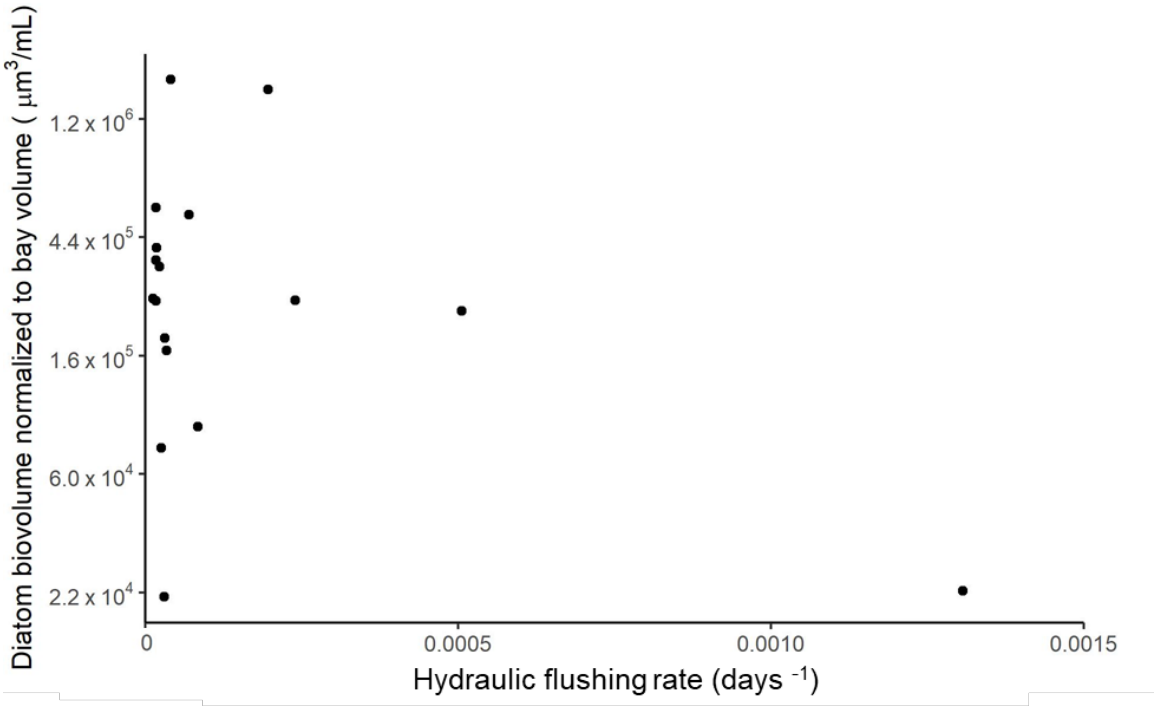

Figure 25. Nueces-Corpus Christi Bay volume-adjusted diatom biovolume, plotted on a natural log scale, over hydraulic flushing rate.

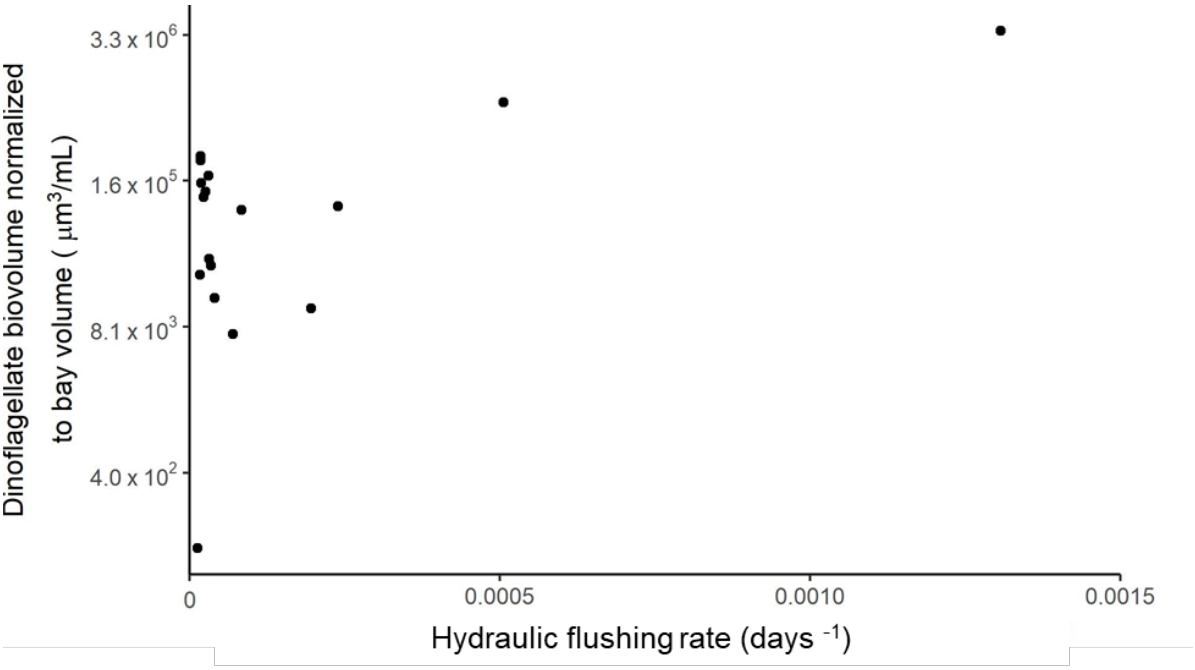

Figure 26. Nueces-Corpus Christi Bay volume-adjusted dinoflagellate biovolume, plotted on a natural log scale, over hydraulic flushing rate.

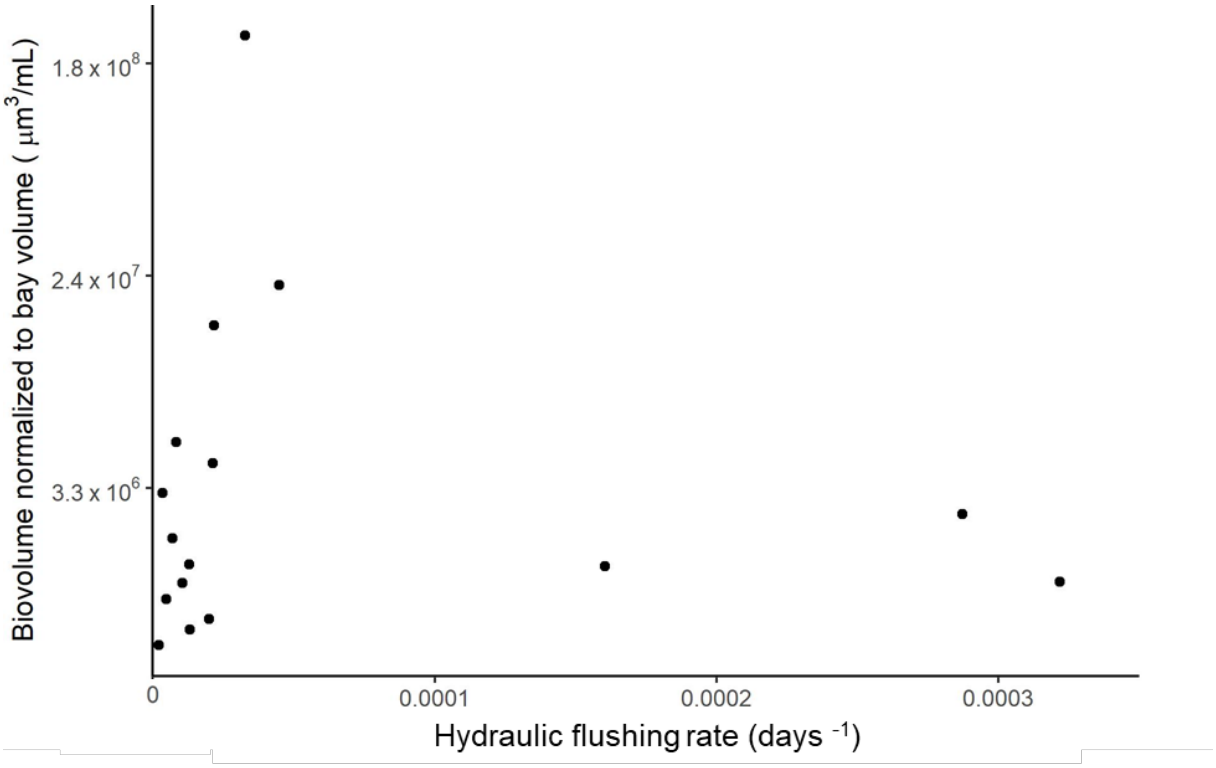

Figure 27. Baffin Bay volume-adjusted total phytoplankton biovolume, plotted on a natural log scale, over hydraulic flushing rate.

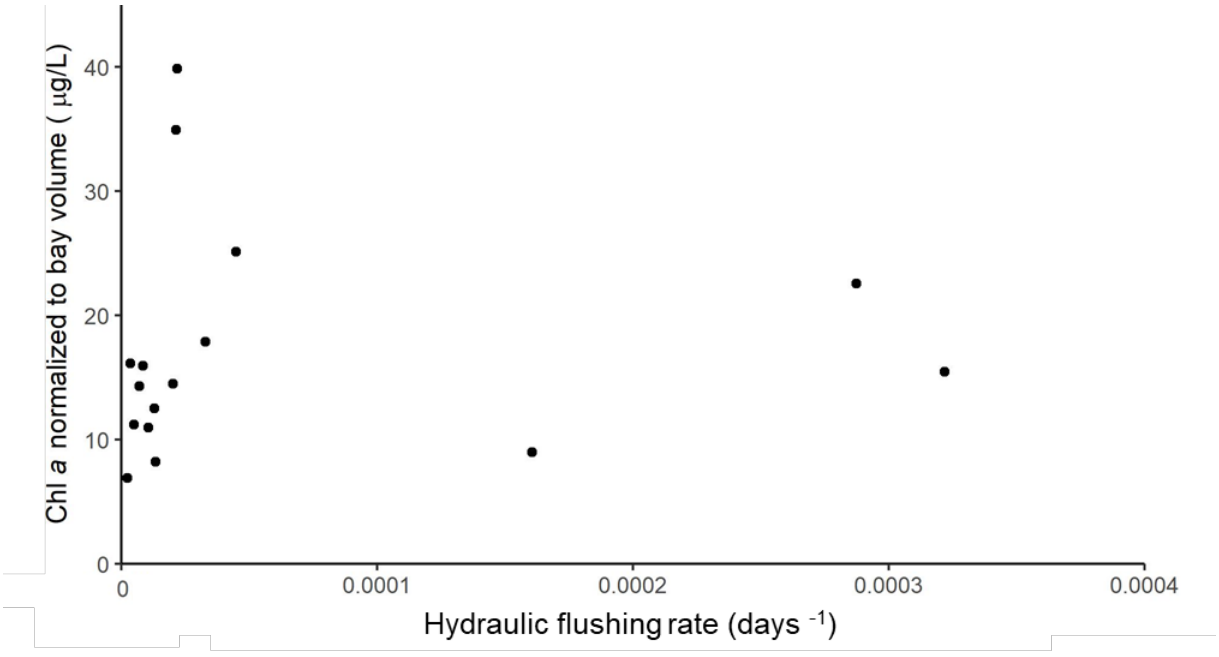

Figure 28. Baffin Bay volume-adjusted total chlorophyll *a* over hydraulic flushing rate.

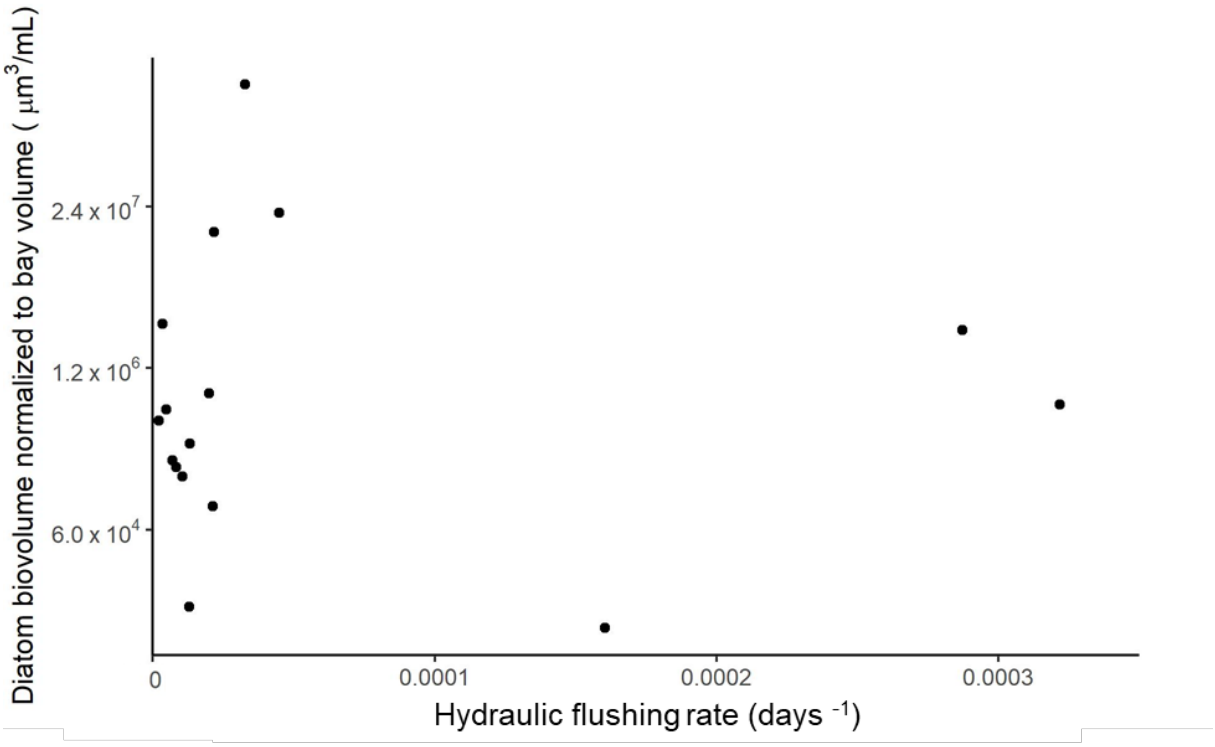

Figure 29. Baffin Bay volume-adjusted diatom biovolume, plotted on a natural log scale, over hydraulic flushing rate.

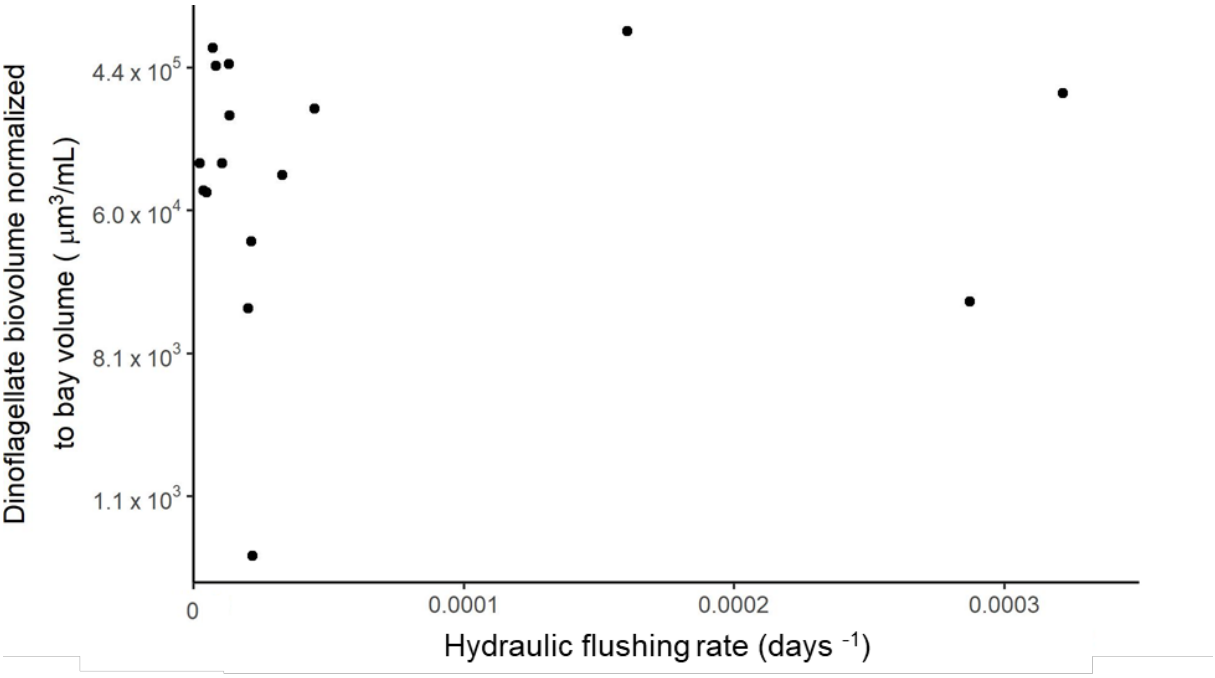

Figure 30. Baffin Bay volume-adjusted dinoflagellate biovolume, plotted on a natural log scale, over hydraulic flushing rate.

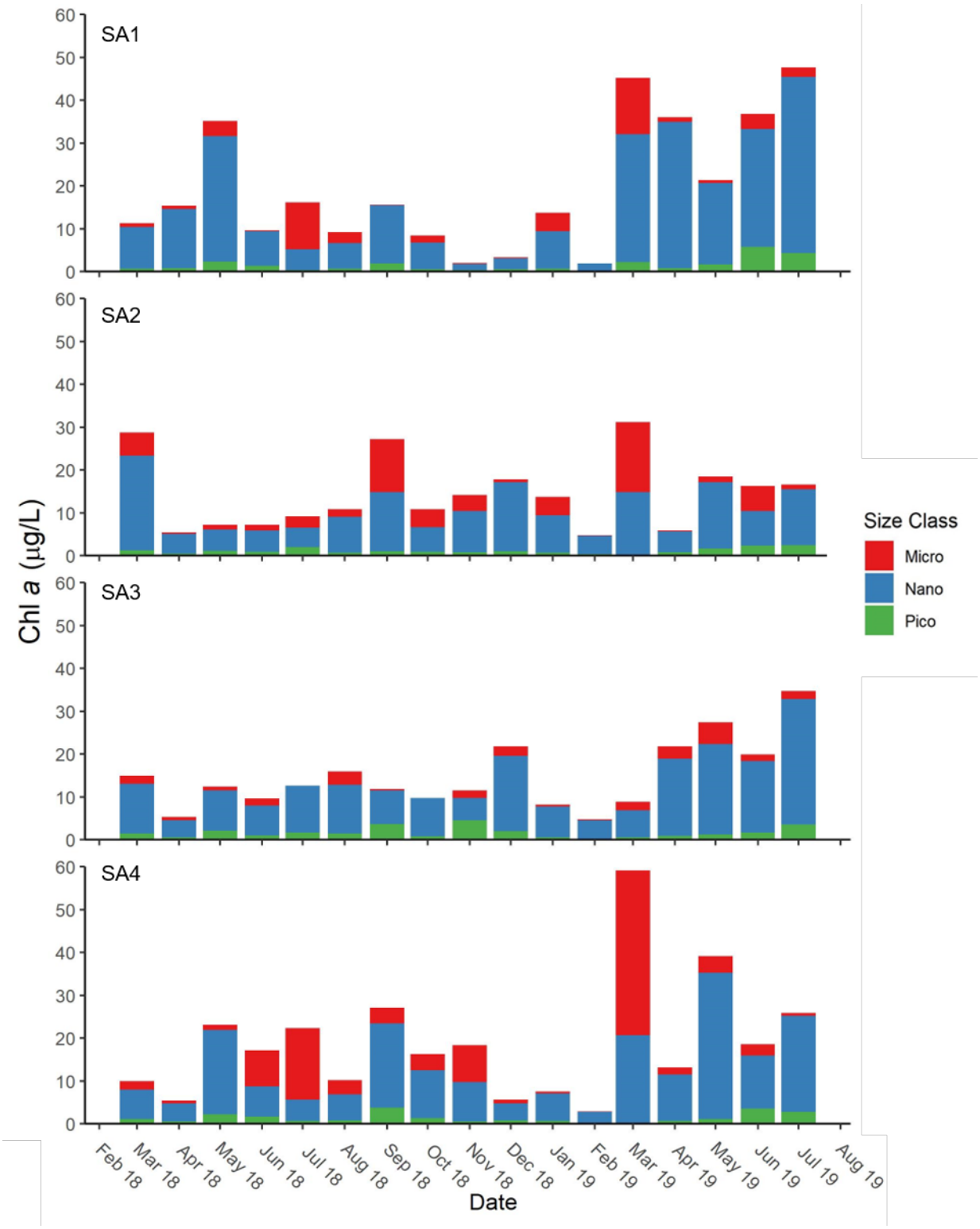

Figure 31. San Antonio Bay size-fractionated chlorophyll *a* by site from March 2018-July 2019.

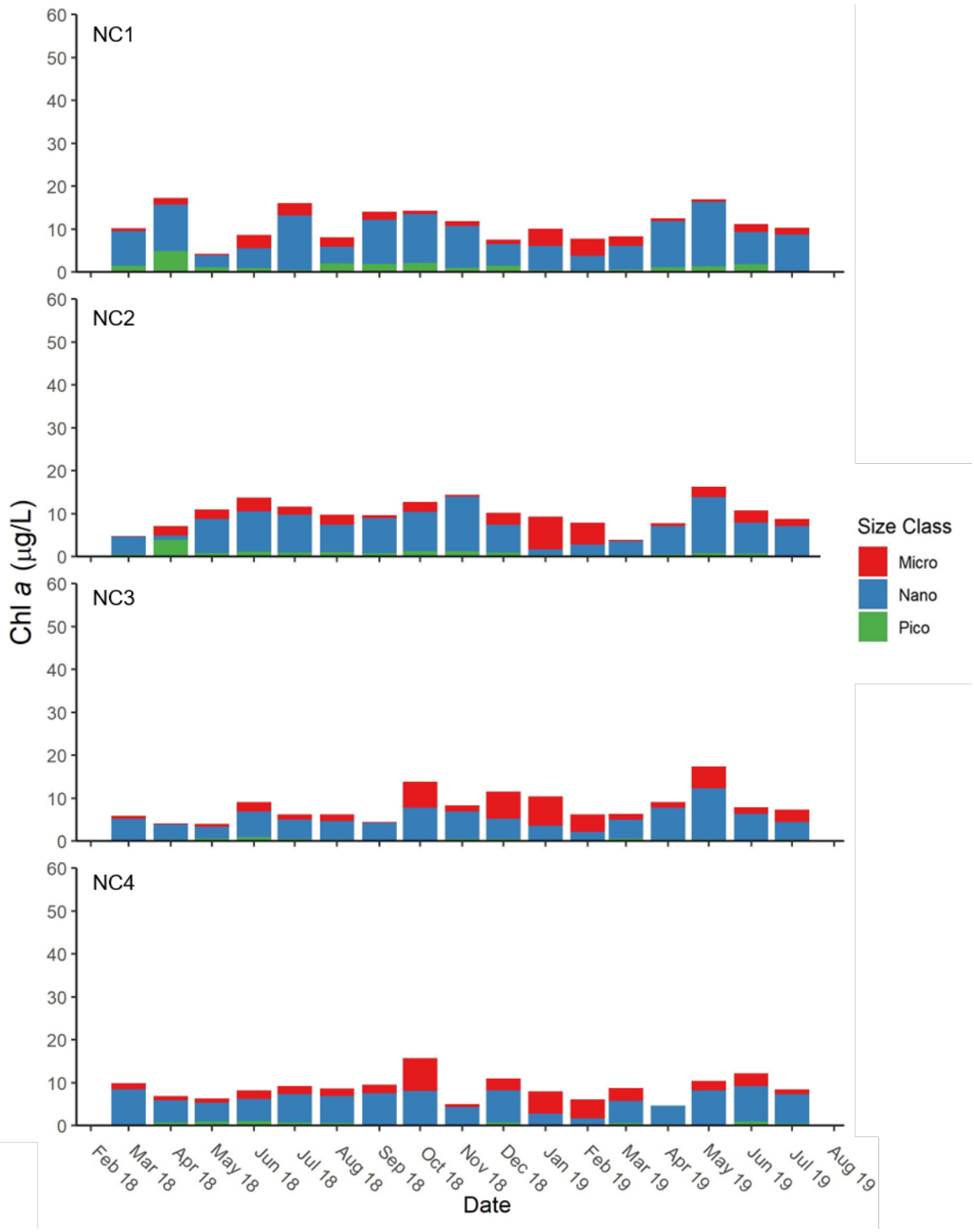

Figure 32. Nueces-Corpus Christi Bay size-fractionated chlorophyll *a* by site from March 2018-July 2019.

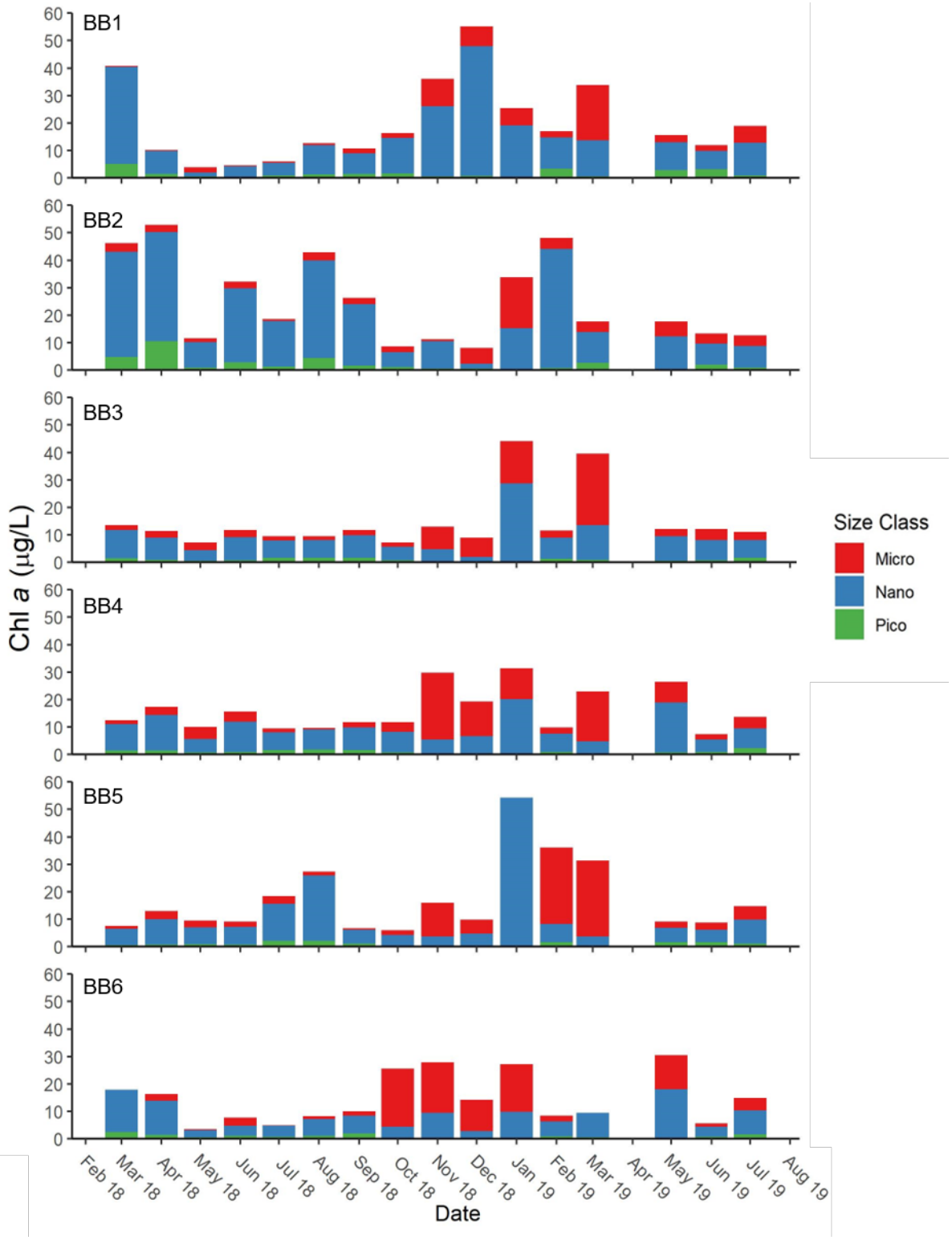

Figure 33. Baffin Bay size-fractionated chlorophyll *a* by site from March 2018-July 2019.

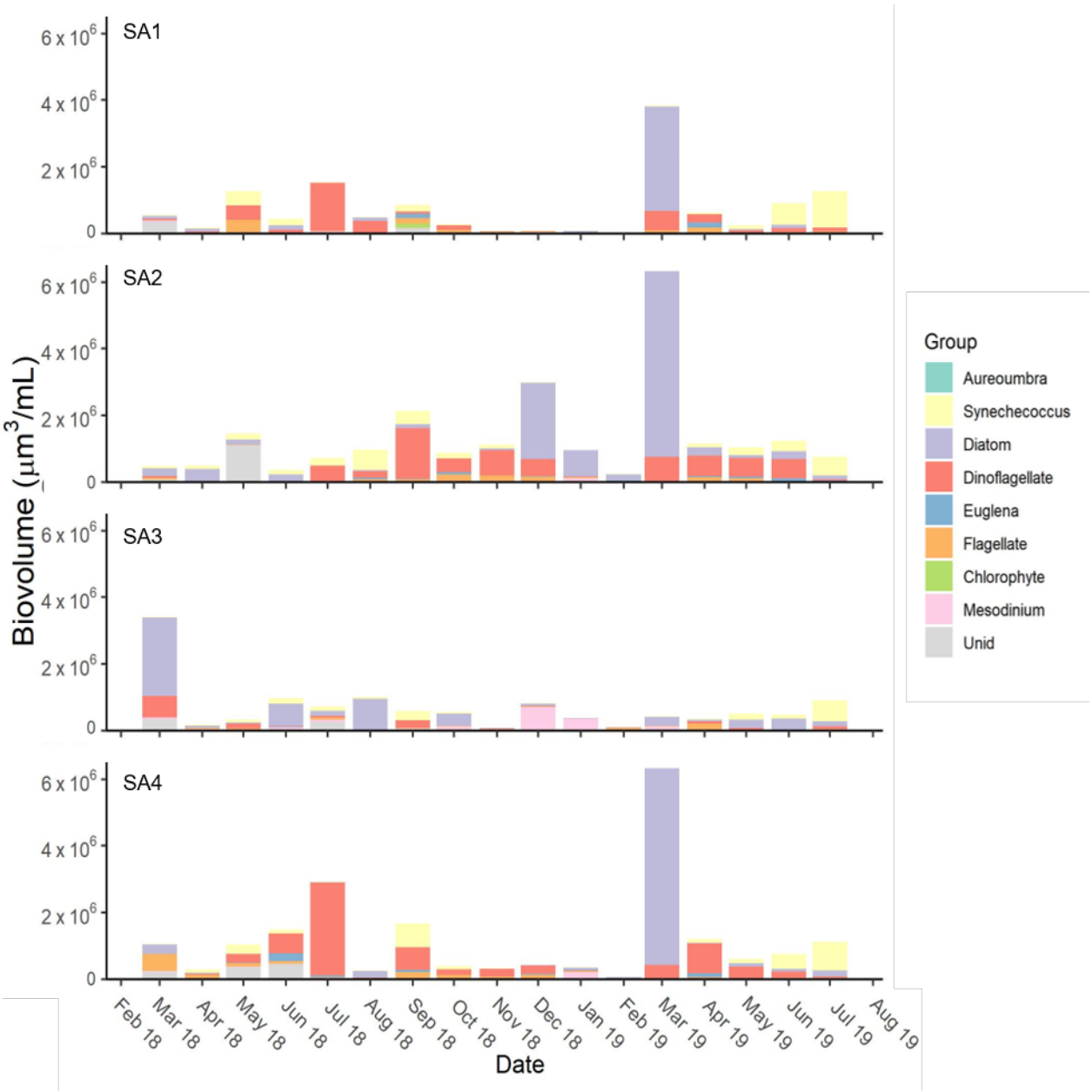

Figure 34. San Antonio Bay phytoplankton biovolume by functional groups from March 2018-July 2019.

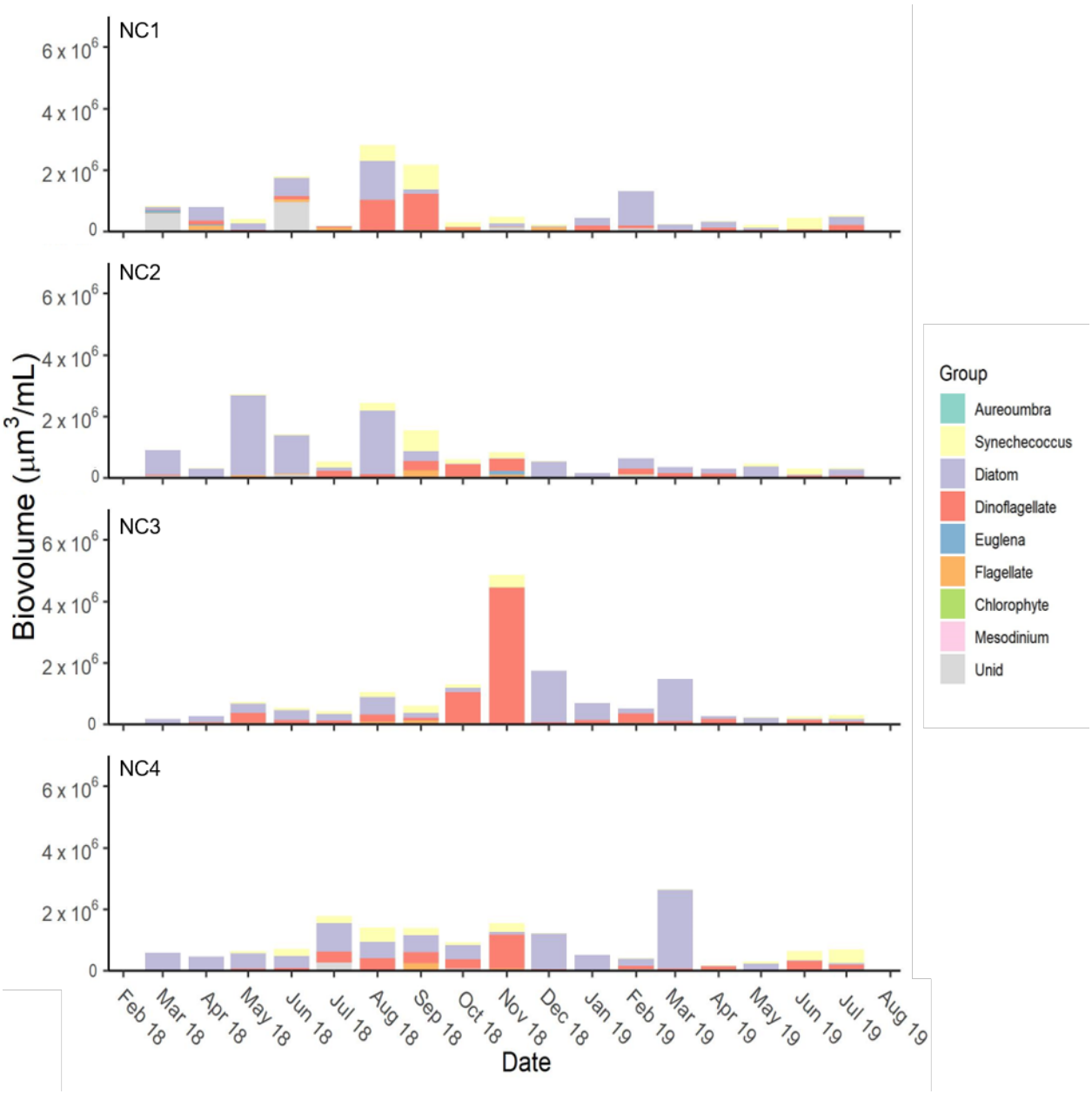

Figure 35. Nueces-Corpus Christi Bay phytoplankton biovolume by functional group from March 2018-July 2019.

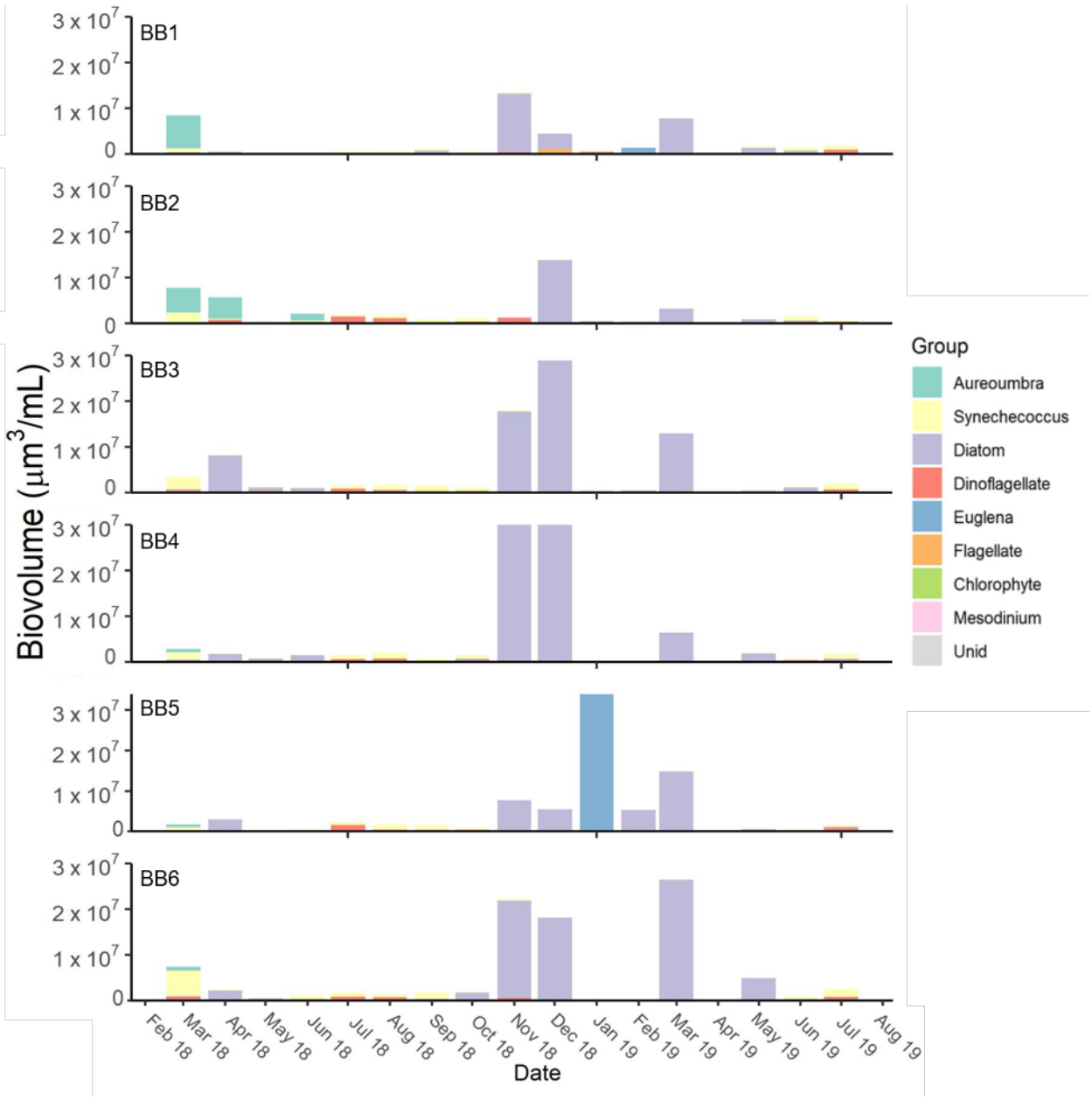

Figure 36. Baffin Bay phytoplankton biovolume by functional group from March 2018-July 2019.

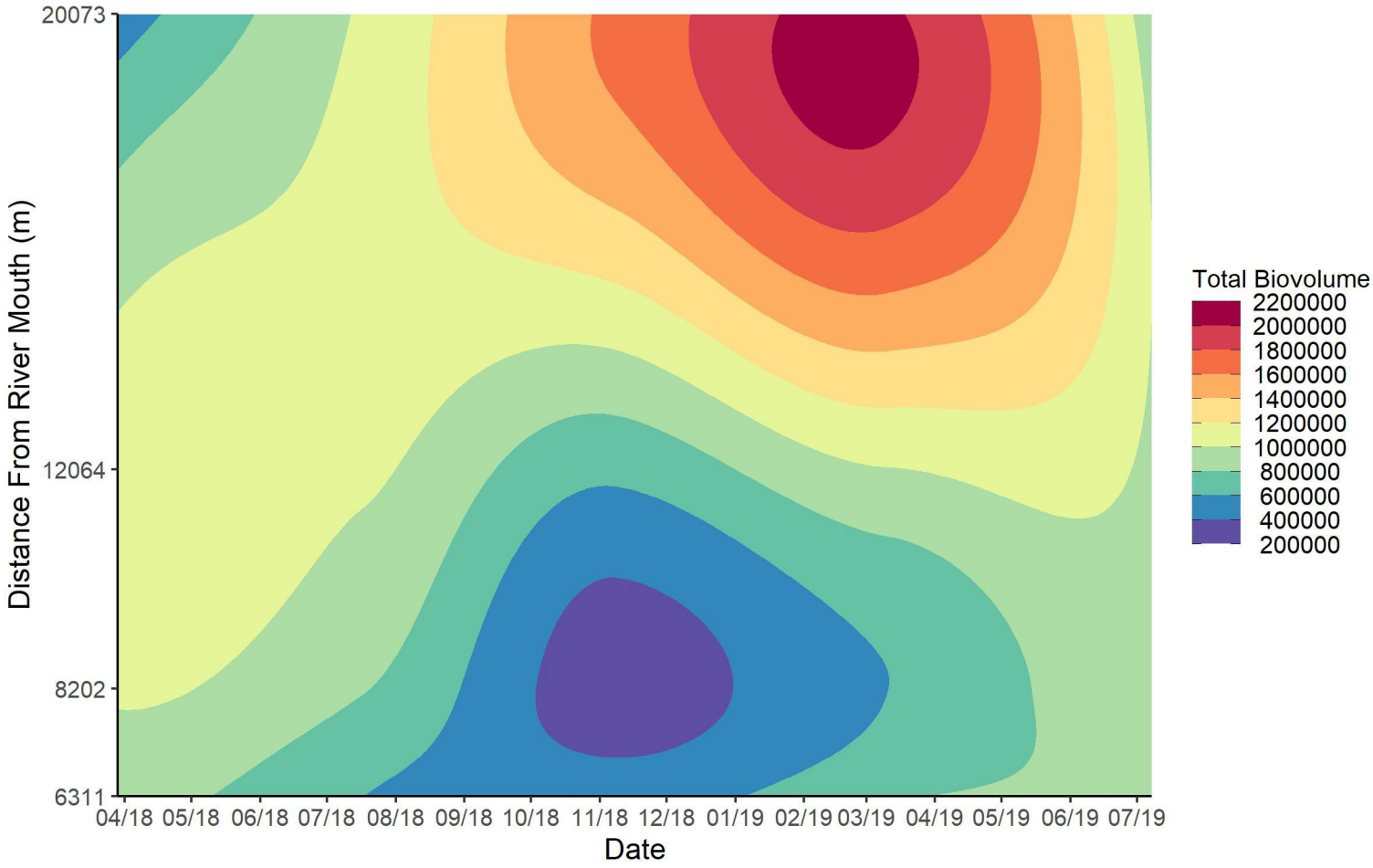

Figure 37. Contour plot showing spatial and temporal patterns in total phytoplankton biovolume in San Antonio Bay, interpolated from the measured values using a loess model in R. Values on the y-axis are the calculated distances of each of the sampling sites from the river mouth. Total biovolume is measured in $\mu m^3\ mL^{-1}$.

TABLES

Table 1. Kendall's tau correlation results between phytoplankton total and functional group biovolume and environmental variables in SA. Highlighted variables indicate significant correlations (α=0.05).

	Diatoms		Dinoflagellates		*Synechoccocus*		*Mesodinium*		Total Biovolume	
	tau	p-value	tau	p-value	tau	p-value	tau	p-value	tau	p-value
Salinity	0.219	0.009	0.238	0.004	0.090	0.280	-0.111	0.195	0.282	0.001
Ammonium (µM)	0.018	0.828	-0.300	<0.001	-0.155	0.063	0.109	0.201	-0.260	0.002
N+N (µM)	-0.160	0.054	-0.361	<0.001	-0.456	<0.001	0.142	0.097	-0.497	<0.001
PO4 (µM)	-0.174	0.036	-0.226	0.007	-0.142	0.087	0.234	0.006	-0.326	<0.001
Silicate (µM)	-0.288	0.001	-0.084	0.314	0.081	0.333	0.084	0.327	-0.121	0.144
DON (µM)	-0.039	0.637	0.007	0.933	0.110	0.187	0.088	0.301	0.024	0.775
DOC (µM)	-0.068	0.417	0.029	0.733	0.119	0.156	0.095	0.269	0.035	0.677
Temperature (°C)	-0.088	0.292	0.175	0.036	0.544	<0.001	-0.050	0.549	0.218	0.009
7-day lag discharge (m^3/sec)	-0.109	0.199	-0.110	0.196	0.050	0.560	-0.001	0.991	-0.161	<0.001
Wind speed (kn)	0.134	0.127	0.054	0.538	0.333	<0.001	0.048	0.597	0.216	0.014
7-day lag wind speed (kn)	0.133	0.143	-0.124	0.171	0.068	0.458	0.049	0.600	0.007	0.939
7-day lag rainfall (in)	0.006	0.945	-0.029	0.734	0.160	0.061	0.007	0.936	0.006	0.941
Secchi depth (m)	-0.101	0.247	0.206	0.019	-0.166	0.058	-0.099	0.271	0.068	0.434

Table 2. Kendall's tau correlation results between phytoplankton total and functional group biovolume and environmental variables in NC. Highlighted variables indicate significant correlations (α=0.05).

	Diatoms		Dinoflagellates		*Synechoccocus*		*Mesodinium*		Total Biovolume	
	tau	p-value	tau	p-value	tau	p-value	tau	p-value	tau	p-value
Salinity	0.274	0.001	0.072	0.387	0.061	0.465	-0.118	0.188	0.169	0.041
Ammonium (µM)	-0.118	0.153	0.076	0.364	0.204	0.014	-0.041	0.648	0.031	0.711
N+N (µM)	-0.040	0.630	0.004	0.966	0.062	0.455	-0.064	0.479	-0.033	0.691
PO4 (µM)	-0.201	0.015	0.039	0.644	0.223	0.008	0.188	0.036	0.070	0.397
Silicate (µM)	-0.135	0.104	0.133	0.114	0.263	0.002	0.154	0.087	0.159	0.055
DON (µM)	-0.095	0.253	0.183	0.029	0.386	<0.001	0.134	0.136	0.217	0.009
DOC (µM)	-0.169	0.041	0.186	0.026	0.371	<0.001	0.124	0.166	0.144	0.083
Temperature (°C)	-0.106	0.205	0.276	0.001	0.476	<0.001	0.097	0.283	0.069	0.412
7-day lag discharge (m^3/sec)	-0.184	0.030	0.115	0.177	0.163	0.055	0.170	0.064	0.069	0.100
Wind speed (kn)	0.119	0.177	0.216	0.016	0.373	<0.001	0.064	0.503	0.139	0.116
7-day lag wind speed (kn)	0.084	0.335	-0.061	0.492	-0.013	0.880	-0.103	0.278	-0.084	0.335
7-day lag rainfall (in)	0.179	0.047	0.041	0.653	-0.108	0.233	0.164	0.094	0.073	0.422
Secchi Depth (m)	-0.057	0.510	0.019	0.826	-0.104	0.234	-0.002	0.986	-0.033	0.704

Table 3. Kendall's tau correlation results between phytoplankton total and functional group biovolume and environmental variables in BB. Highlighted variables indicate significant correlations (α=0.05).

	Diatoms		Dinoflagellates		*Synechoccocus*		*Mesodinium*		Total Biovolume	
	tau	p-value	tau	p-value	tau	p-value	tau	p-value	tau	p-value
Salinity	-0.142	0.040	0.126	0.072	0.320	<0.001	-0.315	<0.001	-0.052	0.449
Ammonium (µM)	0.080	0.251	-0.016	0.822	-0.156	0.025	0.144	0.054	-0.188	0.007
N+N (µM)	0.031	0.655	0.214	0.002	0.133	0.055	-0.083	0.267	0.060	0.386
PO4 (µM)	-0.148	0.033	0.033	0.636	0.062	0.374	-0.047	0.533	-0.051	0.459
Silicate (µM)	-0.428	<0.001	0.106	0.130	0.261	<0.001	-0.225	0.003	-0.180	0.009
DON (µM)	-0.131	0.059	-0.024	0.729	0.086	0.218	-0.075	0.314	-0.210	0.002
DOC (µM)	-0.080	0.248	-0.118	0.092	0.069	0.319	-0.081	0.280	-0.022	0.747
Temperature (°C)	-0.319	<0.001	0.358	<0.001	0.522	<0.001	-0.355	<0.001	-0.159	0.022
7-day lag discharge (m^3/sec)	0.057	0.409	-0.067	0.338	-0.144	0.037	0.227	0.002	0.058	0.038
Wind speed (kn)	-0.133	0.061	0.150	0.038	0.287	<0.001	-0.401	<0.001	-0.148	0.037
7-day lag wind speed (kn)	0.111	0.108	-0.196	0.005	-0.152	0.028	0.016	0.828	-0.039	0.574
7-day lag rainfall (in)	-0.083	0.236	0.022	0.754	-0.105	0.135	-0.032	0.670	-0.030	0.671
Secchi Depth (m)	0.078	0.294	-0.001	0.989	-0.114	0.127	0.067	0.404	0.056	0.451

Table 4. Between bay one-way ANOVA results and mean ± SD for environmental and biomass variables. Different letters (a.b.c) indicate significant differences between bays, as determined by Shaffer post-hoc tests. Variables with the same letter are not significantly different. Asterisk (*) indicates explanatory variable was log-transformed to meet assumptions of normality.

	SA		NC		BB	
	Mean ± SD	Shaffer result	Mean ± SD	Shaffer result	Mean ± SD	Shaffer result
Ammonium (µM)	4.25 ± 4.93	a	1.05 ± 1.51	b	3.89 ± 3.79	a
N+N (µM) *	22.23 ± 27.50	a	0.61 ± 1.04	b	1.50 ± 2.26	c
Orthophosphate (µM) *	3.23 ± 2.39	a	1.46 ± 2.00	b	0.75 ± 1.12	c
Silicate (µM)	149.46 ± 60.51	a	101.56 ± 95.54	b	99.38 ± 55.56	b
DOC (µM)	360.58 ± 77.96	a	364.96 ± 121.42	a	762.20 ± 104.44	b
DON (µM)	34.44 ± 9.56	a	34.29 ± 8.88	a	65.69 ± 9.78	b
DIN:DIP *	12.13 ± 19.47	a	2.59 ± 4.32	b	40.78 ± 119.20	c
DIN:Si *	0.19 ± 0.22	a	0.02 ± 0.02	b	0.11 ± 0.22	c
Secchi depth (m)	0.4 ± 0.3	a	0.7 ± 0.4	b	0.5 ± 0.3	c
total Chl (µg/L) *	16.88 ± 11.73	a	9.49 ± 3.46	b	18.54 ± 3.40	a
Chl %microplankton *	17.36 ± 16.93	a	23.85 ± 18.31	b	29.19 ± 23.21	b
Chl %nanoplankton	73.07 ± 16.27	a	67.77 ± 18.45	a	62.28 ± 21.09	b
Chl %picoplankton	9.77 ± 6.46	a	8.61 ± 7.92	a	8.91 ± 6.00	a
total biovolume ($\mu m^3/mL$) *	$1.02x10^6 \pm 1.25x10^6$	a	$8.64x10^5 \pm 8.57x10^5$	a	$1.36x10^7 \pm 8.42x10^7$	b
Biovolume %diatoms *	25.05 ± 29.76	a	40.30 ± 33.68	b	38.26 ± 40.45	a,b
Biovolume %dinoflagellates *	22.40 ± 25.21	a	19.67 ± 21.50	a	12.40 ± 16.66	b

Table 5. SA site-specific one-way ANOVA results and mean ± SD for environmental and biomass variables. Different letters (a.b.c) indicate significant differences between bays, as determined by Westfall post-hoc tests. Variables with the same letter are not significantly different. Asterisk (*) indicates explanatory variable was log-transformed to meet assumptions of normality.

	SA1		SA2		SA3		SA4	
	Mean ± SD	Westfall result	Mean ± SD	Westfall result	Mean ± SD	Westfall result	Mean ± SD	Westfall result
Ammonium (µM)	5.45 ± 5.28	a	1.95 ± 2.48	a	5.40 ± 6.27	a	4.21 ± 4.46	a
N+N (µM)	38.26 ± 34.57	a	6.12 ± 10.06	b	27.21 ± 28.18	a,c	17.31 ± 21.83	b,c
Orthophosphate (µM)	4.20 ± 2.51	a	1.81 ± 1.59	b	4.15 ± 2.53	a	2.76 ± 2.11	a,b
Silicate (µM)	173.11 ± 54.88	a	109.12 ± 41.32	b	170.93 ± 65.62	a	144.66 ± 58.92	a,b
DOC (µM)	347.29 ± 70.35	a	329.43 ± 51.21	a	412.87 ± 101.39	b	350.90 ± 56.71	a
DIN:DIP	19.75 ± 27.40	a	4.99 ± 6.35	a	14.35 ± 24.03	a	9.43 ± 9.50	a
DON (µM)	32.60 ± 11.12	a	32.55 ± 6.46	a	39.64 ± 9.43	a	32.99 ± 9.49	a
total Chl (µg/L)	19.33 ± 15.06	a	14.45 ± 8.24	a	14.80 ± 8.03	a	18.95 ± 13.96	a
Chl % microplankton	14.07 ± 17.13	a	21.18 ± 15.59	a	10.30 ± 7.08	a	23.89 ± 22.09	a
Chl % nanoplankton	77.75 ± 16.31	a	69.46 ± 15.01	a	77.64 ± 11.38	a	67.42 ± 19.87	a
Chl % picoplankton	8.93 ± 4.86	a	9.36 ± 5.63	a	12.08 ± 9.45	a	8.69 ± 4.76	a
total biovolume ($\mu m^3/mL$)	$7.88x10^5 \pm 9.41x10^5$	a	$1.41x10^6 \pm 1.54x10^6$	a	$7.03x10^5 \pm 7.54x10^5$	a	$1.17x10^6 \pm 1.54x10^6$	a
Biovolume % diatoms *	15.64 ± 22.67	a	32.96 ± 33.78	a	32.45 ± 30.53	a	19.16 ± 29.27	a
Biovolume % dinoflagellates *	22.56 ± 25.56	a	26.59 ± 26.66	a	11.19 ± 13.19	a	29.25 ± 30.24	a

Table 6. NC site-specific one-way ANOVA results and mean ± SD for environmental and biomass variables. Different letters (a.b.c) indicate significant differences between bays, as determined by Westfall post-hoc tests. Variables with the same letter are not significantly different. Asterisk (*) indicates explanatory variable was log-transformed to meet assumptions of normality.

	NC1		NC2		NC3		NC4	
	Mean ± SD	Westfall result	Mean ± SD	Westfall result	Mean ± SD	Westfall result	Mean ± SD	Westfall result
Ammonium (µM)	1.65 ± 2.55	a	0.57 ± 0.55	a	1.09 ± 1.09	a	0.90 ± 0.93	a
N+N (µM) *	1.70 ± 1.66	a	0.27 ± 0.18	b	0.24 ± 0.12	b	0.25 ± 0.17	b
Orthophosphate (µM)	2.76 ± 2.43	a	1.68 ± 2.51	a,b	0.80 ± 1.03	b	0.60 ± 0.66	b
Silicate (µM)	186.67 ± 118.31	a	109.83 ± 95.28	b	57.87 ± 44.47	b	51.87 ± 27.47	b
DOC (µM)	463.07 ± 136.35	a	371.15 ± 117.46	b	301.38 ± 79.15	b	324.23 ± 82.22	b
DIN:DIP	1.63 ± 1.58	a	1.54 ± 2.29	a	2.33 ± 1.66	a	4.87 ± 7.75	a
DON (µM)	41.71 ± 9.00	a	34.42 ± 7.99	b	29.21 ± 6.00	b	31.83 ± 7.57	b
total Chl (µg/L)	11.13 ± 3.67	a	9.99 ± 3.25	a	8.12 ± 3.55	a	8.71 ± 2.79	a
Chl % microplankton	17.54 ± 13.70	a	23.46 ± 20.54	a	28.07 ± 19.07	a	26.35 ± 19.04	a
Chl % nanoplankton	69.78 ± 13.41	a	66.51 ± 23.55	a	66.46 ± 17.72	a	68.32 ± 19.22	a
Chl % picoplankton	12.68 ± 8.19	a	10.04 ± 11.57	a,b	5.47 ± 3.36	b	6.25 ± 3.76	b
total biovolume ($\mu m^3/mL$) *	$8.04x10^5 \pm 7.74x10^5$	a	$8.28x10^5 \pm 7.94x10^5$	a	$8.69x10^5 \pm 1.31x10^6$	a	$9.51x10^5 \pm 6.43x10^5$	a
Biovolume % diatoms	33.05 ± 26.39	a	46.39 ± 38.43	a	29.38 ± 30.66	a	52.40 ± 35.33	a
Biovolume % dinoflagellates	17.38 ± 16.03	a	17.60 ± 20.71	a	24.25 ± 28.51	a	19.42 ± 19.99	a

Table 7. BB site-specific one-way ANOVA results and mean ± SD for environmental and biomass variables. Different letters (a.b.c) indicate significant differences between bays, as determined by Westfall post-hoc tests. Variables with the same letter are not significantly different. Asterisk (*) indicates explanatory variable was log-transformed to meet assumptions of normality.

	BB1		BB2		BB3		BB4		BB5		BB6	
	Mean ± SD	West-fall result	Mean ± SD	West-fall result	Mean ± SD	West-fall result	Mean ± SD	West-fall result	Mean ± SD	West-fall result	Mean ± SD	West-fall result
Ammonium (µM) *	3.85 ± 2.28	a	4.46 ± 4.92	a	4.35 ± 4.58	a	3.55 ± 3.74	a	3.08 ± 3.38	a	4.03 ± 3.74	a
N+N (µM) *	2.76 ± 4.43	a	0.96 ± 0.80	a	1.52 ± 2.01	a	1.48 ± 1.88	a	1.32 ± 1.20	a	0.93 ± 0.74	a
Orthophos-phate (µM)	1.98 ± 1.22	a	0.45 ± 0.30	b	0.36 ± 0.19	b	0.39 ± 0.20	b	0.96 ± 1.98	b	0.38 ± 0.33	b
Silicate (µM)	100.84 ± 67.06	a	122.21 ± 50.71	a	100.21 ± 47.64	a	96.21 ± 58.09	a	95.92 ± 58.51	a	80.91 ± 49.65	a
DOC (µM)	841.30 ± 74.53	a	868.65 ± 110.94	a	729.56 ± 57.47	b	724.31 ± 60.19	b	738.92 ± 71.93	b	670.45 ± 90.46	b
DIN:DIP *	5.06 ± 4.79	a	31.12 ± 47.98	a	76.61 ± 219.03	a	54.72 ± 154.38	a	37.03 ± 90.22	a	40.15 ± 68.29	a
DON (µM)	67.94 ± 9.98	a	68.94 ± 11.94	a	61.80 ± 9.08	a	62.78 ± 6.87	a	68.28 ± 8.12	a	64.37 ± 10.84	a
total Chl (µg/L) *	19.95 ± 14.58	a	25.15 ± 15.44	a	14.64 ± 10.80	a	16.18 ± 7.67	a	17.90 ± 15.06	a	17.45 ± 14.53	a
Chl %micro plankton *	19.33 ± 16.40	a	20.33 ± 19.49	a	31.93 ± 20.01	a	33.47 ± 23.03	a	33.41 ± 26.03	a	36.68 ± 29.35	a
Chl %nano plankton	69.82 ± 15.53	a	71.04 ± 18.99	a	59.55 ± 17.14	a	58.08 ± 19.14	a	58.69 ± 23.55	a	56.47 ± 27.94	a
Chl %pico plankton	10.85 ± 7.40	a	8.63 ± 5.23	a	8.52 ± 5.15	a	8.44 ± 5.98	a	7.90 ± 5.60	a	9.14 ± 6.80	a
total biovolume ($\mu m^3/mL$) *	$2.94x10^6$ ± $3.93x10^6$	a	$2.45x10^6$ ± $2.84x10^6$	a	$5.29x10^6$ ± $8.09x10^6$	a	$5.23x10^7$ ± $1.94x10^8$	a	$5.10x10^6$ ± $8.56x10^6$	a	$5.91x10^6$ ± $8.48x10^6$	a

Biovolume %diatoms *	35.16 ± 36.90	a	10.83 ± 26.92	b	50.17 ± 42.20	a	48.36 ± 42.50	a	39.64 ± 42.58	a	45.37 ± 41.42	a
Biovolume dinoflag-ellates *	9.30 ± 12.37	a	6.08 ± 14.70	a	13.82 ± 16.25	a	15.16 ± 18.40	a	17.86 ± 23.07	a	12.18 ± 12.41	a

LIST OF APPENDICES

APPENDIX PAGE

APPENDICES

Appendix 1. Formulas and assumptions used in biovolume calculations.

Genus	Shape	Formula Source	Assumptions and Comments
Amphiprora	elliptic prism	Sun and Liu (2003)	
Asterionella	cylinder (girdle view) + cone		Combined two shape formulas to match observed morphology
Ceratium furca	ellipsoid 2 cones cylinder	Sun and Liu (2003)	
Ceratium fusus	prolate spheroid + 2 cylinders		Applied formula for *Cylindrotheca* due to morphological similarity
Chaetocerous	elliptic prism	Sun and Liu (2003)	Depth assumed to equal 1/5 width unless otherwise noted
Chattonella	cone halfsphere	Sun and Liu (2003)	
Chroomonas	cone halfsphere	Sun and Liu (2003)	
Cochlodinium	prolate spheroid	Hillebrand et al. (1999)	
Cylindrotheca	prolate spheroid + 2 cylinders	Hillebrand et al. (1999)	Assumed spine width equal to 1 µm
Desmodesmus	prolate spheroid	Sun and Liu (2003)	Applied formula for *Scenedesmus*
Dinophysis	ellipsoid	Sun and Liu (2003)	
Diplopsalis	cone halfsphere	Sun and Liu (2003)	
Ditylum	prism triangle	Sun and Liu (2003)	
Euglena	cone halfsphere cylinder	Sun and Liu (2003)	
Fibrocapsa	prolate spheroid	Hillebrand et al. (1999)	
Gonyaulax	double cone	Hillebrand et al. (1999)	
Guinardia	cylinder (girdle view)	Sun and Liu (2003)	Applied formula for *Leptocylindrus*
Gymnodinium	ellipsoid	Sun and Liu (2003)	*G. sanguineum* depth dimension assumed to equal ¼ width unless otherwise noted
Gyrodinium	ellipsoid	Sun and Liu (2003)	

Hemiaulus	elliptic prism	Sun and Liu (2003)	Applied formula for *Odontella*
Hermesium	double cone		Selected shape formula based on observed morphology
Heterocapsa	double cone	Hillebrand et al. (1999)	
Karenia	ellipsoid	Sun and Liu (2003)	
Katodinium	cylinder cone	Hillebrand et al. (1999)	Assumed cylinder portion equal to 2/3 total length and cone portion equal to 1/3 total length unless otherwise noted
Leptocylindrus	cylinder (girdle view)	Sun and Liu (2003)	
Levanderina	ellipsoid	Sun and Liu (2003)	Applied formula for *Gymnodinium*
Licmophora	gomphonemoid	Sun and Liu (2003)	Assumed depth and width dimensions equal unless otherwise noted
Myrionecta	ellipsoid	Sun and Liu (2003)	Selected formula based on morphology
Navicula	elliptic prism	Sun and Liu (2003)	
Nitzschia	rectangular box	Hillebrand et al. (1999)	
Odontella	elliptic prism	Sun and Liu (2003)	
Oxyphysis	2 cones	Hillebrand et al. (1999)	
Oxyrrhis	prolate spheroid	Hillebrand et al. (1999)	
Peridinium	ellipsoid	Sun and Liu (2003)	
Pleurosigma	elliptic prism	Sun and Liu (2003)	
Polykrikos	ellipsoid	Sun and Liu (2003)	
Prorocentrum	ellipsoid	Sun and Liu (2003)	Exceptions made for certain species, see below
Prorocentrum micans	cone halfsphere	Hillebrand et al. (1999)	Depth assumed to equal 2/5 width unless otherwise noted
Protoperidinium	double cone	Sun and Liu (2003)	Species-specific exceptions noted in

			Hillebrand et al. (1999)
Pseudonitzschia	rectangular box	Hillebrand et al. (1999)	
Pyramimonas	cone	Sun and Liu (2003)	
Pyrodinium	ellipsoid	Hillebrand et al. (1999)	
Rhizosolenia	cylinder (girdle view)	Sun and Liu (2003)	
Scenedesmus	prolate spheroid	Sun and Liu (2003)	
Scrippsiella	cone halfsphere	Sun and Liu (2003)	
Skeletonema	cylinder 2 halfspheres	Sun and Liu (2003)	
Thalassionema	rectangular box	Sun and Liu (2003)	Depth assumed to equal 0.05 x width unless otherwise noted
Thalassiosira	cylinder	Sun and Liu (2003)	